Dissertation

submitted to the

Combined Faculties of the Natural Sciences and Mathematics

of the Ruperto-Carola-University of Heidelberg, Germany,

for the degree of

Doctor of Natural Sciences

Put forward by

Dipl.-Phys. Walter Hahn

born in: Satobolsk, Kazakhstan,

Oral examination: 19.07.2016

Stability of Quantum Statistical Ensembles with Respect to Local Measurements

Referees: Prof. Boris V. Fine
             Prof. Manfred Salmhofer

Abstract:

Ein offenes Problem in den Grundlagen der Quantenstatistik ist die fehlende Rechtfertigung für die Verwendung von statistischen Ensembles mit schmalen Energieverteilungen wie das kanonische oder mikrokanonische Ensemble.

In dieser Doktorarbeit lösen wir dieses Problem, indem wir ein Stabilitätskriterium für quanten-statistische Ensembles einführen, die makroskopische Systeme beschreiben. Wir bezeichnen ein Ensemble als "stabil", wenn eine kleine Anzahl an lokalen Messungen die Wahrscheinlichkeitsverteilung der Gesamtenergie des Systems nicht signifikant modifizieren kann. Wir wenden dieses Kriterium an Gittern von Spins-$\frac{1}{2}$ an und zeigen dabei, dass das kanonische Ensemle fast stabil ist, wohingegen statistische Ensembles mit einer viel breiteren Energieverteilung nicht stabil sind.

Wir testen die analytischen Abschätzungen numerisch, indem wir die Stabilität von quanten-statistischen Ensembles für generische wechselwirkende Spin-Systeme untersuchen. Obwohl die Effekte der endlichen Ausdehnung im Zusammenhang mit lokalen Messungen recht ausgeprägt sind für mikroskopische Systeme, die numerisch untersucht werden können, sind die Ergebinsse der numerischen Untersuchungen konsistent mit den analytischen Ergebnissen.

Zum Schluss führen wir ein Maß für die Makroskopizität von Quantensuperpositionen ein. Wir bezeichnen eine Quantensuperposition als makroskopisch, falls eine lokale Messung eine signifikante Veränderung der Dichtematrizen einer makroskpischen Anzahl der Untersysteme nach sich zieht.

Abstract:

An open problem in the foundations of quantum statistical physics is the missing justification for using statistical ensembles with narrow energy distributions such as the canonical or microcanonical ensembles.

In this thesis, we resolve this problem by introducing a stability criterion for quantum statistical ensembles describing macroscopic systems. An ensemble is called "stable" when a small number of local measurements cannot significantly modify the probability distribution of the total energy of the system. We apply this criterion to lattices of spins-$\frac{1}{2}$, thereby showing that the canonical ensemble is nearly stable, whereas statistical ensembles with much broader energy distributions are not stable.

We test the analytical estimates numerically by investigating the stability of quantum statistical ensembles for generic interacting spin systems. Although the finite-size effects with respect to local measurements are rather pronounced for the microscopic system sizes available in numerical simulations, the results of the numerical studies are consistent with the analytical results.

Finally, we introduce a macroscopicity measure for quantum superpositions. A quantum superposition is called macroscopic if one local measurement can induce a significant change of a macroscopic number of the subsystems' density matrices.

to my parents

Contents

Chapter 1

Introduction

The notion of temperature is rather intuitive. The difference between a hot cup of tea and a piece of ice is familiar to us since childhood. It seems, as a matter of course, that it is always possible to compare two physical bodies of our everyday world and find out which one is warmer and which one is colder. It also comes as no surprise that, in this way, all physical bodies can be put into an order starting with coldest and ending with the hottest objects. In fact, the same order can be characterised by assigning to each object a value which we call temperature. We denote the temperature by the symbol T. An instrument for measuring the temperature is called the thermometer.

First attempts to build thermometers reach back to Galileo Galilei around 1592 (probably even earlier). Back in these days, Galileo actually built a thermoscope which is a thermometer without a temperature scale. Such a device can only indicate changes in the temperature. As illustrated in Fig. 1.1, it consisted of a glass pipe filled with water. On the top of this pipe, a gas vessel was attached. When the temperature varies, the gas inside the vessel changes its volume and, in this way, controls the level of the water in the pipe. First genuine thermometers were introduced in the 18-th century among others by Ole Rømer (1701), Daniel Fahrenheit (1714) and Anders Celsius (1742)[1]. They were made out of more suitable materials and were devised with a useful temperature scale[2].

With the onset of thermodynamics in the first half of the nineteenth century, relations between temperature and other thermodynamic quantities like volume, pressure and heat were established. This development was intimately connected with the industrial revolution, where the primary goal was to make industrial machines more efficient. For exam-
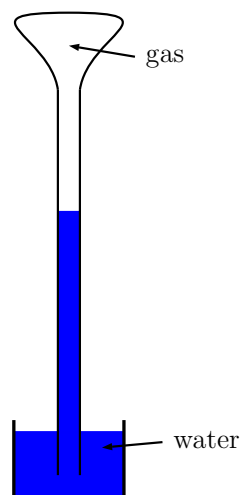
Figure 1.1: A schematic picture of the thermoscope proposed by Galileo Galilei

---

[1]Originally, Celsius defined his temperature scale in reversed order. The temperature of 100°C corresponded to the freezing point of water and 0°C to the boiling point of water. Only later in 1745, this temperature scale was reversed by Carl Linnaeus. It is this corrected temperature scale that we use today.

[2]Today, suitable thermometers are available for a vast number of different experimental settings. A recent work [36] shows that a thermometer can be even made of a single atom.

ple, the work of Sadi Carnot on the today well-known Carnot-cycle was mostly driven by the intention to improve the efficiency of the steam machine. The further development of thermodynamics is connected with many other famous names like James Maxwell, Ludwig Boltzmann, Rudolf Clausius and Willard Gibbs.

During the further scientific development, the theory of classical statistical mechanics emerged, which establishes the relation between macroscopic thermodynamic quantities and microscopic degrees of freedom of the system. Hereby, one makes the assumption that the microscopic dynamics is governed by classical equations of motion. Today, one important subject of research is the dynamical foundation of classical statistical mechanics. This includes, in particular, the relaxation dynamics of non-equilibrium states to thermal equilibrium. This relaxation process is called thermalisation. In order to give an intuitive example, imagine that we intensively shake a system which previously was at thermal equilibrium corresponding to some temperature. Immediately after the shaking, the system is typically out of equilibrium but we expect the system to reach thermal equilibrium later again; possibly with another temperature. Important questions in this respect are: Under which conditions does a system thermalise and what are the relevant time scales? In addition, the role of chaos for thermalisation is not fully clarified.

After the introduction of quantum mechanics at the beginning of the 20th century, attempts to lay down the foundations of quantum statistical mechanics proved to be problematic, as already noticed by Erwin Schrödinger himself [77]. In particular, the superposition principle of quantum mechanics constitutes an apparent obstacle for the thermalisation of non-equilibrium quantum states as will be explained in the following. In this respect, the foundations of the statistical physics for classical systems is in a somewhat better shape than for quantum systems.

A classical isolated system always has a fixed value of the total energy. In contrast, a quantum isolated system can be in a superposition of energy eigenstates. *A priori*, the energy eigenstates as well as superpositions thereof are on the same footing which means that there are no general rules preferring or prohibiting any of the above possibilities. However, a macroscopic quantum system thermalises only if its state is a superposition of energy eigenstates from a *small energy window* [27, 29, 68, 84, 16, 85, 71]. In the opposite case, when the isolated quantum system is described by a superposition of energy eigenstates with significantly different energies, the system does not thermalise, e.g. [19]. At the same time, the Gibbs distribution, which describes a system in thermal equilibrium, works extremely well for predicting experimental outcomes under everyday conditions. The following question arises: Why don't macroscopic quantum systems typically exhibit a broad occupation of energy eigenstates and, hence, non-thermal behaviour?

In the present thesis, we make a proposal for the solution of the above still unsolved problem. This proposal rests upon the concept of stability of quantum statistical ensembles. We argue that quantum statistical ensembles describing stationary states of macroscopic systems must be stable with respect to a small number of any local measurements. We show that broad energy distributions are unstable: Even if initially realised, they would become significantly narrower within an extremely small time interval. Hence, broad energy

distributions can be disregarded for all practical calculations. This justifies the narrow energy window assumption for the energy distribution of macroscopic quantum systems. Therefore, macroscopic quantum systems typically thermalise.

This chapter is organised as follows. After a short overview of the foundations of equilibrium statistical physics for classical and quantum systems, we first precisely formulate the problem addressed in the present thesis. Later, we give an overview of the topics which are related to our proposal and present the novel concept of stability of quantum statistical ensembles. Finally, we provide a preview of our results together with an outline of the thesis.

1.1 Current knowledge and an unsolved problem

1.1.1 Foundations of classical statistical physics of equilibria

The microcanonical ensemble

Let us consider a completely isolated classical system with the Hamilton function $\mathcal{H}(\mathbf{p}, \mathbf{q})$, where $\mathbf{p}$ and $\mathbf{q}$ are generalised momenta and coordinates of the constituents of the system. The momenta $\mathbf{p}$ and coordinates $\mathbf{q}$ span the n-dimensional phase-space. The total energy E of an isolated classical system always has a fixed value $E = E_0$. Therefore, the phase-space dynamics of this system, which is governed by the Hamilton's equations $\frac{d\mathbf{p}}{dt} = -\frac{\partial \mathcal{H}(\mathbf{p}, \mathbf{q})}{\partial \mathbf{q}}$ and $\frac{d\mathbf{q}}{dt} = +\frac{\partial \mathcal{H}(\mathbf{p}, \mathbf{q})}{\partial \mathbf{p}}$, is confined to the $(n-1)$-dimensional hypersurface $\mathcal{H}(\mathbf{p}, \mathbf{q}) = E_0$, which is called the energy shell.

The system's dynamics on the energy shell exhibits ergodic behaviour for typical interacting many-body systems. This implies that a typical phase space trajectory explores the complete energy shell. Therefore, we make the usual assumption that the probability to find the system in a fixed region of the energy shell is proportional to the $(n-1)$-dimensional volume of that region. This assumption is known as the ergodic hypothesis.

Given the above assumption, the phase-space distribution is given by

$$\rho_{\mathrm{mc}}(\mathbf{p}, \mathbf{q}) = \frac{1}{\Omega[E_0]} \delta[\mathcal{H}(\mathbf{p}, \mathbf{q}) - E_0], \tag{1.1}$$

where $\Omega[E_0] = \int \delta[\mathcal{H}(\mathbf{p}, \mathbf{q}) - E_0] d\mathbf{p} d\mathbf{q}$ is the phase-space volume of the energy shell. The corresponding probability distribution of the total energy is

$$g_{\mathrm{mc}}(E) = \delta[E - E_0]. \tag{1.2}$$

The distribution $g_{\mathrm{mc}}(E)$ is called the *microcanonical energy distribution* and the statistical ensemble described by $g_{\mathrm{mc}}(E)$ is called the *microcanonical ensemble.*

Derivation of the Gibbs distribution

Now, we divide the total system into a small subsystem and the rest, which we call heat bath. This is illustrated in Fig. 1.2. We assume that the subsystem and the heat bath exchange energy but do not exchange particles. The following question arises: What is the

energy distribution of the small subsystem provided that the total system is described by the microcanonical ensemble? For the subsequent analysis, we choose the following notations: $\mathbf{p}_1$ and $\mathbf{q}_1$ refer to particles of the subsystem, while $\mathbf{p}_2$ and $\mathbf{q}_2$ refer to particles of the heat bath.

The energy of the total system can be written as a sum of three terms

$$\mathcal{H}(\mathbf{p}, \mathbf{q}) = \mathcal{H}_1(\mathbf{p}_1, \mathbf{q}_1) + \mathcal{H}_2(\mathbf{p}_2, \mathbf{q}_2) + W(\mathbf{p}_1, \mathbf{q}_1, \mathbf{p}_2, \mathbf{q}_2), \tag{1.3}$$

where $\mathcal{H}_1(\mathbf{p}_1, \mathbf{q}_1)$ and $\mathcal{H}_2(\mathbf{p}_2, \mathbf{q}_2)$ are the Hamilton functions for the subsystem and the heat bath, respectively, and $W(\mathbf{p}_1, \mathbf{q}_1, \mathbf{p}_2, \mathbf{q}_2)$ is the interaction term. Usually, the interaction term can be neglected provided a short-range interaction between the individual particles. The reason is that, for a short-range interaction, $W(\mathbf{p}_1, \mathbf{q}_1, \mathbf{p}_2, \mathbf{q}_2)$ grows normally with the surface of the subsystem, while $\mathcal{H}_1(\mathbf{p}_1, \mathbf{q}_1)$ grows with the volume of the subsystem. If we assume that the subsystem is not too small such that $W(\mathbf{p}_1, \mathbf{q}_1, \mathbf{p}_2, \mathbf{q}_2)$ can be neglected, this leads to

$$\mathcal{H}(\mathbf{p}, \mathbf{q}) \approx \mathcal{H}_1(\mathbf{p}_1, \mathbf{q}_1) + \mathcal{H}_2(\mathbf{p}_2, \mathbf{q}_2). \tag{1.4}$$

Now, we calculate the phase-space distribution for the subsystem $\rho_{\text{sub}}(\mathbf{p}_1, \mathbf{q}_1)$. It is given by the integral of $\rho_{\text{mc}}(\mathbf{p}, \mathbf{q})$ over the degrees of freedom of the heat bath

$$
\begin{aligned}
\rho_{\text{sub}}(\mathbf{p}_1, \mathbf{q}_1) &= \int \rho_{\text{mc}}(\mathbf{p}, \mathbf{q}) \, d\mathbf{p}_2 d\mathbf{q}_2 && (1.5)\\
&\approx \frac{1}{\Omega[E_0]} \int \delta[\mathcal{H}_1(\mathbf{p}_1, \mathbf{q}_1) - \mathcal{H}_2(\mathbf{p}_2, \mathbf{q}_2) - E_0] \, d\mathbf{p}_2 d\mathbf{q}_2 && (1.6)\\
&= \frac{\Omega_2[E_0 - \mathcal{H}_1(\mathbf{p}_1, \mathbf{q}_1)]}{\Omega[E_0]}, && (1.7)
\end{aligned}
$$

where $\Omega_2[E_0 - \mathcal{H}_1(\mathbf{p}_1, \mathbf{q}_1)] \equiv \int \delta[\mathcal{H}_1(\mathbf{p}_1, \mathbf{q}_1) - \mathcal{H}_2(\mathbf{p}_2, \mathbf{q}_2) - E_0] \, d\mathbf{p}_2 d\mathbf{q}_2$ is a multi-dimensional integral. It is worth noticing that the dependence of $\rho_{\text{sub}}(\mathbf{p}_1, \mathbf{q}_1)$ on $\mathbf{p}_1$ and $\mathbf{q}_1$ enters the right-hand side in the above expression only through $\mathcal{H}_1(\mathbf{p}_1, \mathbf{q}_1)$. Therefore, $\rho_{\text{sub}}(\mathbf{p}_1, \mathbf{q}_1)$ is the same for all configurations of $\mathbf{p}_1$ and $\mathbf{q}_1$ satisfying $\mathcal{H}_1(\mathbf{p}_1, \mathbf{q}_1) = E$ for some E.

According to the definition, $\Omega_2[E_0 - \mathcal{H}_1(\mathbf{p}_1, \mathbf{q}_1)]$ is a multi-dimensional integral, where the number of integrals is twice the number of particles in the subsystem. If we now vary $\mathcal{H}_1(\mathbf{p}_1, \mathbf{q}_1)$, each of the one-dimensional integrals contributing to $\Omega_2[E_0 - \mathcal{H}_1(\mathbf{p}_1, \mathbf{q}_1)]$ becomes slightly modified. Therefore, the overall dependence of $\rho_{\text{sub}}(\mathbf{p}_1, \mathbf{q}_1)$ on $\mathcal{H}_1(\mathbf{p}_1, \mathbf{q}_1)$
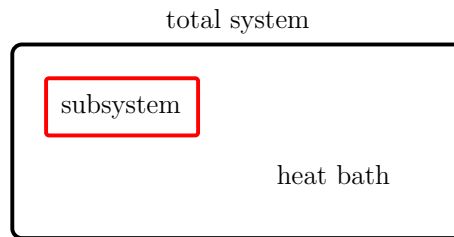
Figure 1.2: The total system is divided into a small subsystem and the heat bath.

can, to a good accuracy, be approximated by an exponential function

$$\rho_{\text{sub}}(\mathbf{p}_1, \mathbf{q}_1) \approx \frac{1}{Z} \, e^{-\frac{\mathcal{H}_1(\mathbf{p}_1, \mathbf{q}_1)}{T}}, \tag{1.8}$$

where $Z = \int \rho_{\text{sub}}(\mathbf{p}_1, \mathbf{q}_1) \, d\mathbf{p}_1 d\mathbf{q}_1$ is the normalisation factor, $k_B = 1$ and temperature T is defined as

$$\frac{1}{T} \equiv \frac{d}{dE} \ln[\Omega_2(E)]. \tag{1.9}$$

The derivative on the right-hand side of Eq. (1.9) is evaluated at the average energy $E_{\text{av}} \equiv \int \mathcal{H}_1(\mathbf{p}_1, \mathbf{q}_1) \rho_{\text{sub}}(\mathbf{p}_1, \mathbf{q}_1) \, d\mathbf{p}_1 d\mathbf{q}_1$. The phase-space distribution in Eq. (1.8) is the *Gibbs distribution*.

Since $\rho_{\text{sub}}(\mathbf{p}_1, \mathbf{q}_1)$ is constant on each energy shell $\mathcal{H}_1(\mathbf{p}_1, \mathbf{q}_1) = E$, the corresponding energy distribution reads

$$g_{\text{can}}(E) = \frac{1}{Z_{\text{can}}} \, e^{-\beta E} \nu(E), \tag{1.10}$$

where $\beta \equiv \frac{1}{T}$ is the inverse temperature, $\nu(E) \equiv \frac{d}{dE} \int_{\mathcal{H}_1(\mathbf{p}_1, \mathbf{q}_1) \leq E} d\mathbf{p}_1 d\mathbf{q}_1$ and $Z_{\text{can}} = \int_{-\infty}^{\infty} e^{-\beta E} \nu(E) dE$ is the canonical partition function. The function $\nu(E)$ normally grows nearly exponentially with energy E and, therefore, $g_{\text{can}}(E)$ typically has a Gaussian shape as illustrated in Fig. 1.3. In the following, we refer to the probability distribution of the energy $g_{\text{can}}(E)$ also as the Gibbs distribution.

The statistical ensemble corresponding to $g_{\text{can}}(E)$ is called the *canonical ensemble*. More precisely, the canonical ensemble is defined as the set of all possible states whose average behaviour is describable by the Gibbs distribution.

Width of the energy distribution for the canonical ensemble

Now, we obtain the width of $g_{\text{can}}(E)$. Let us rewrite Eq. (1.10) as

$$g_{\text{can}}(E) = \frac{1}{Z_{\text{can}}} e^{-\beta E + S(E)}, \tag{1.11}$$
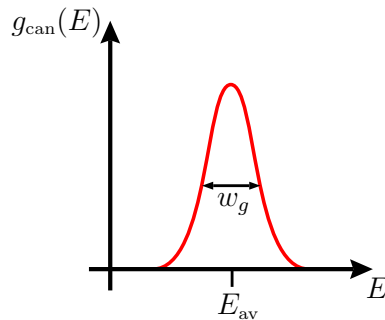
Figure 1.3: A sketch of $g_{\text{can}}(E)$ which is typically of Gaussian shape. We denote the average energy by E_{av} and the width of the energy distribution by w_g. Formal definitions of E_{av} and w_g are given in the next section.

where $S(E) \equiv \ln[\nu(E)]$ is the entropy. As mentioned above, the distribution $g_{\mathrm{can}}(E)$ can be approximated by the Gaussian function

$$g_{\mathrm{can}}(E) \cong \exp\left(-\frac{(E - E_{\mathrm{av}})^2}{2w_g^2}\right). \tag{1.12}$$

In order to obtain the width w_g, we expand the exponent in Eq. (1.11) at E_{av} up to the second order, which leads to

$$w_g = \sqrt{-\frac{1}{\frac{d^2 S(E_{\mathrm{av}})}{dE^2}}} = T(E_{\mathrm{av}})\sqrt{\left.\frac{dE(T)}{dT}\right|_{T(E_{\mathrm{av}})}} = T(E_{\mathrm{av}})\sqrt{C_V(T(E_{\mathrm{av}}))}, \tag{1.13}$$

where $C_V(T) \equiv \frac{dE(T)}{dT}$ is the total specific heat of the system. Typically, $C_V \sim N_s$ and $E_{\mathrm{av}} - E_{\mathrm{min}} \sim N_s$ for a fixed temperature, where E_{min} is the minimal energy of the system. Therefore, $\frac{w_g}{E_{\mathrm{av}} - E_{\mathrm{min}}} \sim \frac{1}{\sqrt{N_s}}$, which means that $g_{\mathrm{can}}(E)$ is sharply peaked for macroscopic systems.

1.1.2 Foundations of quantum statistical physics

The microcanonical ensemble

Let us now turn to quantum statistical physics. The microcanonical energy distribution for quantum systems is defined in analogy to the definition for classical systems in Eq. (1.2). The probability $p_{\mathrm{mc}}(E)$ for occupying an individual energy eigenstate with energy E is

$$p_{\mathrm{mc}}(E) \equiv \begin{cases} const. & E \in [E_0 - \Delta, E_0 + \Delta] \\ 0 & \text{else}, \end{cases} \tag{1.14}$$

where $2\Delta \ll E$ is the width of the narrow energy window.

The statistical ensemble described by $p_{\mathrm{mc}}(E)$ is called the conventional *microcanonical ensemble* for quantum systems. The corresponding probability distribution of the total energy is

$$g_{\mathrm{mc}}(E) = p_{\mathrm{mc}}(E)\nu(E), \tag{1.15}$$

where $\nu(E)$ is the density of states defined as

$$\nu(E) \equiv \sum_i \delta[E - E_i]. \tag{1.16}$$

The sum in the above expression extends over all energy eigenvalues E_i. For macroscopic quantum systems, the energy eigenvalues E_i are exponentially dense such that we consider $\nu(E)$ as a continuous function in the following. Therefore, $g_{\mathrm{mc}}(E)$ can also be considered as a continuous function.

For later purposes, we also define the average energy of $g(E)$

$$E_{\mathrm{av}} \equiv \int E\, g(E)\, dE, \tag{1.17}$$

and the width of $g(E)$

$$w_g \equiv \sqrt{\int (E - E_{\mathrm{av}})^2 g(E) \, dE}. \tag{1.18}$$

The Gibbs distribution for quantum systems

The probability distribution of energy corresponding to the *canonical ensemble* for quantum systems is defined in analogy to the definition for classical systems in Eq. (1.10) as

$$g_{\mathrm{can}}(E) = \frac{1}{Z_{\mathrm{can}}} \, e^{-\beta E} \nu(E), \tag{1.19}$$

where the canonical partition function is now given by $Z_{\mathrm{can}} = \mathrm{Tr}[e^{-\beta \mathcal{H}}]$ and $\mathcal{H}$ is the Hamiltonian of the system. In analogy to the classical case, the width w_g of $g_{\mathrm{can}}(E)$ is given in Eq. (1.13). Therefore, the Gibbs distribution for quantum systems $g_{\mathrm{can}}(E)$ in Eq. (1.19) is also sharply peaked and it is typically of Gaussian shape.

Similar to the above considerations for classical systems, the Gibbs distribution for quantum systems can be derived for subsystems of a large isolated quantum system provided that the large system is described by a microcanonical ensemble, see for example [29]. For this derivation, the large isolated quantum system is described by an incoherent mixture of energy eigenstates with a non-zero occupation probability according to the microcanonical condition.

Quantum thermalisation

So far, we described the conventional quantum statistical physics of equilibrium. The Gibbs distribution, for example, describes quantum systems in thermal equilibrium at some temperature T. Suppose now that we bring a macroscopic system out of equilibrium, for example, by perturbing it or quenching a system's parameter [94]. The usual expectation is that the system is going to relax to thermal equilibrium within a short time interval. The following questions now arise: What are the necessary and sufficient conditions for the wave function in order the quantum system to relax? The answers to these questions are the subject of ongoing research. In the following, we describe recent developments in this research field.

Given an isolated quantum system $\mathcal{A}$, how do we define thermal equilibrium in such a case? It is noteworthy that this setting is different from the one described above, where the system in thermal equilibrium was implied to be a subsystem of a larger system. An isolated quantum system $\mathcal{A}$ described by the density matrix $\rho^{\mathcal{A}}$ is said to be in thermal equilibrium if the reduced density matrix $\rho^{\mathcal{S}}$ of any small subsystem $\mathcal{S}$ is consistent with the Gibbs density matrix $\rho^{\mathcal{A}}_{\mathrm{can}}$ for the large system $\mathcal{A}$

$$\rho^{\mathcal{A}}_{\mathrm{can}} = \frac{1}{Z_{\mathrm{can}}} e^{-\beta \mathcal{H}}, \tag{1.20}$$

where $Z_{\mathrm{can}} = \mathrm{Tr}\left[e^{-\beta \mathcal{H}}\right]$ is the canonical partition function and $\mathcal{H}$ is the Hamiltonian of the system $\mathcal{A}$. In the above definition, "consistent" means that, for *any* local operator $\mathcal{O}$ acting

on the subsystem $\mathcal{S}$, the following relation is satisfied

$$\langle \mathcal{O} \rangle = \mathrm{Tr}_{\mathcal{S}} \left[\mathcal{O} \rho^{\mathcal{S}} \right] \approx \mathrm{Tr} \left[\mathcal{O} \rho_{\mathrm{can}}^{\mathcal{A}} \right], \tag{1.21}$$

where $\mathrm{Tr}_{\mathcal{S}}$ denotes the partial trace over the degrees of freedom of the system $\mathcal{S}$. It is worth stressing that the relation (1.21) must hold for any local operator $\mathcal{O}$. This definition implies that the system $\mathcal{A}$ acts like its own heat bath (compare the Figures 1.4 and 1.2).

In general, there are two aspects about quantum thermalisation: (i) the initial quantum state of the system $\mathcal{A}$ and (ii) the internal dynamics of the system. While the initial quantum state is normally given from outside the system, the dynamics are provided by the internal Hamiltonian of the system. In this thesis, we focus on the first aspect which deals with the initial state. However, in order to make the introduction complete, we now present an overview of the current knowledge on the dynamic aspect of thermalisation. Two important results have been obtained in this direction. In the following, we discuss them separately.

The first important result is the property of *canonical typicality*. Canonical typicality means that, for the overwhelming majority of superpositions of energy eigenstates with energies from a narrow energy window, a system thermalises in the thermodynamic limit, where the size of the system goes to infinity while the energy per particle remains fixed. More explicitly, for any wave function of the total system $\mathcal{A}$

$$|\psi\rangle = \sum c_n |E_n\rangle, \tag{1.22}$$

where the energy eigenstates $|E_n\rangle$ are taken from a small energy window $E_n \in [E-\Delta, E+\Delta]$, the reduced density matrix of any small subsystem $\mathcal{S}$ satisfies Eq. (1.21). Above, we require that Δ satisfies $\frac{\Delta}{E-E_{\min}} \ll 1$, where $E_{\min}$ is the minimal energy of the system. The actual dynamics, which is responsible for the thermalisation, is given by the dephasing of the individual energy eigenstates in Eq. (1.22). This means that the quantum amplitudes c_n acquire quasi-random phases such that the interference terms between the different energy eigenstates can be neglected. It is worth stressing that canonical typicality implies that the system thermalises for pure quantum states. In particular, the average over different pure states is not necessary.

Important contributions to canonical typicality were made by J. Gemmer, M. Michel, G. Mahler [27, 26], by S. Goldstein, J. L. Leibowitz, R. Tumulka, N. Zanghi [29], and by S. Popescu, A. J. Short, A. Winter [68].
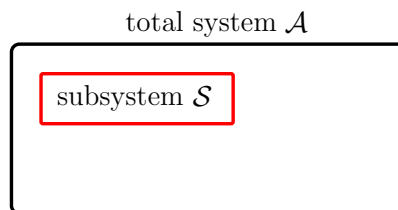

Figure 1.4: Illustration of the total system $\mathcal{A}$ and the small subsystem $\mathcal{S}$.

The second important result in the context of quantum thermalisation is known as the *eigenstate thermalisation hypothesis*[3]. According to this hypothesis, the system $\mathcal{A}$ is in thermal equilibrium if it is described by an individual energy eigenstate

$$|\psi\rangle = |E_n\rangle. \tag{1.23}$$

This is an extreme example for the conventional microcanonical ensemble. In contrast to the superposition considered for the quantum typicality, here, the thermalisation occurs on the level of individual energy eigenstates.

Empirically, the eigenstate thermalisation hypothesis applies to quantum chaotic systems. A quantum system is called chaotic if the corresponding classical system exhibits chaotic behaviour. Further, quantum chaotic systems are known to exhibit the Wigner-Dyson statistics for the spacing between quantum energy levels [66] which is also known as energy level repulsion. However, there is no fully consistent approach to quantum chaos until now.

The same role that ergodicity played for classical equilibration is now taken over by the fact that each energy eigenstate $|E_n\rangle$ is given by a large superposition of different local configurations for the subsystems. In this way, each energy eigenstate incorporates averaging over the classical energy shell, cf. Sec. 1.1.1.

In the context of the eigenstate thermalisation hypothesis, important contributions were made by A. J. Shnirelman [84], J. M. Deutsch [16], M. Srednicki [85], and M. Rigol, V. Dunjko and M. Olshanii [71].

Questions about the thermalisation of quantum systems recently became the subject of particular interest due to experimental advances in isolating quantum systems [91, 75, 40]. In particular, the increasing ability to coherently control systems parameters (as for example the interaction strength, confinement potential or particle number) allows for the experimental investigation of the thermalisation dynamics, see for example [15]. A popular approach in this context is the investigation of the relaxation after a quench [94]. A quench is a sudden change of some parameter of the system such that the system being in equilibrium before the quench is brought out of equilibrium because of the quench.

1.1.3 Unsolved problem: width of the energy distribution

A typical isolated macroscopic quantum system is generally expected to thermalise under the action of its internal dynamics for the overwhelming majority of initial non-equilibrium states appearing in nature or created in a laboratory [13, 47, 28, 27, 29, 68, 70, 4, 67]. As mentioned earlier, thermalisation implies that the density matrix of any small subsystem within the large system approaches a form consistent with the canonical Gibbs density matrix (canonical ensemble) for the large system.

A necessary condition for an isolated many-particle quantum system to thermalise is a sufficiently narrow initial probability distribution of its total energy, as is, for example, the case for the conventional microcanonical ensemble defined in Eq. (1.14). However, since

---

[3]Although this hypothesis is generally expected to be true, there are no analytical results to the best of our knowledge. So far, this hypothesis has been confirmed only by numerical simulations.

quantum systems can be in a superposition of different energy eigenstates, the initial states characterised by a narrow distribution of total energy constitute a rather special case. In fact, narrow energy distribution are not necessarily the most probable ones, as we will see in Sec. 1.1.4. In addition, a total-energy distribution remains constant with time. If a quantum state of an isolated system does not satisfy the condition for thermalisation related to a narrow energy distribution, it will never satisfy that condition and, therefore, it will never thermalise. It is this possibility of superpositions which poses an additional problem for the foundations of quantum statistical physics as compared to the foundations of classical statistical physics.

Let us formulate the above considerations more precisely. Suppose that the initial wave function of the total system is

$$|\psi(0)\rangle = \sum_n c_n(0)|E_n\rangle, \tag{1.24}$$

where $|E_n\rangle$ is the total-energy eigenstate with energy E_n. The above sum extends over all energy eigenstates. The occupation probability of $|E_n\rangle$ is $|c_n(0)|^2$. This occupation probability is a constant of motion, i.e., $|c_n(t)|^2 = |c_n(0)|^2$. To show this, we rewrite $|\psi(0)\rangle$ at a later time t

$$|\psi(t)\rangle = \sum_n c_n(t)|E_n\rangle, \tag{1.25}$$

where $c_n(t) = c_n(0) \, e^{-iHt}$. This leads to $|c_n(t)|^2 = |c_n(0)|^2$.

As explained above, isolated quantum systems with a broad initial distribution of the total energy do not thermalise. An example here is a quantum superposition of states with two different temperatures [19]

$$|\phi_{\beta_1\beta_2}\rangle \cong \sqrt{\frac{1}{Z_1}} \sum_i e^{-\frac{1}{2}\beta_1 E_i}|E_i\rangle + \sqrt{\frac{1}{Z_2}} \sum_i e^{-\frac{1}{2}\beta_2 E_i}|E_i\rangle, \tag{1.26}$$

where β_1 and β_2 are inverse temperatures ($\beta_1 \neq \beta_2$), and Z_1 and Z_2 are the corresponding canonical partition functions. Given such a superposition, the corresponding probability distribution of the total energy $g(E)$ entails two peaks as illustrated in Fig. 1.5. What is important here is that a superposition of states with two or more different temperatures as in Eq. (1.26) cannot be described by a state corresponding to a single temperature. In general, even more complex situations may occur which can lead, for example, to the superstatistics [7], the non-extensive statistics [90] or the generalised Gibbs ensembles [38, 39, 72].

Given that the Gibbs distribution works extremely well for predicting experimental outcomes under everyday conditions, the description of isolated quantum systems by the conventional microcanonical ensemble appears empirically justified. However, a thorough theoretical justification for choosing the conventional microcanonical ensemble remains elusive. In this thesis, we propose a justification for choosing narrow energy distributions.

Why don't the initial non-equilibrium quantum states of macroscopic systems normally exhibit the broad participation of energy eigenstates and hence non-Gibbs statistics for

Figure 1.5: A sketch of $g(E)$ corresponding to the coherent superposition of two states corresponding to different temperatures in Eq. (1.26).

small subsystems?

A priori, it is not clear why the definition of the microcanonical ensemble for classical systems is to be transferred to the quantum domain as in Eq. (1.14). An alternative definition for the microcanonical ensemble for quantum system is known as "quantum microcanonical" (QMC) ensemble [93, 12, 1, 21, 19, 61]. The definition of the QMC ensemble fixes the average energy E_{av} but allows any superpositions of the energy eigenstates. As explained in the next subsection, if a macroscopic isolated quantum system is described by the QMC ensemble, it was shown [19, 22, 23, 20] that non-Gibbs equilibrium emerges for small subsystems. Therefore, narrow energy distributions are not necessarily the most probable ones.

1.1.4 Quantum micro-canonical (QMC) ensemble

In Sec. 1.1.2, we introduced the conventional microcanonical ensemble for quantum systems. In this section, we describe an alternative definition of the microcanonical ensemble which is known as the QMC ensemble. By doing this, we also show that the probability distributions of the total energy $g(E)$ which are as narrow as those corresponding to the conventional microcanonical ensemble $g_{mc}(E)$ in Eq. (1.15) are not necessarily the most probable ones.

The QMC ensemble is defined as follows: We fix the average energy E_{av} without further restricting the participating eigenstates. This ensemble is fully characterised by the following three constraints

$$\sum_{i=1}^{N} p_i = 1, \tag{1.27}$$

$$p_i \geq 0, \tag{1.28}$$

$$\sum_{i=1}^{N} E_i p_i = E_{av}, \tag{1.29}$$

where $p_i = |c_i|^2$ is the probability for occupying the eigenstate $|E_i\rangle$ and N is the dimension of the Hilbert space. The first two constraints are the usual constraints of the quantum-mechanical description, whereas the last relation fixes the average energy. It is noteworthy that the sums in the above expressions are not restricted to any energy interval as for the definition of the conventional microcanonical ensemble.

Given that a macroscopic system with a non-degenerate ground state is described by the

QMC ensemble, the probability for occupying individual energy eigenstates is given by [19]

$$\langle p_1 \rangle \;\; \approx \;\; \frac{E_{\mathrm{av}}}{E_{\mathrm{min}}} \tag{1.30}$$

$$\langle p_k \rangle \;\; = \;\; \frac{1}{N\left(1 + \frac{E_k - E_{\mathrm{av}}}{E_{\mathrm{av}} - E_{\mathrm{min}}}\right)}, \tag{1.31}$$

where $\langle p_1 \rangle$ is the average occupation probability for the ground state, $\langle p_k \rangle$ with $k \geq 2$ corresponds to higher energy eigenstates, and N is again the dimension of the Hilbert space. The occupation probability $\langle p_k \rangle$ as a function of the energy E_k decays slowly with the energy which is in contrast to the definition of the conventional microcanonical ensemble in Eq. (1.14). The energy distribution in Eqs. (1.30) and (1.31) is a broad energy distribution. The energy distribution $g(E)$ thus has a form of two distinct peaks, cf. Fig. 1.5. This implies that narrow energy distributions are not necessarily the most probable ones.

Given that the total system is described by the QMC ensemble, one obtains non-Gibbs statistics for small subsystems [19]. The diagonal elements of the subsystem's reduced density matrix written in the energy basis are given by [19]

$$\langle \rho_1 \rangle \;\; = \;\; \frac{E_{\mathrm{av}}}{E_{\mathrm{min}}} + \frac{1}{N_1}\left(1 - \frac{E_{\mathrm{av}}}{E_{\mathrm{min}}}\right) \tag{1.32}$$

$$\langle \rho_\alpha \rangle \;\; = \;\; \frac{1}{N_1}\left(1 - \frac{E_{\mathrm{av}}}{E_{\mathrm{min}}}\right), \tag{1.33}$$

where $\langle \rho_1 \rangle$ corresponds to the lowest subsystem energy state, $\langle \rho_\alpha \rangle$ with $\alpha \geq 2$ corresponds to higher energy states and N_1 is the number of states of the subsystem. In fact, the energy distribution for subsystems is a sum of two Gibbs distributions with the temperatures $T = 0$ and $T = \infty$. In the case $T = 0$, only the lowest energy state is occupied, and, in the case $T = \infty$, all states have equal probability of occupation.

1.2 Concept of stability of quantum statistical ensembles

In this thesis, we address the unsolved problem of why the description of isolated macroscopic quantum systems by narrow total-energy distributions is justified. Hereby, macroscopic means that the total number of particles or microscopic subsystems is $N_s \sim 10^{23}$.

Macroscopic systems cannot be completely isolated under any realistic circumstances and, therefore, inevitably interact with the environment. This can be, for example, the interaction with an accidentally passing photon. Such an interaction with the environment corresponds to a decoherence process as will be explained in the next section. The decoherence theory, which describes the effects of the interactions with the environment, is concerned with predicting the average effect. In contrast, the individual realisations occurring in nature and laboratory cannot be accounted for by this description of the average effects. Since we want to consider concrete realisations, we introduce ideal local measurements described by projective operators. Hereby, local means localised in the physical three-dimensional space.

Due to the random nature of the interactions with the environment, we assume the measurements to occur randomly in space and time. Moreover, the Hilbert space basis, in which the measurements occur, is also random for each individual measurement.

Although the measurements are local, the outcomes of these measurements can be correlated with the total energy of the total system. At first sight, this seems to contradict the fact that the energy eigenstates of generic many-body systems are typically given by large superpositions of different local configurations for the subsystems. Therefore, the total energy of the system cannot be fully discriminated by measuring local observables. However, local measurements can induce modifications of the occupation of the total-energy eigenstates because one local configuration can be more likely for one energy than for another.

Let us consider a simple example of an ideal gas in one dimension consisting of identical particles. For a moment, we assume that the system is described by the canonical ensemble with the inverse temperature β. In this case, the probability distribution of the velocity for each particle is given by the so-called Maxwell distribution

$$g(v) \cong e^{-\beta \frac{mv^2}{2}}, \tag{1.34}$$

where v is the velocity and m is the mass of the particle. This distribution is illustrated in Fig. 1.6 for different values of β.

Now, let us assume that the system is in a superposition state of two inverse temperatures β_1 and β_2 with equal probability, cf. Eq. (1.26). Depending on the temperature, $g(v)$ has a different shape. For the sake of the argument, let us assume that $\beta_1 = \beta_{\text{blue}}$ and $\beta_2 = \beta_{\text{green}}$ in Fig. 1.6. Now, suppose that the velocity of a single particle is accidentally measured and that the measurement outcome is $v_{\text{m}} = 10$. This outcome favours the case with β_{green} because the probability of this outcome for β_{blue} is practically zero. The post-measurement probability of the Gibbs distribution with β_{green} is larger than that for β_{blue}. Therefore,
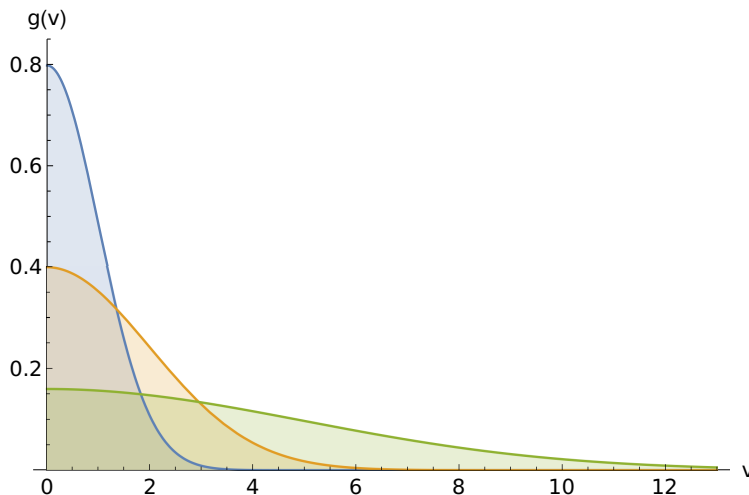

Figure 1.6: Probability distribution $g(v)$ of the velocity for the one-dimensional ideal gas in Eq. (1.34). The distribution $g(v)$ is shown for different values of the temperature. The relations for the inverse temperatures are $\beta_{\text{blue}} > \beta_{\text{orange}} > \beta_{\text{green}}$, where the index denotes the colour of the corresponding curve.
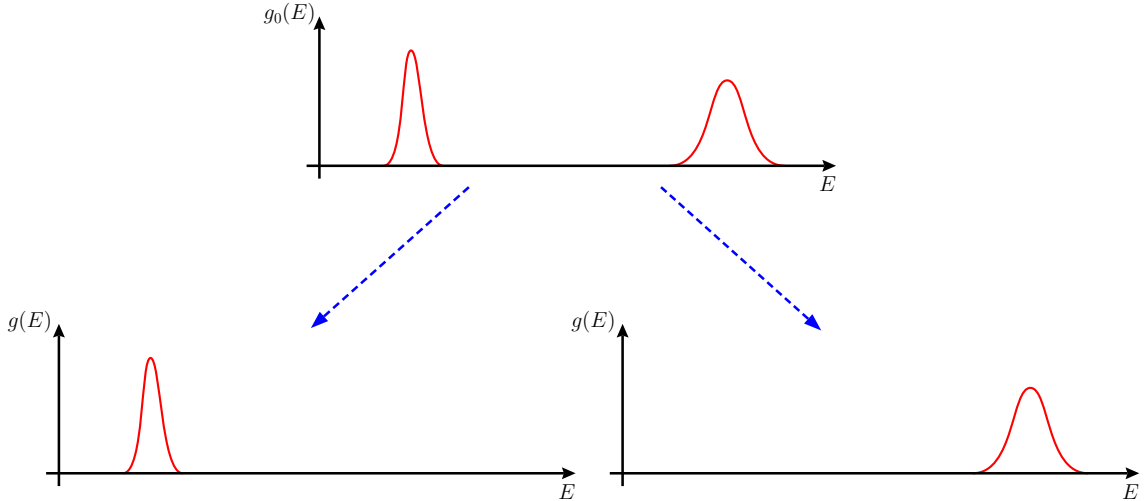
Figure 1.7: Sketch of the narrowing effect of local measurements with respect to an initial broad $g(E)$ consisting of two peaks. Either left peak or the right peak becomes completely suppressed after multiple measurements. Since the width of the individual peaks is much smaller than the distance between the peaks, this effectively corresponds to a narrowing of $g(E)$.

this measurement would modify the probabilities for different β.

Let us also consider another measurement outcome, for example $v_m = 1$. In such a case, the first measurement would not lead to a significant change of the probabilities since, in both cases $\beta_1 = \beta_{\text{blue}}$ and $\beta_2 = \beta_{\text{green}}$, the velocity $v_m = 1$ has non-zero probability. However, if the subsequent measurements also yield $v_m \approx 1$, this would indicate that the system is in the state corresponding to β_{blue}.

From an information-theoretic viewpoint, the outcomes of local measurements constitute a source of partial information about the total energy of the system. Each local measurement whose outcome is correlated with the total energy thus leads to a better estimate of the total energy and, in turn, to a narrower probability distribution of the total energy [5]. Coming back to the example of two temperatures in Sec. 1.1.3, this narrowing of the probability distribution of the total energy corresponds to the suppression of one peak as indicated in Fig. 1.7.

We have seen that local measurements can indeed lead to a significant modification of $g(E)$. This result naturally leads to the notion of *stability of quantum statistical ensembles with respect to local measurements*. For macroscopic systems, the local measurements are expected to occur very frequently. Therefore, only stable ensembles are realisable in nature and laboratory. The unstable ensembles can be disregarded for their lifetime being usually unmeasurably short as we will see below.

1.2.1 Relation to quantum decoherence and quantum measurements

A part of the endeavour of explaining the quantum-to-classical transition is the quantum decoherence theory [41, 42, 99, 37, 64]. In essence, quantum decoherence is the suppression of observable coherences in a given system of interest due to the interaction with the environmental degrees of freedom. If we consider the density matrix of the system in a suit-

able basis, its off-diagonal elements, which quantify the coherence in the system, become suppressed. Hence, decoherence leads to a nearly diagonal reduced density matrix of the system, where nearly diagonal means that only matrix elements close to the diagonal can be non zero. Effectively, such a density matrix resembles a classical mixture of quantum systems being in different states. Therefore, measurements of observables of the system normally do not exhibit quantum interference.

Let us now consider a simple toy model consisting of a spatially delocalised dust grain described by the state

$$
|\psi\rangle = \frac{1}{\sqrt{2}}\big[|G_{x_1}\rangle + |G_{x_2}\rangle\big], \tag{1.35}
$$

where $|G_{x_1}\rangle$ is a state corresponding to a spatially localised dust grain around a space point x_1, and likewise $|G_{x_2}\rangle$. For simplicity, we assume a Gaussian shape of these states, cf. Fig. 1.8. Further, we assume that $|x_1 - x_2|$ is sufficiently large such that the overlap between the states is negligible, i.e., $\langle G_{x_1}|G_{x_2}\rangle \approx 0$.

Now, let us imagine that a photon passes accidentally the region at x_1 as illustrated in Fig. 1.8. For the photon, there are two possibilities: either the photon passes this region unaffected or it becomes scattered. Each case corresponds to the position measurement of the dust grain: a scattered photon indicates that the dust grain is at x_1 and, otherwise, the dust grain is at x_2[4].

In order to illustrate the decoherence effect, we denote the scattered state of the photon as $|s\rangle$ and, in the case it passes unaffected, the state is $|p\rangle$. The interaction with the photon can thus be described as

$$
\frac{1}{\sqrt{2}}\big[|G_{x_1}\rangle + |G_{x_2}\rangle\big]|\text{before}\rangle \;\rightarrow\; \frac{1}{\sqrt{2}}\big[|G_{x_1}\rangle|s\rangle + |G_{x_2}\rangle|p\rangle\big], \tag{1.36}
$$

where $|\text{before}\rangle$ is the state of the photon before the interaction[5].

The change of the reduced density matrix of the dust grain as a consequence of the

---

[4]We assume that the dust grain is opaque such that the photon cannot fly through the dust grain

[5]An implicit assumption that we make here is that the dust grain is sufficiently heavy such that the interaction with a single photon does not significantly change its state, for example the recoil of the dust grain can be neglected.

Figure 1.8: A sketch of the setting. Indicated are the spatial probability distributions of the dust grain (red) and the photon (green).

interaction reads analogously to Eq. (1.36)

$$\frac{1}{2}\big[|G_{x_1}\rangle + |G_{x_2}\rangle\big]\big[\langle G_{x_1}| + \langle G_{x_2}|\big] = \begin{pmatrix} \frac{1}{2} & \frac{1}{2} \\ \frac{1}{2} & \frac{1}{2} \end{pmatrix} \to \begin{pmatrix} \frac{1}{2} & 0 \\ 0 & \frac{1}{2} \end{pmatrix} = \frac{1}{2}\big[|G_{x_1}\rangle\langle G_{x_1}| + |G_{x_2}\rangle\langle G_{x_2}|\big].$$

(1.37)

As anticipated, the off-diagonal elements vanished[6].

Above, the photon discriminates the states of the dust grain with different spatial distributions. In general, the interaction could lead to the same process in another basis. In Eq. (1.36), we would obtain on the right-hand site $\frac{1}{\sqrt{2}}\big[|a_1\rangle|s\rangle + |a_2\rangle|p\rangle\big]$, where $|a_1\rangle$ and $|a_2\rangle$ are some states. In such a case, the off-diagonal elements of the reduced density matrix of the dust grain vanish in the basis corresponding to $|a_1\rangle$ and $|a_2\rangle$ but not in the basis $|G_{x_1}\rangle$ and $|G_{x_2}\rangle$. The basis which diagonalises the density matrix is called the *preferred basis* [42]. The interaction with environment selects out of the infinitely many possible bases a preferred one. This process in known as environmentally induced selection, or *einselection* [99]. If the Hamiltonian of the system is local which means that the interaction extends only over a few neighbouring particles, the preferred basis is typically a local basis, where the local basis states can be written as product states of local quantities.

The quantum decoherence theory describes the average situation. In the above toy model, the density matrix on the right hand site of Eq. (1.37) is averaged over the situations with the scattered and not scattered photon. Therefore, the nearly diagonal density matrix describes the result of many repeated realisations. In this thesis, however, we are interested in individual realisations rather than on the average situation. In each individual case, the photon is either scattered or it is not scattered. In order to consider the single realisations, we introduce projective measurements. Coming back to the above toy model again, we consider the cases of the scattered and not scattered photon individually by projecting the state of the dust grain either on $|G_{x_1}\rangle$ or on $|G_{x_2}\rangle$.

1.2.2   Instability as a macroscopicity measure for quantum superpositions

In a later chapter of this thesis, we will rethink the concept of stability and formulate a macroscopicity measure for quantum superpositions of macroscopically distinct states which can be interpreted as a measure of instability of individual quantum superpositions. In this section, we introduce the notion of macroscopicity and put it into a general context of ongoing research.

Until today, there was not any clear evidence that quantum mechanics breaks down at any physical scale. In order to advance the forefront of research, the current agenda is to extend the parameter range, where effects of quantum mechanics have been observed experimentally. One of the directions of research is to observe superpositions of macroscopically distinct states.

Different experiments have been devised so far in order to test quantum mechanics on ever increasing scales. They encompass

---

[6]In the above toy model, the off-diagonal elements become zero after the interaction with a single environmental particle. Typically, this happens only after many successive interactions because the environmental particles cannot fully discriminate between different states of the system.

- Matter-wave double-slit interference experiments with neutrons [56, 98], atoms [63, 44, 83, 31, 14], Bose-Einstein condensates [2], Buckey-balls [3] and other big organic molecules [33, 37].

- Preparation of superposition states of counter-propagating currents in a superconducting SQUID loop [24, 35, 48].

- Opto-mechanical entanglement between macroscopic mechanical devices like oscillating membranes or levitating nano-spheres and photons [59, 73].

In order to assess the degree of macroscopicity that was achieved in the experiments, one needs a well-defined measure of macroscopicity. On the basis of such a measure, one could also decide on the future experimental investigations [54].

Although the notion of macroscopicity appears intuitive, its precise formulation turns out to be rather involved. As an example, the states describing a living and a dead cat are clearly macroscopically distinct states. However, when it comes to introducing a formal measure of macroscopicity, it is not clear how to tackle the problem. In particular, it remains unclear which mathematical objects should be used for the definition of the macroscopicity in order to obtain a universally applicable measure. For example, the overlap $\langle \psi_L | \psi_D \rangle$ between the state $| \psi_L \rangle$ describing a living cat and $| \psi_D \rangle$ describing a dead cat is not a suitable measure of macroscopicity. The reason is that the overlap already vanishes when a few molecules of the cat occupy orthogonal states but the rest of the cat is the same in both cases.

Different proposals have been made so far for the measure of macroscopicity. They include proposals based on the information-theoretic framework using quantum Fisher information [25], the observable consequences of a minimal extension of quantum mechanics [62], the ability to discriminate the superposed states by classical detectors [81, 80] and others [53, 17, 8, 49, 58, 52, 95, 96]. However, the above proposals are applicable only to specific systems, for example to spin systems, to mechanical systems or systems of photons. Therefore, it is difficult to compare the different proposals. A definitive answer to the question of a proper measure of macroscopicity for the superpositions of macroscopically distinct states remains elusive.

1.3 Brief summary of results and the structure of the thesis

In Chapter 2, we first provide a precise formulation of the stability criterion on the basis of which the statistical ensembles are to be called stable or unstable. For spins-$\frac{1}{2}$, we analytically derive a relation which describes the modifications of the probability distribution due to local measurements. We show that the basic effect of measurements is the narrowing of the energy distributions. Therefore, ensembles with broad energy distributions are unstable. For spins in a magnetic field and for the Ising model, the modification mentioned above amounts to "cutting" the probability distribution of the total energy by a linear function. We also show that similar results apply to general interacting spin systems.

We consider two shapes for the probability distributions, namely a distribution consisting of two narrow peaks and a distribution of a Gaussian shape. In the former case, the measurements induce the suppression of one of the peaks, as shown in Fig. 1.7. For the Gaussian distribution, the measurements narrow the Gaussian, cf. Fig. 1.9.

Further, we show that lifetimes of broad ensembles are unmeasurably short. In contrast, the statistical ensembles, whose energy distributions have a width comparable to that of the canonical Gibbs distribution, are nearly stable in the absolute sense. This means that the narrowing effect of measurements described above compensates the broadening effect of measurements which is due to the off-diagonal elements of the projection operators when written in the total-energy basis.

In Chapter 3, we present the results of the numerical investigation of interacting spin systems. We simulate numerically one-dimensional lattices with up to $N_s = 24$ spins. Due to the limitation of numerical investigations to microscopic system sizes, these investigations cannot be applied to the systems considered in Chapter 2. However, we show that the results of the numerical calculations are in qualitative agreement with the analytical results.

First, we explicitly show that the finite-size effects with respect to the local measurements is rather pronounced for computationally accessible systems. These finite-size effects become smaller with increasing system size. However, even for the largest spin systems available for numerical investigations $N_s = 24$, these effects are still non-negligible. Further, we consider the effect of measurements on a two-peak $g(E)$ on the basis of the stability measure. For the two-peak $g(E)$, it is possible to suppress the finite-size effects such that the narrowing effect can be investigated thoroughly.

In Chapter 4, we introduce a measure of macroscopicity for quantum superpositions. This measure is based on the notion of instability of individual quantum states with respect to one local measurement. This macroscopicity measure quantifies the change of the reduced density matrices of small subsystems due to the local measurement. A quantum state is called unstable if a local measurement significantly changes a macroscopic number of density matrices of small subsystems. We apply the measure of macroscopicity to lattices of spins-$\frac{1}{2}$ and explicitly derive an expression for the measure of macroscopicity which is based on spin polarisations and spin-spin correlations. In the end, we present two examples.
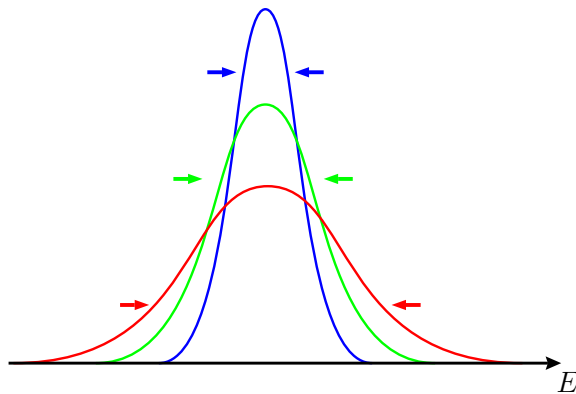
Figure 1.9: Illustration of the narrowing effect of local measurements for a broad Gaussian distribution of total energy.

In Chapter 5, we summarise the results of the thesis.

The second chapter of this thesis is based on the following article:

- Stability of Quantum Statistical Ensembles with Respect to Local Measurements,
  W. Hahn and B. V. Fine, arXiv:1601.06402

During the PhD time, the author of this thesis also contributed to the following article:

- Improvement of the Finite Basis Set for the Solution of the Two-Centre Dirac Equation in Cassini Coordinates,
  W. Hahn, A. N. Artemyev and A. Surzhykov, preprint

Further, the author of this thesis contributed to the following article:

- Non-Entangling Channels for Multiple Collisions of Quantum Wave Packets,
  W. Hahn and B. V. Fine, Phys. Rev. A 85, 032713 (2012)

1.4 Conventions and notations

Throughout this thesis, we use the following conventions unless explicitly specified otherwise:

- $k_B = 1$,

- $\hbar = 1$.

Further, the symbols are used with the following meaning:

- "$\equiv$" denotes a definition,

- "$\sim$" denotes the order of magnitude,

- "$\cong$" denotes proportionality,

- "$\lesssim$" denotes "smaller or approximately the same value".

Chapter 2

Stability of Quantum Statistical Ensembles with Respect to Local Measurements

In this Chapter, we give a precise formulation of our stability criterion for quantum statistical ensembles which is suitable for a broad variety of many-particle systems. Our primary focus is on the macroscopic quantum systems, where the number of microscopic subsystems is $N_s \sim 10^{23}$. After formulating and discussing the stability criterion, we apply the criterion to lattices of spins-$\frac{1}{2}$.

Let us start with a few general considerations. A statistical ensemble is defined by the probability $p(E)$ of occupying a state with total energy E. In classical physics, a system is fully characterised by the momenta and the coordinates of all constituents of the system. In quantum physics, a system is fully characterised by a density matrix. In the quantum-mechanical formalism of density matrices, $p(E)$ equals the diagonal elements of the system's density matrix expressed in the total-energy basis.

Given the density of energy eigenstates $\nu(E)$, the probability distribution of the total energy is

$$g(E) = p(E)\nu(E). \tag{2.1}$$

We define the average energy E_{av} of $g(E)$ as

$$E_{\mathrm{av}} \equiv \int_{-\infty}^{\infty} E \ g(E)dE \tag{2.2}$$

and the variance w_g^2 of $g(E)$ as

$$w_g^2 \equiv \int_{-\infty}^{\infty} (E - E_{\mathrm{av}})^2 \ g(E)dE. \tag{2.3}$$

In this thesis, we primarily focus on broad probability distribution $g(E)$. We call $g(E)$ broad, when

$$\frac{w_g}{E_{\mathrm{av}} - E_{\mathrm{min}}} \sim 1, \tag{2.4}$$

21

where $E_{\min}$ is the ground state energy of the system. As an example, a canonical ensemble with a positive temperature T is narrow from the above perspective because, in this case, [20]

$$\frac{w_g}{E_{\mathrm{av}} - E_{\min}} \sim \frac{1}{\sqrt{N_s}} \ll 1, \tag{2.5}$$

where $N_s \sim 10^{23}$. This relation is obtained in Sec. 1.1.1.

As discussed in the previous chapter, the description of isolated quantum systems by narrow $g(E)$ is only poorly justified. Broad $g(E)$ typically do not thermalise and, hence, exhibit non-equilibrium statistics for subsystems. In order to resolve this discrepancy, we formulate a stability criterion.

2.1 Stability criterion

Accidental measurements of microscopic particles in a macroscopic system cannot be excluded under any foreseeable natural or experimental conditions. We, therefore, introduce the following stability criterion: *A physically realisable quantum statistical ensemble describing a stationary state of a macroscopic system must be stable with respect to a small number of any arbitrarily chosen local measurements within the system. The measurement is called "local" if the measured quantity is localised in the three-dimensional physical space. The number of measurements n is called small, if $n \ll \sqrt{N_s}$, where N_s is the number of particles or microscopic subsystems in the system. The ensemble is called stable if*

$$\Delta G(n) \equiv \int_{-\infty}^{+\infty} |g_n(E) - g_0(E)| \, dE \ll 1, \tag{2.6}$$

where $g_0(E)$ and $g_n(E)$ are the probability distributions of the total energy before and after the measurements, respectively.

In this thesis, we mainly focus on "strong instability", which we define as the case when less than ten measurements lead to $\Delta G \gtrsim 0.1$ independent of N_s.

Let us also stress that the stability measure (2.6) is not unique. Both, the stability measure $\Delta G(n)$, could be defined in alternative ways without changing qualitatively the general concept of stability of quantum statistical ensembles. In fact, we introduce alternative stability measures in Chapter 3 and apply them to the results of our numerical investigations.

The above criterion can also be used to determine the lifetime of unconventional quantum ensembles in experiments with non-macroscopic isolated quantum clusters which become increasingly available these days. Hereby, examples are experiments with trapped ions [75], matter-wave experiments [33], NV-centres [40], few-fermion systems [91] and experiments with bose-gas [89, 45].

2.2 Qualitative discussion

In order to investigate the stability of quantum statistical ensembles, we study the evolution of the stability measure $\Delta G(n)$ with the number of measurements n. The stability measure

$\Delta G(n)$ quantifies the difference between the energy distribution after n measurements $g_n(E)$ and the initial energy distribution $g_0(E)$. Therefore, in order to understand the evolution of $\Delta G(n)$, we focus on how the measurements modify $g(E)$ in general. Below, we will learn that the main effects of the local measurements on $g(E)$ are the narrowing and the broadening of $g(E)$. This is why we will often refer to the variance w_g^2 of $g(E)$ when studying the stability of $g(E)$.

Qualitatively, measurements can lead to both narrowing and broadening of $g(E)$. The broadening effect of a single measurement is due to the off-diagonal elements of the projection operator describing the measurement in the basis of the total-energy eigenstates. The narrowing effect originates from correlations between the total energy of the system and the measurement outcomes. It can be understood as follows: Broad probability distributions $g(E)$ can be represented as a mixture of microcanonical (or canonical) ensembles corresponding to different temperatures $T(E)$, which, in turn, imply different probability distributions of local variables. When a given measurement outcome is much more likely for one represented temperature than for another, the post-measurement distribution can be significantly narrower than the initial one.

In terms of the energy scales, the increase of the variance w_g^2 due to the off-diagonal elements of a local projection operator should normally be of the order of ϵ_1^2, cf. Appendix A.1, where ϵ_1 is an appropriately chosen single-particle energy. At the same time, the decrease of w_g^2 for broad $g(E)$ can easily be of the order $\epsilon_1^2 N_s^2$, i.e. much larger. Since we focus primarily on broad $g(E)$, we neglect the broadening effect of the measurements unless explicitly specified otherwise. We further limit our derivations to $g(E)$ satisfying inequality $\left| \frac{dg(E)}{dE} \right| \lesssim \frac{g(E)}{w_{\text{can}}}$, where w_{can} is the width of the energy distribution corresponding to the canonical ensemble with the same average energy as that of $g(E)$, cf. Appendix A.3.

Random measurements typically lead to the change of E_{av} associated with heating, cf. Appendix A.1. In the case of the canonical ensemble, $\sqrt{N_s}$ measurements may easily lead to the increase of E_{av} by the value of the order of w_g, which would mean $\Delta G \sim 1$. The condition $n \ll \sqrt{N_s}$ allows us to neglect the heating for not too low E_{av}. Technically, heating can be dealt for macroscopic systems with by introducing a coarse-graining of the energy axis, cf. Appendix A.2.

2.3 Local measurements

In our analysis, we assume that the local measurements occur naturally. An example here is a passing photon which becomes entangled with the system and, later, accidentally becomes measured. While such a process corresponds to an indirect measurement of the system [11, 9], in this thesis, we simplify the analysis by assuming random instantaneous projective measurements of individual particles in the system [55, 6, 32, 30, 43]. We particularly focus on local measurements because the interactions involved in the measurement process are typically local. In the following, we assume that only one particle of the system interacts with the environmental particle for simplicity.

Let us now elaborate in detail on why we can describe the interaction with the en-

vironment by assuming projective measurements. An interaction of the system's particle with the environmental particle describes a decoherence event [41, 42, 99, 54, 97, 76], cf. Sec. 1.2.1. The density matrix ρ_S of the system S after the interaction is obtained from the joint density matrix ρ_SP by tracing over the degrees of freedom of the environmental particle P: $\rho_\mathrm{S} = \mathrm{Tr}_\mathrm{P}\left[\rho_\mathrm{SP}\right]$. The trace operation in turn corresponds to the average over all possible measurement outcomes for the particle

$$\rho_\mathrm{S} = \mathrm{Tr}_\mathrm{P}\left[\rho_\mathrm{SP}\right] \;=\; \sum_n \langle n|\rho_\mathrm{SP}|n\rangle \tag{2.7}$$

$$=\; \sum_n \langle n|\mathcal{P}_n\rho_\mathrm{SP}\mathcal{P}_n|n\rangle \tag{2.8}$$

$$=\; \sum_n \langle n|\left(\frac{\mathcal{P}_n\rho_\mathrm{SP}\mathcal{P}_n}{\mathrm{Tr}\left[\mathcal{P}_n\rho_\mathrm{SP}\mathcal{P}_n\right]}\right)|n\rangle \; \mathrm{Tr}\left[\mathcal{P}_n\rho_\mathrm{SP}\mathcal{P}_n\right] \tag{2.9}$$

$$=\; \sum_n \langle n|\rho_{\mathrm{SP},n}|n\rangle \; p(n), \tag{2.10}$$

where $|n\rangle$ is a basis of the Hilbert space corresponding to the given environmental particle, $\mathcal{P}_n = |n\rangle\langle n|$ is the projection operator on the state $|n\rangle$, $p(n) \equiv \mathrm{Tr}\left[\mathcal{P}_n\rho_\mathrm{SP}\mathcal{P}_n\right]$ is the probability[1] for measuring the particle in the state $|n\rangle$ and

$$\rho_{\mathrm{SP},n} \equiv \frac{\mathcal{P}_n\rho_\mathrm{SP}\mathcal{P}_n}{\mathrm{Tr}\left[\mathcal{P}_n\rho_\mathrm{SP}\mathcal{P}_n\right]} \tag{2.11}$$

is the joint density matrix of the system and the particle which is measured[2] in state $|n\rangle$.

The density matrix ρ_S in Eq. (2.10) is the incoherent weighted sum of reduced density matrices corresponding to different measurement outcomes for the environmental particle. Therefore, quantum decoherence, which leads to ρ_S, describes the average behaviour of repeated experiments. However, in each individual case in nature and the experiment, only a single possibility becomes realised. Therefore, by introducing projective measurements, we focus on the concrete realisations instead on the average behaviour.

After a measurement of the environmental particle, the state of the system is factorised into the term describing the system and the term describing the environmental particle. Therefore, we can disregard the term of the environmental particle for the subsequent analysis. Moreover, a measurement of the environmental particle can be effectively described as a measurement of the system's particle it interacted with. This is why we consider local measurements of the system's particles in this thesis.

---

[1] In the sum of Eq. (2.9), we leave out the terms with vanishing probability $p(n) = \mathrm{Tr}\left[\mathcal{P}_n\rho_\mathrm{SP}\mathcal{P}_n\right] = 0$.

[2] The density matrix in Eq. (2.11) can be referred to as "conditional density matrix" [79] because the measurements of the particle are to be understood as effectively arising from the trace operation and are, therefore, hypothetical.

2.4 Formulation for lattices of spins-$\frac{1}{2}$

We consider a lattice of N_s spins-$\frac{1}{2}$ and examine how multiple random local measurements affect $g(E)$. We implement an individual local measurement by selecting a random spin at a random time and then measuring its projection on a random axis. The measurements are assumed to occur very rarely with constant average rate per spin τ_{m}^{-1} (τ_{m} is much longer than the characteristic time of microscopic dynamics). We label measurements by index n. Each measurement is characterised by the parameters $\{m_n, \vartheta_n, \varphi_n\}$, where m_n labels the lattice site of the measured spin and (ϑ_n, φ_n) are the polar and azimuthal spherical angles indicating the orientation of the spin after the measurement. The n-th measurement is represented by the projection operator $\mathcal{P}_n$.

2.4.1 Projective operator for a local measurement

Technically, the local projection operator $\mathcal{P}_n$ is defined as

$$\mathcal{P}_n = \cdots \mathbf{1}_{m_n-1} \otimes [|\vartheta_n \varphi_n\rangle\langle\vartheta_n \varphi_n|]_{m_n} \otimes \mathbf{1}_{m_n+1} \cdots, \tag{2.12}$$

where $\mathbf{1}_i$ is the unit matrix acting on the Hilbert space associated with spin i and

$$|\vartheta_n \varphi_n\rangle = \cos\left(\frac{\vartheta_n}{2}\right)|\uparrow\rangle + \sin\left(\frac{\vartheta_n}{2}\right)e^{i\varphi_n}|\downarrow\rangle \tag{2.13}$$

is the quantum state of a spin polarised into the direction given by the spherical angles $\{\vartheta_n, \varphi_n\}$. The operator $[|\vartheta_n \varphi_n\rangle\langle\vartheta_n \varphi_n|]_{m_n}$ acts on the Hilbert space associated with lattice site m_n. The operator $\mathcal{P}_n$ is hermitian $\mathcal{P}_n^\dagger = \mathcal{P}_n$ and satisfies the relation of a projector $\mathcal{P}_n\mathcal{P}_n = \mathcal{P}_n$. It is related to the spin operator S_n as

$$\mathcal{P}_n = \frac{1}{2}\mathbf{1} + S_n, \tag{2.14}$$

where S_n is the operator of the m_n-th spin projection on the axis pointing in the direction $\{\vartheta_n, \varphi_n\}$ [74]. Is satisfies the relation $S_n|\vartheta_n\varphi_n\rangle = \frac{1}{2}|\vartheta_n\varphi_n\rangle$. The operator S_n can be formally obtained as

$$S_n = \mathcal{U}(\vartheta_n, \varphi_n)\, S_{m_n z}\, \mathcal{U}^\dagger(\vartheta_n, \varphi_n), \tag{2.15}$$

where $\mathcal{U}(\vartheta_n, \varphi_n)$ is the spin rotation operator for the spin at lattice site m_n, which rotates the z-axis such that it points into the direction given by (ϑ_n, φ_n) after rotation. The corresponding eigenstates of S_n are given by $\mathcal{U}(\vartheta_n, \varphi_n)|\uparrow\rangle$ with eigenvalue $+\frac{1}{2}$, and $\mathcal{U}(\vartheta_n, \varphi_n)|\downarrow\rangle$ with eigenvalue $-\frac{1}{2}$.

As an example, for $\varphi_n = 0$ and arbitrary ϑ_n, $\mathcal{U}(\vartheta_n, \varphi_n) = \exp\left(-i\vartheta_n S_y\right)$. This leads to

$$S_n = \cos\left(\vartheta_n\right)S_{m_n z} + \sin\left(\vartheta_n\right)S_{m_n x}, \tag{2.16}$$

and the corresponding eigenstates of S_n are

$$
|\vartheta_n 0\rangle \;=\; \cos\left(\frac{\vartheta_n}{2}\right)|\uparrow\rangle_z + \sin\left(\frac{\vartheta_n}{2}\right)|\downarrow\rangle_z, \tag{2.17}
$$

$$
|\overline{\vartheta_n 0}\rangle \;=\; \cos\left(\frac{\vartheta_n}{2}\right)|\uparrow\rangle_z - \sin\left(\frac{\vartheta_n}{2}\right)|\downarrow\rangle_z, \tag{2.18}
$$

where $|\vartheta_n 0\rangle$ and $|\overline{\vartheta_n 0}\rangle$ are defined such that $S_n|\vartheta_n 0\rangle = \frac{1}{2}|\vartheta_n 0\rangle$ and $S_n|\overline{\vartheta_n 0}\rangle = -\frac{1}{2}|\overline{\vartheta_n 0}\rangle$.

In principle, the stability criterion introduced above also allows for a broader definition of local measurements. Any arbitrary measurements of observables which can be written as a sum of local observables can also be admitted for the stability measure $\Delta G(n)$.

2.4.2 Modification of the energy distribution due to measurements

We denote the initial density matrix of the total system as ρ_0 and the initial $g(E)$ as $g_0(E)$. The same two quantities after n measurements are denoted as ρ_n and $g_n(E)$. The transformation from ρ_{n-1} to ρ_n reads

$$
\rho_n = \frac{\mathcal{P}_n e^{-i\mathcal{H}(t_n - t_{n-1})}\rho_{n-1}e^{i\mathcal{H}(t_n - t_{n-1})}\mathcal{P}_n^\dagger}{\mathrm{Tr}\left[\mathcal{P}_n e^{-i\mathcal{H}(t_n - t_{n-1})}\rho_{n-1}e^{i\mathcal{H}(t_n - t_{n-1})}\mathcal{P}_n^\dagger\right]}, \tag{2.19}
$$

where t_n is the time of the n-th measurement. Although $\mathcal{P}_n$ is hermitian, we keep the notation $\mathcal{P}_n^\dagger$ for a moment for the sake of clarity. Based on the relation (2.19), one obtain

$$
g_n(E) = \frac{1}{B}\left[\mathcal{P}_1^\dagger e^{i\mathcal{H}(t_2 - t_1)}\mathcal{P}_2^\dagger \cdots \mathcal{P}_n^\dagger \mathcal{P}_n \cdots \mathcal{P}_2 e^{-i\mathcal{H}(t_2 - t_1)}\mathcal{P}_1\right]_{\mathrm{diag}}(E)\, g_0(E), \tag{2.20}
$$

where $[\cdots]_{\mathrm{diag}}(E)$ denotes the diagonal elements of the operator in the energy basis averaged over suitably chosen energy bins[3]. It is important to notice that Eq. (2.20) is a relation between $g_n(E)$ and $g_0(E)$ which is local in energy. We present the derivation of Eq. (2.20) in Appendix A.3.

For long τ_m, the effect of individual measurements in Eq. (2.20) normally factorises, which leads to

$$
g_n(E) = \frac{1}{B_n}\left[\mathcal{P}_n\right]_{\mathrm{diag}}(E)\, g_{n-1}(E), \tag{2.21}
$$

where B_n is the normalisation factor, and, according to Eq. (2.14),

$$
\left[\mathcal{P}_n\right]_{\mathrm{diag}}(E) = \frac{1}{2} + \left[S_n\right]_{\mathrm{diag}}(E). \tag{2.22}
$$

The action of each measurement thus consists of multiplying of $g(E)$ by $[\mathcal{P}_n]_{\mathrm{diag}}(E)$ and then renormalising the result.

The derivation of Eq. (2.21) goes as follows. For a long time delay between measurements τ_m, the system typically loses the memory of the previous measurements locally by the time a new measurement occurs [57]. Here, we use the concept of memory loss in the sense that, for all practical purposes, the density matrix before the next measurement can be

---

[3]For details, see Appendix A.2.

approximated as being diagonal in the energy basis. This allows us to treat measurements iteratively by using the same approximation as the one that led to Eq. (2.20), namely, we replace $g_0(E)$ by $g_{n-1}(E)$ and $\mathcal{O}$ by $\mathcal{P}_n$ thereby obtaining

$$g_n(E) = \frac{1}{B_n} \left[\mathcal{P}_n^\dagger \mathcal{P}_n \right]_{\mathrm{diag}} (E) \; g_{n-1}(E) = \frac{1}{B_n} \left[\mathcal{P}_n \right]_{\mathrm{diag}} (E) \; g_{n-1}(E), \qquad (2.23)$$

which is the same as Eq. $(2.21)^4$. Above, we used $\mathcal{P}_n^\dagger = \mathcal{P}_n$ and $\mathcal{P}_n \mathcal{P}_n = \mathcal{P}_n$. This concludes our derivation.

Applying relation (2.21) iteratively n times, we obtain

$$g_n(E) = \prod_{i=1}^{n} \frac{1}{B_i} \left[\mathcal{P}_i \right]_{\mathrm{diag}} (E) g_0(E). \qquad (2.24)$$

Finally, for the stability measure (2.6) averaged over all possible outcomes of n measurements, we obtain

$$\overline{\Delta G}(n) = \int \overline{\left| \prod_{i=1}^{n} \frac{1}{B_i} \left[\mathcal{P}_i \right]_{\mathrm{diag}} (E) - 1 \right|} g_0(E) dE, \qquad (2.25)$$

where the bar denotes the result of averaging.

The average in Eq. (2.25) is to be taken over all free parameters. For each measurement, there are four parameters: a pair of spherical angles $\{\vartheta_n, \varphi_n\}$ for the measurement outcome, the lattice site m_n and the measurement time t_n. Therefore, $\Delta G(n)$ is, in principle, to be averaged over $4n$ parameters.

2.4.3   Relation to the Bayes' theorem

Before applying the above results to lattices of spins-$\frac{1}{2}$, let us focus on the relations in Eq. (2.20) and Eq. (2.23) which describe the modifications of $g(E)$ due to measurements. In this section, we argue that these relations are intimately connected with the Bayes' theorem known from statistics. First, we recapitulate the Bayes' theorem which is usually stated as

$$P(A|B) = \frac{1}{P(B)} P(B|A) P(A), \qquad (2.26)$$

where A and B denote probabilistic events, $P(A)$ and $P(B)$ are the probabilities of the individual events, $P(A|B)$ is the conditional probability for observing event A provided event B occurred and likewise for $P(B|A)$. An example here is the process of throwing a dice and individual events in this context can be A: "throw a 5" and B: "throw an odd number".

---

[4]In practice, Eq. (2.23) is valid as long as the delay between measurements τ_{m} is much longer than the characteristic time scales of system's microscopic dynamics. These characteristic time scales are, for example, of the order of $\frac{1}{H_z}$ for Hamiltonian (2.27), or of the order of $\frac{1}{J}$ for interacting spin systems, where J is the typical coupling constant in Hamiltonian (2.42). There may be anomalous situations, when the above limit is not realisable. An example is the Ising model defined by $J_x = J_y = 0$ in Hamiltonian (2.42). In this case, a single-spin measurement is not correlated with the total energy of the system, while the measurement of two neighbouring spins is correlated, and, at the same time, the system has anomalously many local integrals of motion (z-components of spins). As a result, the expression (2.20) for the measurement of a pair of neighbouring spins cannot be approximated by the result of two successive applications of Eq. (2.23) no matter how long the delay between the two measurements is.

The formulation of the Bayes' theorem in Eq. (2.26) resembles the Eq. (2.20) and Eq. (2.23). For simplicity, we focus on Eq. (2.23) in the following and establish the relations between the individual objects in Eq. (2.23) and Eq. (2.26). The events A and B correspond to A: "measuring energy E" and B: "measuring the outcome described by the projector $\mathcal{P}_n$". Therefore, in Eq. (2.23), $g_n(E)$ can be interpreted as the conditional probability distribution of energy given the n-th measurement outcome. The bin average $[\mathcal{P}_n]_{\mathrm{diag}}(E)$ in turn is the conditional probability for the measurement outcome described by the projector $\mathcal{P}_n$ given the microcanonical energy distribution at energy E. The normalisation coefficient B_n is the total probability for obtaining the above measurement outcome and $g_{n-1}(E)$ is probability distribution of energy corresponding to $P(A)$ in Eq. (2.26).

The discussion is to emphasise the correlations between the total energy E and the measurement outcomes $\mathcal{P}_n$. As a result of this correlation, the cutting function $[\mathcal{P}_n]_{\mathrm{diag}}(E)$ is not a constant function. Applying the cutting function to $g(E)$, therefore, modifies $g(E)$ and induces narrowing in this way.

2.5 Specific examples of lattices of spins-$\frac{1}{2}$

In this section, we apply the general formulation for spins-$\frac{1}{2}$ to non-interacting spins in a magnetic field and to spin systems with nearest-neighbour interaction.

2.5.1 Spins in magnetic field

Let us now turn to the specific example of non-interacting spins in a uniform magnetic field H_z with Hamiltonian

$$\mathcal{H} = -H_z \sum_i S_{iz}, \tag{2.27}$$

where S_{ix}, S_{iy} and S_{iz} are spin operators on the i-th lattice site.

In this case, the outcome of a single spin measurement normally correlates with the total energy of the system and, therefore, leads to a significant narrowing of $g(E)$ governed by Eq. (2.21). A calculation based on Eq. (2.22) gives

$$[\mathcal{P}_n]_{\mathrm{diag}}(E) = \frac{1}{2} - \cos(\vartheta_n) \frac{E}{E_{\max} - E_{\min}}, \tag{2.28}$$

where $E_{\max} = \frac{H_z N_s}{2}$ is the highest energy eigenstate and $E_{\min} = -\frac{H_z N_s}{2}$ is the lowest energy eigenstate.

The expression (2.28) can either be obtained by the following consideration or by an explicit calculation presented in Appendix A.1. Since the Hamiltonian $\mathcal{H}$ in Eq. (2.27) is diagonal in the product basis of individual spin states $|\uparrow\rangle_z$ and $|\downarrow\rangle_z$, we obtain for the expectation value of the z-polarisation of spin n

$$\langle S_{nz} \rangle = \frac{\langle (S_z)_{\mathrm{tot}} \rangle}{N_s} = -\frac{E}{N_s H_z} = -\frac{E}{E_{\max} - E_{\min}}, \tag{2.29}$$

where $\langle (S_z)_{\text{tot}} \rangle \equiv \sum_n \langle S_{nz} \rangle$. With $\langle S_n \rangle = \langle S_{nz} \rangle \cos(\vartheta_n)$, this yields

$$[S_n]_{\text{diag}} (E) = - \cos(\vartheta_n) \frac{E}{E_{\max} - E_{\min}}. \tag{2.30}$$

Substituting this result into Eq. (2.14) gives Eq. (2.28). This concludes our derivation.

The expression (2.28) together with Eq. (2.21) thus yields

$$g_n(E) = \frac{1}{B_n} \left(\frac{1}{2} - \cos(\vartheta_n) \frac{E}{E_{\max} - E_{\min}} \right) g_{n-1}(E). \tag{2.31}$$

The action of this transformation consists of "cutting" $g_{n-1}(E)$ by function $[\mathcal{P}_n]_{\text{diag}}(E)$ and then renormalising the result. This "cutting" normally makes $g_n(E)$ narrower than $g_{n-1}(E)$. The outcome of the next measurement can, in principle, lead to the opposite effect, but it is more probable that it will lead to further narrowing because the probability of subsequent measurement outcomes is determined by the narrower $g_n(E)$. After many iterations, the drastic narrowing of $g(E)$ becomes overwhelmingly probable.

Figure 2.1 schematically illustrates the effect of a sequence of transformations (2.21) applied to an initial two-peak distribution which we approximate by

$$g_0(E) \approx \frac{1}{2}[\delta(E - E_1) + \delta(E - E_2)], \tag{2.32}$$

where $\delta(...)$ is Dirac delta-function. This approximation is valid as long as the width of each individual peak is much smaller than the distance between the peaks $E_2 - E_1$. In this case, one of the two peaks dominates $g_n(E)$ for $n \to \infty$.

Figure 2.2 presents computed $\overline{\Delta G}(n)$ for the above $g_0(E)$. In each case, we obtain $\overline{\Delta G}(n) > 0.1$ after nine measurements independently of the number of spins in the system, which implies "strong instability". In Fig. 2.2, we also show an analytical approximation, namely,

$$\overline{\Delta G}(n) \approx \sqrt{1 - e^{-\lambda n}}, \tag{2.33}$$

where

$$\lambda \cong u^2 (E_2 - E_1)^2 \tag{2.34}$$

and

$$u \equiv \overline{\left| \frac{d \left[\mathcal{P}_n \right]_{\text{diag}} (E)}{dE} \right|} \sim \frac{1}{E_{\max} - E_{\min}}. \tag{2.35}$$

The derivation of this approximation is given in Appendix A.4. In Fig. 2.2, all three curves have been plotted with the same value for the parameter κ such that $\lambda = 0.3 \left(\frac{E_1 - E_2}{E_{\max} - E_{\min}} \right)^2$.

As an example for the narrowing of a general broad $g(E)$, we sketch the effect of a sequence of transformations (2.21) in Fig. 2.3.

Let us also consider the initial Gaussian distribution

$$g_0(E) \cong \exp \left[-\frac{(E - E_0)^2}{2w_{g,0}^2} \right] \tag{2.36}$$

defined by parameters E_0 and $w_{g,0}$, where $w_{g,0} \ll E_{\max} - E_{\min}$. After n measurements,
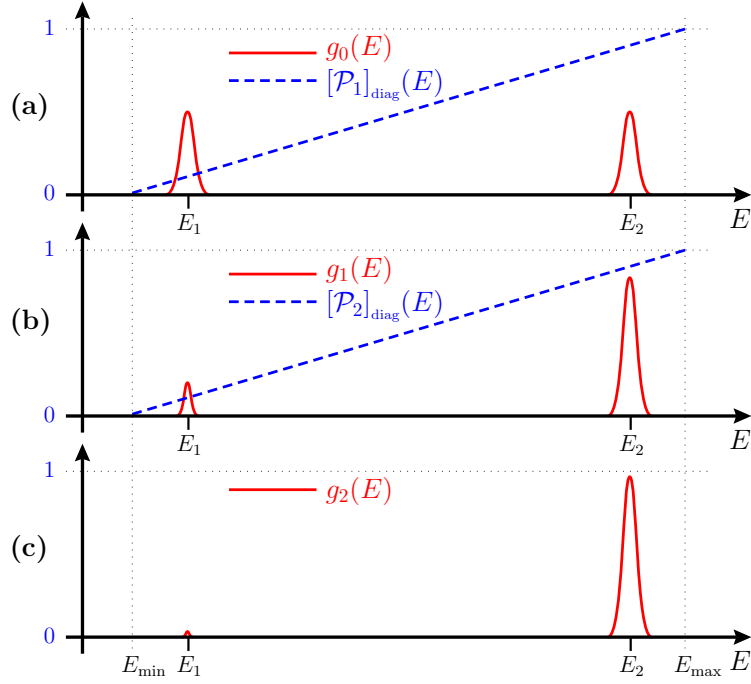
Figure 2.1: (Colour online) Schematic representation of the evolution of a two-peak energy distribution $g_n(E)$ (solid red lines) governed by Eq. (2.21): $g_0(E) = 1/2[\delta(E - E_1) + \delta(E - E_2)]$; $g_1(E) \cong [\mathcal{P}_1]_{\mathrm{diag}}(E)\, g_0(E)$; $g_2(E) \cong [\mathcal{P}_2]_{\mathrm{diag}}(E)\, g_1(E)$. Here $[\mathcal{P}_1]_{\mathrm{diag}}(E)$ and $[\mathcal{P}_2]_{\mathrm{diag}}(E)$ (dashed blue lines) correspond to two single-spin measurements with respective outcomes $\vartheta_1 = \pi$ and $\vartheta_2 = \pi$ substituted in Eq. (2.28).
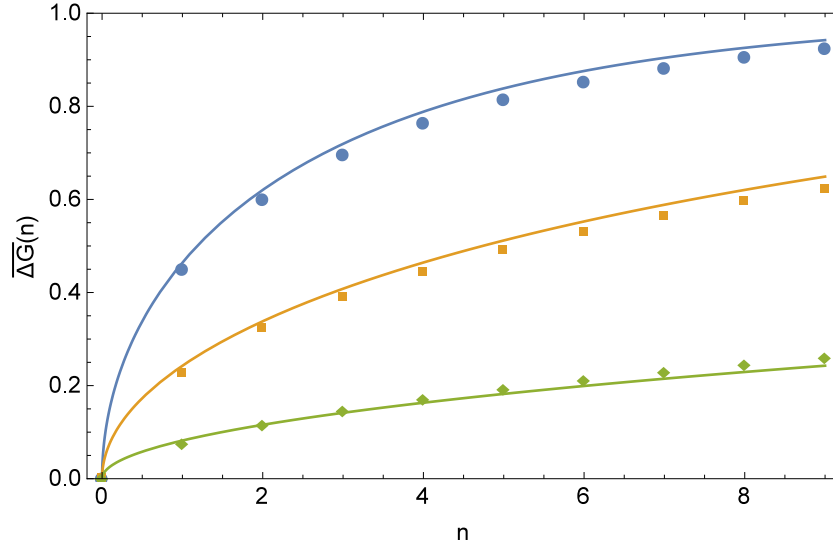
Figure 2.2: (Colour online) Averaged ensemble stability measure $\overline{\Delta G}(n)$ as a function of the number of measurements n for a two-peak initial distribution $g_n(E)$. Points represent exact numerically computed results. Lines correspond to the approximated expression $\overline{\Delta G}(n) \approx \sqrt{1 - e^{-\lambda n}}$ with $\lambda = 0.3\, \frac{(E_1 - E_2)^2}{(E_{\max} - E_{\min})^2}$. Different colours represent different pairs of values for (E_1, E_2): blue (circles) $(-0.9, 0.9)$, yellow (squares) $(-0.9, 0.0)$, green (rhombi) $(-0.9, -0.6)$ in units where $E_{\min} = -1$ and $E_{\max} = 1$.

Figure 2.3: (Colour online) Schematic representation of the evolution of a broad $g_n(E)$ (solid red lines) governed by Eq. (2.21). Here $[\mathcal{P}_i]_{\mathrm{diag}}(E)$ (dashed blue lines) correspond to single-spin measurements with given outcomes substituted in Eq. (2.28).

31

$g_n(E)$ remains approximately Gaussian with the width $w_{g,n}$ following the relation
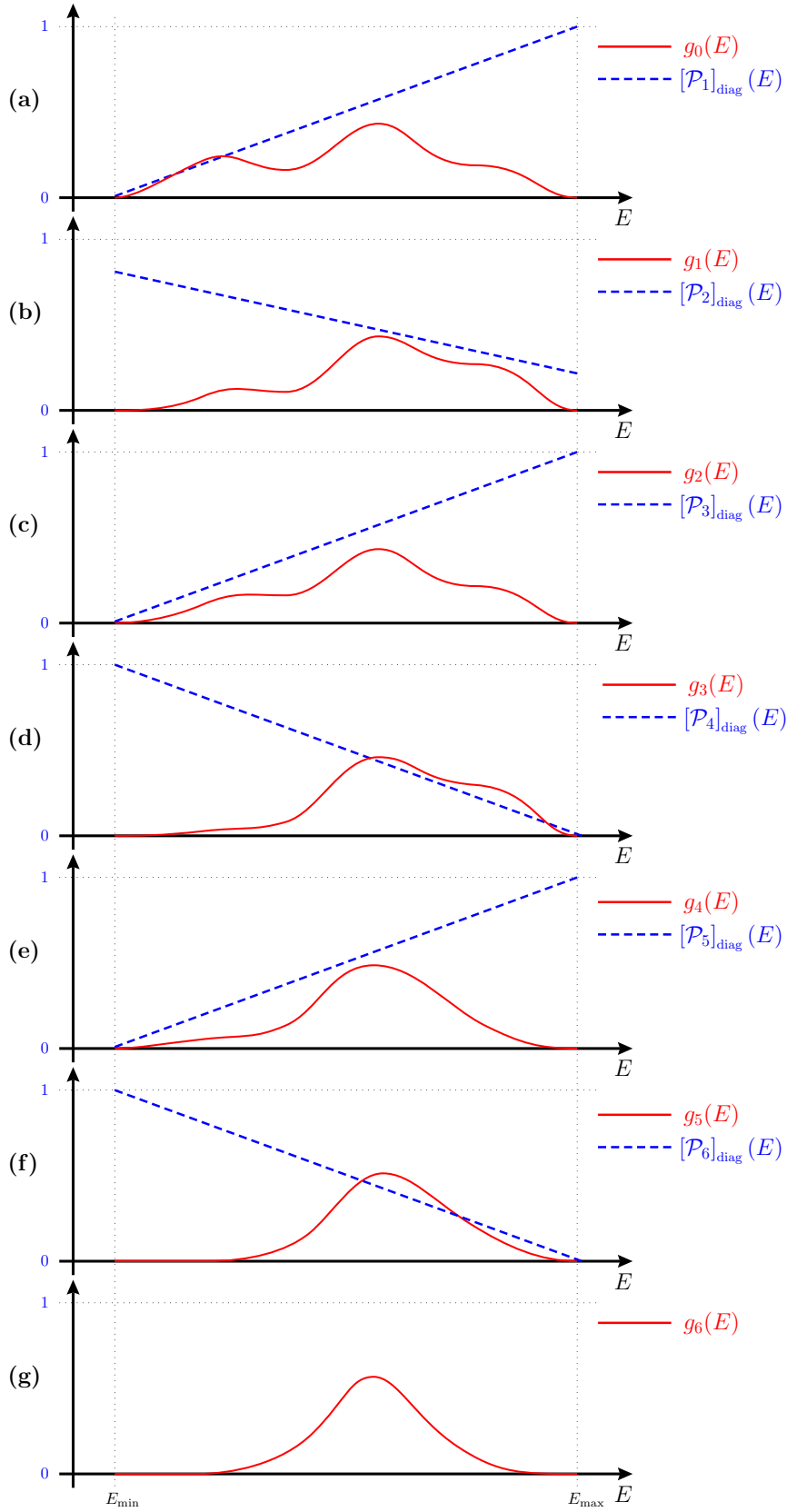
$$\overline{\left[\frac{1}{w_{g,n}^2}\right]} = \frac{1}{w_{g,0}^2} + u^2 n, \tag{2.37}$$

cf. Appendix A.5. This relation leads to $\overline{\Delta G}(n) \sim 1$ when $\overline{\frac{1}{w_{g,n}^2}} \sim \frac{2}{w_{g,0}^2}$, which corresponds to the number of measurements $n_{cr} \sim \frac{1}{w_{g,0}^2 u^2}$. According to our criterion, the border case for the ensemble stability corresponds to $n_{cr} \sim \sqrt{N_s}$, which implies that the ensemble is unstable for

$$w_{g,0} \gg \frac{E_{\max} - E_{\min}}{\sqrt[4]{N_s}}. \tag{2.38}$$

An ensemble with $w_{g,0} \lesssim (E_{\max} - E_{\min})/\sqrt[4]{N_s}$ may still become narrower due to measurements, but the criterion calls it "stable", because the narrowing is relatively slow.

We finally note that, for $w_{g,0} \sim \epsilon_1 \sqrt{N_s}$, where $\epsilon_1 \equiv \frac{E_{\max} - E_{\min}}{N_s}$ is the characteristic single-spin energy, the decrease of the variance as a result of one measurement is

$$w_{g,1}^2 - w_{g,0}^2 \approx w_{g,0}^4 u^2 \sim \epsilon_1^2, \tag{2.39}$$

which is of the same order of magnitude as the increase of w_g^2 due to the broadening effect mentioned earlier. Therefore, it is reasonable to expect that, for some

$$w_{g,0} \sim \epsilon_1 \sqrt{N_s}, \tag{2.40}$$

the narrowing effect would compensate the broadening effect, and hence such an ensemble is absolutely stable with respect to measurements. Remarkably, this $w_{g,0}$ is of the order of the width of the canonical ensemble [60, 46] for $T \gtrsim \epsilon_1$. In Fig. 2.4, we provide an overview of the different regimes of stability or instability of a Gaussian $g(E)$ as a function of the width w_g.

Given that the system is measured on average once per time $\frac{\tau_m}{N_s}$, the above estimates for λ and for n_{cr} imply that the characteristic time for gaining $\Delta G \sim 1$ is

$$\tau_1 \sim \tau_m \frac{\epsilon_1^2 N_s}{w_g^2}. \tag{2.41}$$
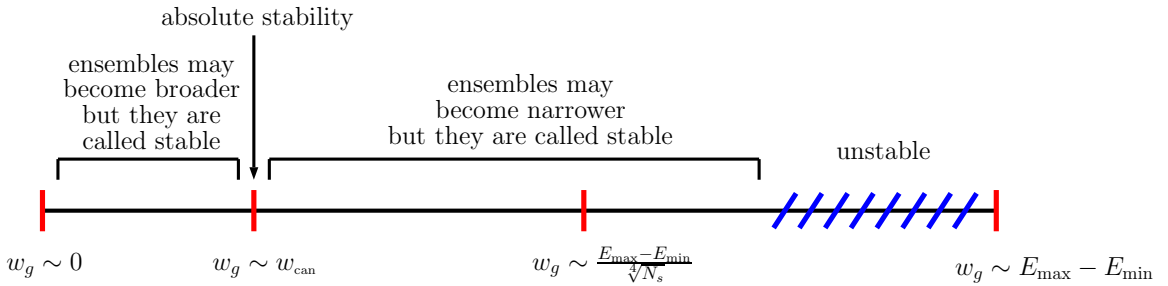

Figure 2.4: Illustration of the stability and instability of quantum statistical ensembles with a Gaussian energy distribution depending on the value of the width w_g. The horizontal axis is the logarithm of w_g.

For a macroscopic system, τ_1 is extremely short unless $w_g \leq \epsilon_1 \sqrt{N_s}$.

2.5.2 Systems of interacting spins

Now, we turn to a lattice of interacting spins-$\frac{1}{2}$. We consider the following general Hamiltonian with nearest-neighbour interaction

$$\mathcal{H} = -\sum_{i<j} J_x S_{ix} S_{jx} + J_y S_{iy} S_{jy} + J_z S_{iz} S_{jz}, \tag{2.42}$$

where J_x, J_y and J_z are the coupling constants. In contrast to the previous case of spins in a magnetic field in Eq. (2.27), the outcome of a single measurement here is not correlated with the total energy of the system and, hence, does not induce narrowing of $g(E)$. At least two accidental measurements sufficiently close in space and time are required for this. The reason is that the energy E now depends on the relative orientation of spins but not on the orientation of each spin relative to an external magnetic field.

Let us now consider two such measurements n and $n-1$ at times $t_n > t_{n-1}$. The same treatment that led to Eq. (2.21) now gives

$$g_n(E) = \frac{1}{B_n} \left[\mathcal{A}_{n,n-1}^\dagger \mathcal{A}_{n,n-1} \right]_{\text{diag}} (E) \ g_{n-2}(E), \tag{2.43}$$

where $\mathcal{A}_{n,n-1} = \mathcal{P}_n e^{-i\mathcal{H}(t_n-t_{n-1})} \mathcal{P}_{n-1}$. Substituting Eq. (2.14), we obtain

$$\begin{aligned}
\left[\mathcal{A}_{n,n-1}^\dagger \mathcal{A}_{n,n-1} \right]_{\text{diag}} (E) &= \frac{1}{4} - \frac{1}{2} \left[\left\{ S_n(t_n), S_{n-1}(t_{n-1}) \right\} \right]_{\text{diag}} (E) \\
&\quad + \left[S_{n-1}(t_{n-1}) S_n(t_n) S_{n-1}(t_{n-1}) \right]_{\text{diag}} (E),
\end{aligned} \tag{2.44}$$

where $\left\{ S_n(t_n), S_{n-1}(t_{n-1}) \right\} \equiv S_n(t_n) S_{n-1}(t_{n-1}) + S_{n-1}(t_{n-1}) S_n(t_n)$ is anti-commutator of spin operators.

The derivation of Eq. (2.44) goes as follows. Substituting $\mathcal{A}_{n,n-1} = \mathcal{P}_n e^{-i\mathcal{H}(t_n-t_{n-1})} \mathcal{P}_{n-1}$ into the function $\left[\mathcal{A}_{n,n-1}^\dagger \mathcal{A}_{n,n-1} \right]_{\text{diag}} (E)$ in Eq. (2.43), we first obtain

$$\begin{aligned}
\left[\mathcal{A}_{n,n-1}^\dagger \mathcal{A}_{n,n-1} \right]_{\text{diag}} (E) &= \left[\mathcal{P}_{n-1}^\dagger(0) \mathcal{P}_n^\dagger(t_n-t_{n-1}) \mathcal{P}_n(t_n-t_{n-1}) \mathcal{P}_{n-1}(0) \right]_{\text{diag}} (E) \\
&= \left[\mathcal{P}_{n-1}(0) \mathcal{P}_n(t_n-t_{n-1}) \mathcal{P}_{n-1}(0) \right]_{\text{diag}} (E).
\end{aligned} \tag{2.45}$$

Further, substituting the relation $\mathcal{P}_n = \frac{1}{2}\mathbf{1} + S_n$ in Eq. (2.45) leads to Eq. (2.44) if $[S_n]_{\text{diag}}(E) = 0$. This concludes our derivation.

Once the spin projections measured in the $(n-1)$-th and n-th measurements are specified and the value of energy E is fixed, the last two terms on the right-hand side of Eq. (2.44) can be considered as spin correlation functions associated with the corresponding microcanonical ensemble[5]. This relation is formulated more precisely below. The two terms

---

[5]For the usual definition of the correlation function, the product of individual spins expectation values is subtracted from the spin-spin expectation value. Therefore, the usual spin correlation function is governed by the fluctuations of the spin-spin expectation value around its mean value. In Eq. (2.44), we call solely the

depend on the time delay and the distance between the two measurements. We characterise the overall behaviour of the above two terms by correlation time $\tau_{\text{corr}}(E)$ and correlation length $\xi(E)$. This behaviour is, in principle, accessible experimentally.

The three-spin term in Eq. (2.44) should typically be significantly smaller than the two-spin term. First, the three-spin term is smaller than the two-spin term by a factor of $\frac{1}{2}$ due to the definition of the spin operator $S_{ix} = \frac{1}{2}\sigma_{ix}$, where σ_{ix} is a Pauli matrix. Further, for the time delay $t_n - t_{n-1} = 0$, the three-spin term vanishes if $m_{n-1} \neq m_n$, which means that different spins were measured.

Relation to conventional spin correlation functions

The expressions

$$[\{S_n(t_n - t_{n-1}), S_{n-1}(0)\}]_{\text{diag}}(E) \tag{2.46}$$

and

$$[S_{n-1}(0)S_n(t_n - t_{n-1})S_{n-1}(0)]_{\text{diag}}(E) \tag{2.47}$$

on the right-hand side of Eq. (2.44) mean the microcanonical average for the energy bin corresponding to energy E. Therefore, these expressions can be related to the conventional equilibrium spin correlation function at temperature T corresponding to the average energy $E_{\text{av}} = E$ (the relation $T(E_{\text{av}})$ is defined in Sec. 1.1.1). We use canonical typicality, which means that arbitrary quantum superpositions chosen from a narrow energy interval typically lead to same expectation values. Therefore, the expectation value for the bin corresponding to energy E equals the expectation value for the microcanonical ensemble corresponding to temperature $T(E)$.

To give an example, let us assume that the outcome of the 1st measurement is $\vartheta_1 = 0, \varphi_1 = 0$ (spin 1 points into the positive z-direction) and the outcome of the 2-nd measurement is $\vartheta_2 = \frac{\pi}{2}, \varphi_2 = 0$ (spin 2 points into the positive x-direction). For the two-spin term, we then obtain[6]

$$\left[\{S_2(t_2 - t_1), S_1(0)\}\right]_{\text{diag}}(E) = \langle\{S_x(\vec{r}_2 - \vec{r}_1, t_2 - t_1), S_z(0)\}\rangle_{T(E)}, \tag{2.49}$$

where $\vec{r}_n$ is the position of the n-th measured spin.

It is also noteworthy that conventional spin correlation functions are accessible experimentally, possibly by means of the fluctuation-dissipation theorem [50].

---

spin-spin expectation value as the spin correlation function. For this correlation function, the fluctuations of the spin-spin expectation value play a minor role.

[6]These correlation functions are not to be confused with those, where the product of individual expectation values for the individual operators is subtracted as for example

$$\langle\delta S_x \delta S_z\rangle = \langle S_x S_z\rangle - \langle S_x\rangle\langle S_z\rangle, \tag{2.48}$$

where $\delta S_x \equiv S_x - \langle S_x\rangle$. Such correlation functions are primarily useful for studying the fluctuation properties of the given operators which play a minor role for our treatment.

Characteristic time required to gain $\Delta G \sim 1$

Now, we estimate the characteristic time τ_2 required to gain $\Delta G \sim 1$. We make the assumption justified by the final result that $\tau_2 \ll \tau_{\mathrm{corr}}(E)$ for all energies E. Therefore, we set the time delay in Eq. (2.44) effectively to zero. The value of τ_2 is strongly influenced by the presence of magnetic order within the range of energies covered by $g_0(E)$. If all or a significant part of $g_0(E)$ is within the magnetically ordered phase, where $\xi(E)$ is infinite, then each measurement correlates with all previous ones. The overall situation resembles the case of Hamiltonian (2.27), with external magnetic field substituted by the local field created by the ordered neighbours of each spin. In such a case, $\tau_2 \sim \tau_1$ given by Eq. (2.41).

In the paramagnetic (non-ordered) phase, $\xi(E)$ is finite. For the estimate of τ_2, let us assume that $\xi(E)$ is equal to the nearest-neighbour distance. In this case, Eq. (2.44) implies that sufficiently many accidental measurements of the pairs of nearby spins must occur to make $\Delta G \sim 1$, which makes τ_2 significantly longer than for the ordered phase. Specifically, we obtain in Sec. A.6 that

$$\tau_2 \sim \tau_1 \sqrt{N_s} \gg \tau_1. \tag{2.50}$$

This estimate, together with Eq. (2.41) implies that, for $w_g \sim E_{\max} - E_{\min}$, $\tau_2 \cong \frac{\tau_{\mathrm{m}}}{\sqrt{N_s}}$, which is still very short. However, since $n \sim \sqrt{N_s}$ measurements are required to gain $\Delta G \sim 1$, our criterion defines the ensemble as stable with respect to single-spin measurements. This, however, does not mean the overall stability: measurements of the total spin of nearest neighbours, which are also admitted by our stability criterion as "local", would easily lead to

$$\tau_2 \ll \frac{\tau_{\mathrm{m}}}{\sqrt{N_s}} \tag{2.51}$$

and $n \ll \sqrt{N_s}$ thus rendering the ensemble unstable.

We additionally note here that applying an external magnetic field to the paramagnetic phase would drastically shorten τ_2, because, in this case, single-spin measurements described by Eq. (2.28) would cause a much faster ensemble narrowing.

Ising model

In order to further illustrate the above considerations, we study the Ising model, which is a special case of the Hamiltonian in Eq. (2.42) with $J_x = 0$ and $J_y = 0$

$$\mathcal{H}_{\mathrm{Ising}} = -\sum_{i<j} J_z S_{iz} S_{jz}. \tag{2.52}$$

The application of the above general results to the Ising model is rather problematic because of the many integrals of motion associated with the z-component of each spin. This can be readily realised by checking the relation

$$[\mathcal{H}_{\mathrm{Ising}}, S_{lz}] = 0, \tag{2.53}$$

for each spin at lattice site l. The consequence is that the total effect of n measurements in Eq. (2.20) cannot be decomposed into effects of measurements of individual spin-pairs as

in Eq. (2.43).

Nevertheless, we shall assume in this section that the total effect of measurements is describable by the effects of spin-pair measurements and that only measurements of nearest neighbours correlate with total energy. This may be a good assumption particularly in the high-temperature limit. Further, we assume that the three-spin term in Eq. (2.44) can be neglected. In this case, Eq. (2.44) results in

$$\left[\mathcal{A}_{n,n-1}^{\dagger}\mathcal{A}_{n,n-1}\right]_{\text{diag}}(E) = \frac{1}{4} - \frac{1}{2}\cos(\vartheta_n)\cos(\vartheta_{n-1})\frac{E}{E_{\max} - E_{\min}}, \qquad (2.54)$$

where $E_{\max} = \frac{J_z N_s}{4}$ and $E_{\min} = -\frac{J_z N_s}{4}$. The application of the expression in Eq. (2.54) leads to the same kind of narrowing of $g(E)$ as Eq. (2.28).

Let us now briefly sketch the derivation of Eq. (2.54). For the nearest-neighbour Ising model with Hamiltonian (2.52), the total energy of the system is a function of the number of parallel and anti-parallel spin-pairs

$$\langle S_{nz}S_{(n-1)z}\rangle = \frac{\langle\left(S_z S_{(n-1)z}\right)_{\text{tot}}\rangle}{N_s} = -\frac{E}{N_s J_z} = -\frac{1}{2}\frac{E}{E_{\max} - E_{\min}}. \qquad (2.55)$$

With $\langle S_n S_{n-1}\rangle = \langle S_{n-1}S_n\rangle = \langle S_{nz}S_{(n-1)z}\rangle\cos(\vartheta_n)\cos(\vartheta_{n-1})$, the nearest-neighbour spin correlation function for the Ising model in the non-ordered (paramagnetic) phase reads

$$\frac{1}{2}\left[\{S_n(t_n - t_{n-1}), S_{n-1}(0)\}\right]_{\text{diag}}(E) = \frac{1}{2}\cos(\vartheta_n)\cos(\vartheta_{n-1})\frac{E}{E_{\max} - E_{\min}}. \qquad (2.56)$$

Given Eq. (2.44), this leads to Eq. (2.54) when neglecting the three-spin term. This concludes our derivation.

2.5.3   Interacting spins in a magnetic field

Now, we consider the effect of local measurements for a general spin lattice with a short-range interaction in an external magnetic field. We expect in this case that a local measurement, whose possible outcomes correlate with the total energy of the system, would have a narrowing effect comparable to that of the single-spin measurement for Hamiltonian (2.27). The effect is to be describable by Eq. (2.21) with the cutting functions $[\mathcal{P}_n]_{\text{diag}}(E)$ expressed in terms of appropriate projection operators. These functions are, in general, not linear in E, but

$$\left|\frac{d\left[\mathcal{P}_n\right]_{\text{diag}}(E)}{dE}\right| \sim \frac{1}{\epsilon_1 N_s}, \qquad (2.57)$$

meaning that the estimate (2.41) for the ensemble-narrowing time and the argument for the proximity of the canonical ensemble to the absolute stability threshold remain valid.

Let us for a moment also consider a more general spin Hamiltonian. We define the k-local spin Hamiltonian as

$$\mathcal{H}_k = \sum_i \mathcal{H}_{k,i}, \qquad (2.58)$$

where each operator $\mathcal{H}_{k,i}$ involves k spin operators. For example, the Hamiltonian (2.27) for

a spins in an external magnetic field is a 1-local Hamiltonian, and the Hamiltonian (2.52) for the Ising model is a 2-local Hamiltonian. Such k-local Hamiltonians are often used in the quantum complexity theory.

For a spin system with a k-local Hamiltonian, the measurement outcomes of k measurements of single spins within a sufficient short time interval are normally correlated with the total energy of the system. The measurement outcomes of less than k measurements are, in general, not correlated with the total energy of the system.

In the definition (2.58), the k spin operators entering the terms $\mathcal{H}_{k,i}$ are not constrained to a spatially localised subsystem. For physical systems, though, the set of k spin operators for each $\mathcal{H}_{k,i}$ is usually confined to small subsystems in the three-dimensional physical space. Therefore, the measurement outcomes of k measurements correlate with total energy when the measured spins also lie within a small subsystem.

2.6   Discussion and summary of results

Before summarising, let us first make the following two remarks.

1. According to our stability criterion, ensembles with broad $g(E)$ are not stable. In particular, the QMC ensemble [19] introduced in Sec. 1.1.4 is not stable with respect to local measurements, because it implies a broad $g(E)$. In particular, the energy distribution for small subsystems has the form of two widely separated peaks corresponding to $T = 0$ and $T = \infty$ respectively [19].

2. Experiments aiming at protecting unconventional statistical ensembles for finite spin systems should avoid: (i) external magnetic fields, (ii) long-range order, (iii) local constants of motion. Effectively, each of the above points increase the measurement frequency and thereby decrease the lifetime of a statistical ensemble.

Let us now conclude by summarising the results of this chapter. First, we formulated a stability criterion for statistical ensembles describing macroscopic systems which is suitable for a broad range of many-body systems. An ensemble is called "stable" when a small number of local measurements cannot significantly modify the probability distribution of the total energy of the system. We applied this stability criterion to lattices of spins-$\frac{1}{2}$ and analytically derived relations which describe the effect of local measurements on the probability distribution of the total energy $g(E)$. The results are somewhat non-intuitive as, for example, that the cutting function $[\mathcal{P}_n]_{\mathrm{diag}}(E)$ for spins in a magnetic field is a linear function of the total energy E.

Further, we have shown that even relatively rare local measurements impose strict constraints on quantum statistical ensembles. Quantum statistical ensembles characterised by $g(E)$ which is significantly broader than that of a canonical ensemble are unstable. In contrast, quantum statistical ensembles characterised by $g(E)$ having a width which is of the same order as that of the Gibbs distribution are nearly stable in its absolute sense; namely, for this width, the broadening effect and the narrowing effect compensate each other.

The above results justify the use of statistical ensembles with narrow $g(E)$ for equilibrium description of macroscopic systems. Provided that a quantum system is prepared in a quantum state corresponding to a broad $g(E)$, this quantum state will be modified in a rather short time interval during which $g(E)$ becomes significantly narrower. Typically, the lifetime of broad $g(E)$ is short to such extent that a narrow $g(E)$ can be assumed for all practical calculations.

The analytical treatment of lattices of spins-$\frac{1}{2}$ presented in this chapter is based on derivations which involve system-specific mathematical techniques such that the results may be not applicable beyond spin lattices. However, the basic concept of the stability of statistical ensembles can be applied to all physical systems in principle. Moreover, we are confident that similar results as that described above may also be obtained for other systems, for example systems with mechanical degrees of freedom.

Chapter 3

Numerical Investigation of the Stability of Quantum Statistical Ensembles

In this chapter, we numerically investigate the stability of quantum statistical ensembles for lattices of interacting spins-$\frac{1}{2}$. The motivation for this study is to test the analytical results of the previous chapter. There, we were able to derive a relation describing the modifications of $g(E)$ due to local measurements for spins in a magnetic field and for the Ising model in the high-temperature regime. We have also made estimates for general interacting systems which are difficult to treat analytically. The aim of this chapter is, therefore, to simulate interacting spins systems and to compare the numerical results with the expectations from the analytical treatment.

In our numerical approach, we employ the property of quantum systems known as quantum typicality[1]. Quantum typicality means that, for quantum systems of increasing size, each wave function with a given energy distribution $g(E)$ behaves in an increasingly typical manner. If we draw wave functions with a given $g(E)$ at random, the system exhibits locally the same behaviour for almost all wave functions. Therefore, it seems as if the properties of the system are governed by $g(E)$. This is why, we can identify a randomly chosen wave function with its energy distribution $g(E)$. By repeating the numerical simulation for different initial wave functions each of which corresponds to the given $g(E)$, we obtain the stability of $g(E)$.

Before going into details, let us make a few remarks about the system sizes that are available in numerical investigations on modern computers. The results of the previous chapter were derived for macroscopic systems with the number of spins being $N_s \sim 10^{23}$. In numerical calculations, though, these system sizes are not accessible without resorting to semi-classical or classical approximations. Since we do not make such approximations here, we are limited to system sizes of $N_s \lesssim 24$ which are microscopic.

The limitation to $N_s \lesssim 24$ is due to the following reasons. The Hilbert space of N_s

---

[1]We already encountered a special case of quantum typicality, namely canonical typicality introduced in Sec. 1.1.2.

spins has the dimension 2^{N_s} and, hence, the wave function of the system, when written as a vector, has 2^{N_s} complex entries or, equivalently, $2 \cdot 2^{N_s}$ real entries. A real entry in double precision occupies 8 bytes (64 bits) of memory. Thus, for the storage of a single wave function, $8 \cdot 2 \cdot 2^{N_s}$ bytes are needed, which, for $N_s = 25$, amounts to 512 MB and, for $N_s = 30$, to 16 GB. It is noteworthy, hereby, that the wave function should be preferably stored in the primary storage, not on the hard disk. Therefore, when it comes solely to storing the wave function, we are limited to $N_s \lesssim 35$ with modern computers. Moreover, in order to manipulate this wave function, one needs much more storage. This leads to a further limitation for the system sizes.

In principle, the above storage limitations can be circumvented by employing appropriate numerical techniques. This includes, for example, the parallelisation of the algorithm and the implementation of sparse matrices and vectors which we describe below. However, even with the best computational architectures and algorithms available today, we are still limited to microscopic system sizes.

In this chapter, we show that the numerical results are in a *qualitative agreement* with the analytical expectations. This applies to all effects of local measurements analysed in the previous chapter: the broadening, narrowing and the heating effects. In the following, we first describe the methods that we use in our numerical approach and briefly discuss the individual routines. Later, we investigate the finite-size effects and, finally, study the stability of a two-peak $g(E)$.

3.1 Methods for the numerical calculations

One possible method to simulate quantum systems, is to diagonalise the Hamiltonian matrix and, thereby, obtain the energy eigenstates and the energy eigenvalues. Then, after expanding the initial wave function in the energy eigenbasis, the time evolution of the system amounts to manipulating the phases of the quantum amplitudes. However, the diagonalisation of large matrices is a rather time consuming procedure. Therefore, the diagonalisation method is limited to system sizes of $N_s \lesssim 20$ on modern computer architectures. Since we would like to reach still larger N_s, we use methods which do not rely on the diagonalisation.

Our algorithm consists of the following four main blocks:

1. Initialisation of the wave function with a given energy distribution $g(E)$,

2. Time evolution of the wave function and repeated local measurements,

3. Calculation of $g(E)$ from a given wave function,

4. Calculation of a stability measure.

In this section, we describe the necessary methods for the realisation of these blocks.

Before starting, we define the *Ising basis* which we will often refer to in the following. The elements of this basis are the product states $|\psi\rangle = |\uparrow\rangle_1|\uparrow\rangle_2|\downarrow\rangle_3|\uparrow\rangle_4 \cdots$, where $|\uparrow\rangle_i$ and $|\downarrow\rangle_i$ are the eigenstates of the spin operator in the z-direction for the lattice site i. Below, we simplify the notation by identifying $|\uparrow\rangle_1|\uparrow\rangle_2|\downarrow\rangle_3|\uparrow\rangle_4 \cdots = |\uparrow\uparrow\downarrow\uparrow\rangle \cdots$.

3.1.1 Structure of the Hamiltonian matrix

We consider one-dimensional lattices of spins-$\frac{1}{2}$ with nearest-neighbour interaction. The Hamiltonian is

$$\mathcal{H} = -\sum_{i<j} \left[J_{ij}^x S_{ix} S_{jx} + J_{ij}^y S_{iy} S_{jy} + J_{ij}^z S_{iz} S_{jz} \right] - \sum_j H_j S_{jz}, \qquad (3.1)$$

where J_{ij}^x, J_{ij}^y and J_{ij}^z are the coupling coefficients between sites i and j, and H_j is the magnetic field into the z-direction at lattice site j. In principle, the spin lattice can be of any dimension, but, in our simulations, we consider one dimensional lattices. We assume that the results obtained do not depend essentially on the dimensionality of the lattice. For simplicity, we always consider periodic boundary conditions.

The energy of the spin systems is bounded not only from below but also from above. We denote the minimal energy, or the ground state energy, as $E_{\min}$ and the maximal energy as $E_{\max}$. The difference $E_{\max} - E_{\min}$, we call the spectral width. Due to the existence of a maximal energy, negative temperatures can be defined in analogy to the usual definition of (positive) temperatures, cf. Eq. (3.6), [69, 10].

Block-diagonal form of the Hamiltonian

When working with large matrices, as for example the spin Hamiltonian matrix, a significant advantage is if this matrix can be written in a block-diagonal form as indicated in Fig. 3.1. In particular, the advantage of such a form is that the individual blocks can be dealt with independently. Moreover, if we think of matrix manipulations in general, the number of individual scalar multiplications approximately scales as D^2, where D is the dimension of the matrix. If the matrix can be written in a block diagonal form with m blocks of average dimension $\frac{D}{m}$, then the number of individual scalar multiplications for matrix manipulations approximately scales as $m \left(\frac{D}{m} \right)^2 = \frac{1}{m} D^2$ instead of D^2. Thus, the number of individual scalar manipulations is reduced by the factor $\frac{1}{m}$. Moreover, a block-diagonal form allows for working with each individual block on different computers in parallel.

Now, we make a physically natural, yet very important choice that guarantees that $\mathcal{H}$
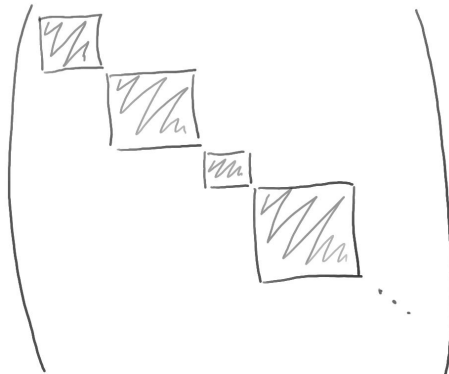

Figure 3.1: An illustration a matrix with block structure. The shaded area indicates non-zero matrix elements.
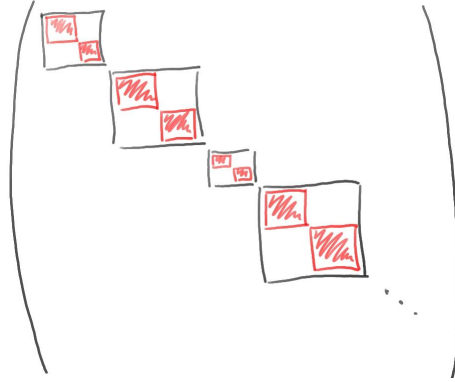
Figure 3.2: An illustration of a matrix with finer block structure than that in Fig. 3.1. The shaded area indicates the non-zero matrix elements.

can be written in a block-diagonal form with N_s blocks: *We choose the Hamiltonian $\mathcal{H}$ to be translational invariant.* The proof that translational invariance indeed leads to a block-diagonal form is given in Appendix B.1. For the Hamiltonian in Eq. (3.1), translational invariance means in particular

$$
\begin{aligned}
J_{ij}^x &= J^x(\vec{r}_i - \vec{r}_j) & (3.2) \\
J_{ij}^y &= J^y(\vec{r}_i - \vec{r}_j) & (3.3) \\
J_{ij}^z &= J^z(\vec{r}_i - \vec{r}_j) & (3.4) \\
H_j &= H, & (3.5)
\end{aligned}
$$

where $\vec{r}_i$ is the position of the i-th lattice site. The transformation to a block diagonal form corresponds to a change of the Hilbert-space basis.

Beside the translational invariance, the Hamiltonian $\mathcal{H}$ in Eq. (3.1) also conserves the quantity $[N_\downarrow \mod 2]$, where $N_\downarrow$ is the number of spins down in z-direction. $N_\downarrow$ is well defined, for example, for the states of the Ising basis. If we choose an Ising state $|\psi_\text{o}\rangle$ with an odd number of spins down and $|\psi_\text{e}\rangle$ with an even number of spins down, the corresponding matrix element of $\mathcal{H}$ is guaranteed to be $\langle\psi_\text{e}|\mathcal{H}|\psi_\text{o}\rangle = 0$.

Since the conservation of $[N_\downarrow \mod 2]$ is compatible with the translational invariance, this symmetry leads to a further splitting of each block into two smaller blocks as illustrated in Fig. 3.2. In Appendix B.2, we show that $\mathcal{H}$ in Eq. (3.1) indeed conserves the quantity $[N_\downarrow \mod 2]$. The translational invariance together with the conservation of $[N_\downarrow \mod 2]$ leads to the splitting of the Hamiltonian $\mathcal{H}$ into $2N_s$ blocks.

In principle, other symmetries of $\mathcal{H}$ which are compatible with the two above would lead to a further splitting into blocks as described above. Symmetries that are often encountered in similar calculations are: the rotational symmetry, the spin-inversion symmetry and the parity symmetry.

Sparsity of the Hamiltonian

Another feature of $\mathcal{H}$ which is helpful in numerical investigations is the sparsity. The overwhelming majority of matrix elements of $\mathcal{H}$ in the Ising basis is 0. From the viewpoint

of numerical calculations, sparsity of a matrix usually makes matrix manipulations faster and one needs less storage[2]. In Appendix B.3, we show that $\mathcal{H}$ is indeed sparse in the Ising basis and that, furthermore, when $\mathcal{H}$ is written in the basis that leads to the block structure, each reduced block is also sparse. In addition, one needs to store either the upper or the lower half of $\mathcal{H}$ including the diagonal elements since the Hamiltonian matrix is Hermitian[3].

3.1.2 Preparation of the initial energy distribution

Since we do not diagonalise the Hamiltonian, we are somewhat limited in the choice of the initial energy distribution associated with the initial wave function. We prepare the Gibbs distribution and any superpositions thereof by employing the so-called *imaginary-time propagation method*. In principle, this method is based on following the relation between the time evolution operator and the Boltzmann-Gibbs factor

$$e^{-\beta\mathcal{H}}|\psi\rangle = e^{-i\mathcal{H}t}|\psi\rangle, \tag{3.6}$$

where $t = -i\beta$.

In practice, this corresponds to the following procedure. We first prepare the Gibbs distribution in the infinite temperature limit by random sampling. Details of this sampling are given in Appendix B.4. The infinite temperature limit corresponds to an equal occupation probability for all energy eigenstates. Next, we apply the operator $e^{-\beta\mathcal{H}}$ to the corresponding wave function $|\psi\rangle$ by employing the relation (3.6), cf. [88]. In this way, we reduce the preparation of the Gibbs distribution to the time evolution of the wave function which we describe below.

We repeat our algorithm several times, where each time we initialise the wave function with a given energy distribution anew. By averaging the outcomes of all repetitions, we obtain result which do not depend on the particular realisation of the wave functions but only on the given energy distribution. With increasing system sizes, we need to make less repetitions in order to obtain good statistics. This is related to quantum typicality which we introduced above and, in particular to canonical typicality introduced in Sec. 1.1.1.

3.1.3 Time evolution of the wave function

Given that the Hamiltonian is time-independent, the quantum-mechanical time-evolution operator is

$$\mathcal{U}(\Delta t) = e^{-i\mathcal{H}\Delta t}. \tag{3.7}$$

Propagating the wave function $|\psi(t)\rangle$ by the time step Δt, therefore, amounts to

$$|\psi(t + \Delta t)\rangle = \mathcal{U}(\Delta t)|\psi(t)\rangle. \tag{3.8}$$

---

[2]In our numerical calculations, we used the numerical libraries GSL (GNU Scientific Library) and MKL (Math Kernel Library) which have special routines for sparse matrices and sparse vectors.

[3]A high degree of sparseness of the Hamiltonian allows for an alternative approach with a minimal demand for storage space, namely to build the Hamiltonian matrix each time anew without storing it. However, this alternative approach is less storage consuming at the expense of the computation time.

For a sufficiently small time step Δt, we can make a Taylor expansion of $\mathcal{U}(\Delta t)$ at $\Delta t = 0$, where the first terms provide a good approximation of $\mathcal{U}(\Delta t)$. We terminate the Taylor expansion of $\mathcal{U}(\Delta t)$ after the fourth-order term and obtain

$$\mathcal{U}(\Delta t) \approx 1 - i\mathcal{H}\Delta t - \frac{1}{2!}(\mathcal{H}\Delta t)^2 + i\frac{1}{3!}(\mathcal{H}\Delta t)^3 + \frac{1}{4!}(\mathcal{H}\Delta t)^4. \tag{3.9}$$

This fourth-order Taylor expansion is equivalent to the so-called fourth-order Runge Kutta method for solving linear differential equations with time-independent coefficients. Such an equation is the Schrödinger equation with a time-independent Hamiltonian. Therefore, we call the method using Eq. (3.9) the *Runge-Kutta method* in the following [86, 87].

It is the Runge-Kutta method which allows to avoid the diagonalisation of the Hamiltonian. According to Eq. (3.8), the time evolution of the wave function amounts to simple matrix-vector multiplications. Indeed, only matrix-vector multiplications are involved because the higher-order terms of $\mathcal{H}$ in Eq. (3.9) can be obtained by iteratively applying $\mathcal{H}$ to the wave function. Apart from that, the sparsity of the Hamiltonian makes these matrix-vector multiplications fast and less storage consuming[4].

Empirically, it was shown in [18] for a similar Hamiltonian that the Runge-Kutta method is stable and accurate enough for $\Delta t \leq \frac{0,02}{\overline{J}}$, where $\overline{J} \equiv \sqrt{J_x^2 + J_y^2 + J_z^2}$ is the r.m.s.-average of the coupling coefficients of the Hamiltonian. When applying the approximation (3.9) repeatedly, the error is bound by $|1 - \langle \psi_{\mathrm{rk}}(t)|\psi_{\mathrm{ex}}(t)\rangle| < 10^{-4}$ for $\overline{J}t \leq 50$ for interacting spin systems with $N_s = 20$, where $|\psi_{\mathrm{ex}}(t)\rangle$ is the propagated wave function without any approximations and $|\psi_{\mathrm{rk}}(t)\rangle$ is calculated using the Runge-Kutta method.

The implementation of the local measurements amounts to matrix-vector multiplications $\mathcal{P}|\psi\rangle$, where the projection operator $\mathcal{P}$ can be readily obtained by using the expression in Eq. (2.12). When written in the Ising basis, the matrix of the projection operator $\mathcal{P}$ is also sparse.

3.1.4 Retrieval of the final energy distribution

Given the wave function $|\psi(t')\rangle$, how to obtain the energy distribution of this wave function without knowing the energy eigenstates $|E_n\rangle$? We use the method shown in [34], which is based on the Fourier transform of the function $f(t) \equiv \langle \psi(t + t')|\psi(t')\rangle$. This function can be written as

$$f(t) = \langle \psi(t + t')|\psi(t')\rangle = \sum_j |c_j|^2 e^{-iE_j t}, \tag{3.10}$$

where $c_j = \langle E_j|\psi(t')\rangle$ and E_j are the energy eigenvalues. Now, calculating the Fourier transform of $f(t)$ yields

$$F(\omega) \equiv \int f(t)e^{i\omega t}dt \cong \sum_j |c_j|^2 \delta(\omega - E_j). \tag{3.11}$$

---

[4]When dealing with multiple matrix-matrix and matrix-vector multiplications in high-dimensional vector spaces, one needs to take care of the accumulating rounding error. In our algorithm, we made tests in order to make sure that we can neglect this source of error.

The left-hand site of this relation is proportional to the energy distribution corresponding to the wave function $|\psi\rangle$. Thus, in order to obtain the energy distribution $g(E)$, $F(E)$ must be normalised to 1.

In numerical calculations, $f(t)$ is a discrete time series. Therefore, a discrete Fourier transform must be applied to $f(t)$[5]. Moreover, $f(t)$ is also finite which implies that the result of the discrete Fourier transform is $F(\omega)$ multiplied by the Fourier transform of the window function. In order to achieve a good resolution for the energy distribution, we multiply $f(t)$ by the Kaiser-Bessel function before applying the discrete Fourier transform. In Appendix B.5, we present the Kaiser-Bessel function and provide further details for the procedure of the discrete Fourier transform.

3.1.5 Parallelisation of the algorithm

An important computational technique which is indispensable for reaching system sizes above $N_s \approx 20$ is parallelisation. This means that the total workload is distributed among several working units (processor with a local storage). Each working unit then solves a partial problem. A necessary requirement for an efficient parallelisation is that the total problem is reducible to smaller subproblems such that the individual working units can work mutually independent. If the working units often need to communicate between each other, this makes the process significantly slower[6].

The simulation of spin systems is suitable for parallelisation if the Hamiltonian can be written in a block-diagonal form. In such a case, each processor works with its own Hamiltonian block and operates with it on the wave function. In total, the following steps described above can be made by the processors mainly in parallel: the initialisation of the wave function, the propagation in time and the Fourier transform.

An exception hereby is the measurement process which, in general, does not respect the block diagonal structure of the Hamiltonian. Broadly speaking, a measurement induces transitions between individual blocks. This necessitates an extensive communication between the working units and noticeably slows down the calculation.

3.2 Finite-size effects with respect to local measurements

In this section, we investigate the finite-size effects with respect to local measurements. This investigation is particularly important because we expect the finite-size effects to be rather pronounced for microscopic system sizes. Since only microscopic systems can be simulated numerically, we need to asses the finite-size effects before investigating the more interesting narrowing effect.

The finite-size effects manifest themselves in a pronounced heating and the broadening of $g(E)$. For the macroscopic systems considered in the analytical treatment, we neglected these effects. In order to contrast the microscopic systems and the macroscopic systems

---

[5]In our numerical calculations, we used the numerical library FFTW, which employs the Fast Fourier Transform algorithm.

[6]In our numerical calculations, we used the OpenMPI library and the Intel MPI library.

treated analytically in Chapter 2, let us first recall the constraints that we imposed in our analytical investigation and check their applicability to microscopic systems.

In the analytical investigations, we neglected the heating effect by requiring

$$n \ll \sqrt{N_s}. \tag{3.12}$$

For the largest system sizes available in our numerical calculations $N_s = 24$, though, $\sqrt{24} \approx 5$. Therefore, the condition (3.12) is already not satisfied by the first measurement ($n = 1$).

Further, we considered $g(E)$ on a coarse-grained energy axis in Chapter 2. The corresponding width of the energy bins Δ_e satisfies the two constraints given in Eq. (A.33) that we repeat here for the sake of convenience

$$\epsilon_1 \ll \Delta_e \ll T(E_{av})\sqrt{C_V(E_{av})}, \tag{3.13}$$

where ϵ_1 is a suitably chosen one-particle energy and $T(E_{av})\sqrt{C_V(E_{av})}$ is the width of the Gibbs distribution at temperature T. For the system sizes available in numerical calculations, the constraints in Eq. (3.13) cannot be satisfied by an appropriately chosen Δ_e because the basic constraint $\epsilon_1 \ll T(E_{av})\sqrt{C_V(E_{av})}$ is already not satisfied. This means that the results obtained in the previous chapter cannot be directly applied to the systems investigated numerically.

The above results imply that we need to find new ways in order to suppress the finite-size effects. Coarse-graining of the energy axis as well as requiring $n \ll \sqrt{N_s}$, does no work for microscopic systems.

3.2.1 The heating effect

In order to study the heating effect, we consider the quantity[7] $\frac{E_{av,n} - E_{av,0}}{\Delta_{sw}}$ as a function of n, where $E_{av,n}$ is the average energy after n measurements, $E_{av,0}$ is the initial average energy and $\Delta_{sw} \equiv E_{max} - E_{min}$ is the spectral width. The quantity $\frac{E_{av,n} - E_{av,0}}{\Delta_{sw}}$ is, therefore, the deviation of the average energy from its initial value on the scale of the spectral width. The results are shown in Fig. 3.3.

In order to obtain the results shown in Fig. 3.3, we consider one-dimensional spin systems of different sizes with nearest-neighbour interaction. The Hamiltonian is given in Eq. (3.1) with the following parameters

$$J_x = 0.47 \quad J_y = -0.37, \quad J_z = -0.79, \quad H = 0, \tag{3.14}$$

which satisfy $J_x^2 + J_y^2 + J_z^2 = 1$. The initial state of the system is a wave function with a Gibbs energy distribution of inverse temperature $\beta = 10$. For the measurements, the spins are chosen randomly and the measurement axes are also chosen randomly. The time delay between the measurements is 1. The results shown are averaged over many iterations[8].

---

[7]We do not need to consider the absolute value of energy difference $|E_{av,n} - E_{av,0}|$ because the heating effect makes $E_{av,n}$ drift towards values corresponding to larger entropy. The opposite process is very unlikely.

[8]The results obtained are averaged over the following numbers of independent calculations $N_s = 16$: 100, $N_s = 17$: 100, $N_s = 18$: 100, $N_s = 19$: 100, $N_s = 20$: 100, $N_s = 21$: 87, $N_s = 22$: 83, $N_s = 23$: 45,
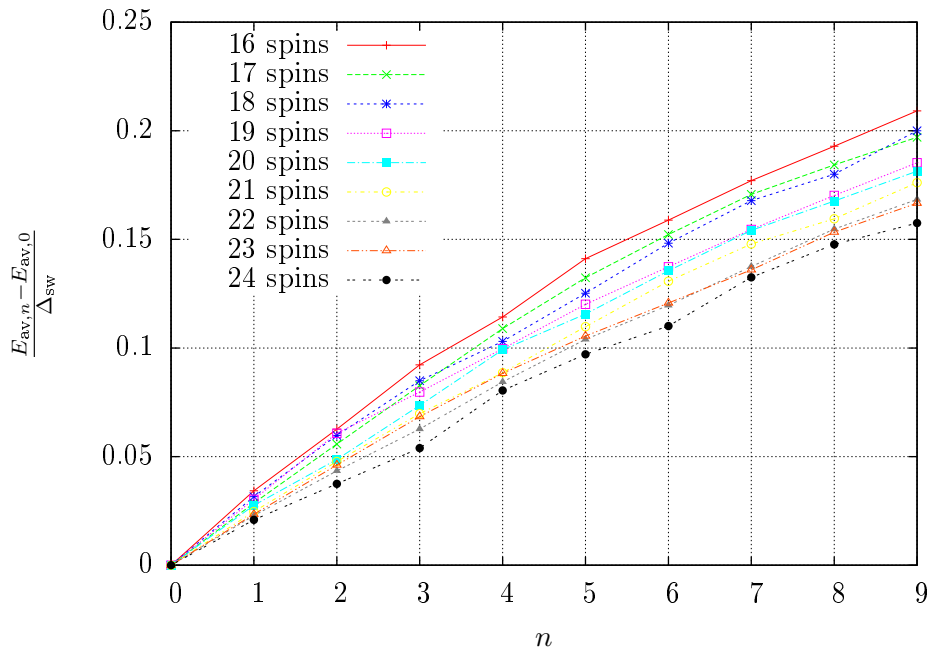
Figure 3.3: The quantity $\frac{E_{\mathrm{av},n} - E_{\mathrm{av},0}}{\Delta_{\mathrm{sw}}}$ is shown for interacting spin systems of different system sizes as indicated in the legend. The plotted values have been averaged over many iterations. The points are connected by a line in order to guide the eye. See text for further details.

Figure 3.4: The function $\frac{w_{g,n} - w_{g,0}}{\Delta_{\mathrm{sw}}}$ is shown for interacting spin systems of different system sizes as indicated in the legend. The plotted values have been averaged over many iterations. The points are connected by a line in order to guide the eye. See text for further details.
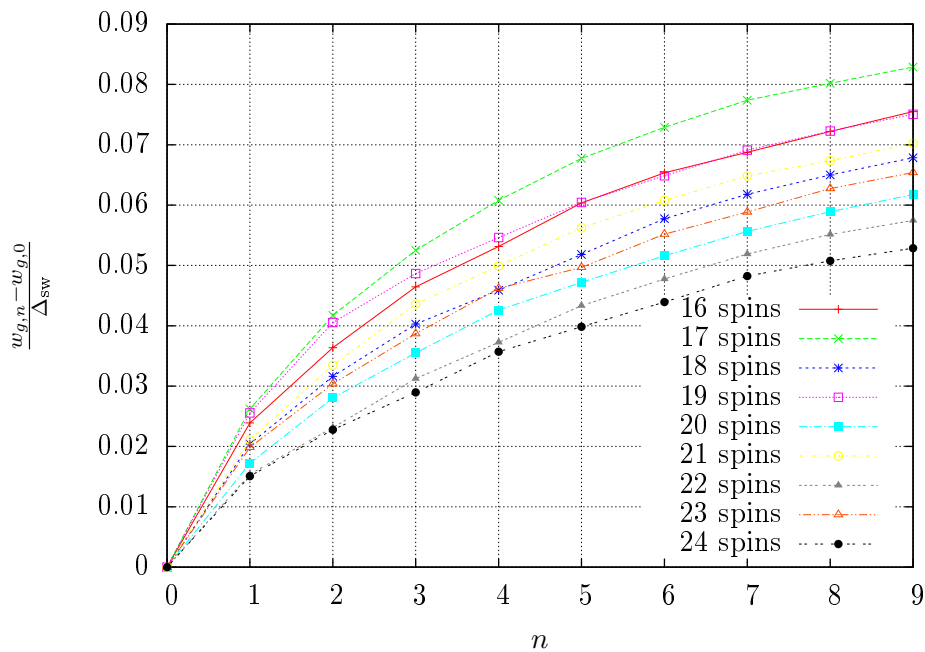

$N_s = 24$: 19.

The results in Fig. 3.3 show that the deviation of the average energy is significant. For smaller system sizes ($N_s = 16$), the deviation after 9 measurements amounts to $E_{\mathrm{av},14} - E_{\mathrm{av},0} \approx 0.2\Delta_{\mathrm{sw}}$. Especially important is that, for $n = 1$, the deviation is approximately $E_{\mathrm{av},1} - E_{\mathrm{av},0} \approx 0.025\Delta_{\mathrm{sw}}$ for all system sizes which is significant as well. Although the deviation of $E_{\mathrm{av},n}$ is slower for larger system sizes, it remains of the same order.

Let us now compare the results shown in the figure with the analytical estimates. In Chapter 2, we showed that evolution of $E_{\mathrm{av},n}$ can be approximately described as $E_{\mathrm{av},n} \approx E_{\mathrm{av},n-1} + \epsilon_1$, where $\epsilon_1 = \frac{\Delta_{\mathrm{sw}}}{N_s}$ is the single-spin energy. This leads to $\frac{E_{\mathrm{av},1} - E_{\mathrm{av},0}}{\Delta_{\mathrm{sw}}} \approx \frac{\epsilon_1}{\Delta_{\mathrm{sw}}} = \frac{1}{N_s}$. For the system sizes considered in the numerical calculations, $\frac{1}{N_s} \approx 0.06$ for $N_s = 16$ and $\frac{1}{N_s} \approx 0.04$ for $N_s = 24$. These values are of the same order as that in Fig. 3.3, where $\frac{E_{\mathrm{av},1} - E_{\mathrm{av},0}}{\Delta_{\mathrm{sw}}} \approx 0.025$ on average. Therefore, the numerical results are consistent with the analytical estimates. In the macroscopic limit, the heating can be neglected as stated in Chapter 2.

3.2.2 The broadening effect

Another manifestation of the finite-size effects is the broadening of $g(E)$. The broadening occurs due to the off-diagonal elements of the measurement operators when written in the energy basis. In Fig. 3.4, we show $\frac{w_{g,n} - w_{g,0}}{\Delta_{\mathrm{sw}}}$ as a function of n, where $w_{g,n}$ is the width of $g(E)$ after n measurements. All parameters of the calculations are the same as that for Fig. 3.3.

The results in Fig. 3.4 show that the broadening effect is rather pronounced. The broadening shows a dependence on the parity of N_s. For even N_s, the broadening is less pronounced than for comparable even N_s. However, the overall tendency is that the broadening occurs slower for larger systems.

Let us also compare these results with the analytical estimates. Using the relation $w_{g,n}^2 \approx w_{g,n-1}^2 + \epsilon_1^2$ and neglecting the initial width, we obtain after the first measurement $\frac{w_{g,1} - w_{g,0}}{\Delta_{\mathrm{sw}}} \approx \frac{1}{N_s}$ which is on the average 0.05 as we have seen above. This result is in agreement with the computed result which is about 0.02 on the average. In the macroscopic limit, the broadening can be neglected as stated in Chapter 2.

In Appendix B.6, we illustrate examples of the finite-size effects.

3.2.3 Introduction of a two-peak energy distribution

The above results imply that we cannot neglect neither the heating nor the broadening effect in our numerical simulations. Even after the first measurement, both effects turn out to be rather pronounced. An important result, though, is that the finite-size effects become smaller for an increasing N_s. In contrast, the narrowing effect is independent of N_s. Therefore, the narrowing effect dominates for larger system sizes, in particular for the macroscopic systems.

In order to minimise the finite-size effects for the microscopic systems, we limit our further numerical investigations to a two-peak $g(E)$. The width of individual peaks of this $g(E)$ is smaller than the distance between the peaks. As long as the two peaks do not overlap, we can distinguish between a two-peak $g(E)$ and a one-peak $g(E)$. Here, the

evolution of ΔG is still strongly influenced by the heating and the broadening. Nevertheless, one can at least observe qualitatively the disappearance of one of the two peaks, as expected in the macroscopic limit.

In practice, we prepare such two-peak $g(E)$ by coherently superposing two wave functions exhibiting the Gibbs energy distribution with two different temperatures. We choose the inverse temperatures $\beta_1 = 10$ and $\beta_2 = -10$.

3.3 Results of the numerical investigation for a two-peak energy distribution

In this section, we present the results of our numerical investigations of the stability of a two-peak $g(E)$. First, we give an example by explicitly showing the effect of 10 measurements on a given wave function corresponding to a two-peak $g(E)$. Then, we investigate the evolution of the stability measure $\overline{\Delta G}(n)$ introduced in the previous chapter. Finally, we discuss other possible measures of stability and study their evolution as a function of n.

3.3.1 Example: Evolution the energy distribution

Before studying the average evolution of the stability measures, let us focus on a particular example. We show the individual $g_n(E)$ after each local measurement in order to illustrate possible individual realisations. We choose the initial two-peak $g(E)$ by coherently superposing two wave functions exhibiting the Gibbs energy distributions with temperatures $\beta_1 = +10$ and $\beta_2 = -10$.

The Figures 3.5, 3.6 and 3.7 show $g_n(E)$ after the individual measurements as indicated in the figures. On the horizontal axis, the energy per spin is given, where the minimal and maximal energies per spin approximately correspond to $E_{\min} = -0.22$ and $E_{\max} = 0.28$, respectively. Dots which lie outside the energy interval $[E_{\min}, E_{\max}]$ can be ignored because there are no states available or, equivalently, $\nu(E) = 0$ in this region.

The parameters for the calculation are as follows. The Hamiltonian of the system with nearest-neighbour interaction is given in Eq. (3.1) with the parameters given in Eq. (3.14). Additionally, we switched on a small magnetic field along the z-direction $H = 0.05$. We measure 10 spins in pairs which means that the first and the second measured spins are neighbours, the third and fourth spins are the same, and so forth. The time delays between individual measurements were randomly chosen from the interval $[0, 2]$. For each measurement, the measurement axis is the z-axis which is the direction of the largest coupling coefficient. We chose to measure spin-pairs along the direction of the strongest interaction in order to accelerate the narrowing effect of measurements and to keep the broadening and heating as small as possible. In principle, a measurement of a spin-pair along the same axis could also occur accidentally. However, we would need to wait many measurements in order for such measurement configuration to occur accidentally. Therefore, the broadening and heating would be rather pronounced. Aside from that, if we would measure along another fixed axis, the same narrowing process would normally take place but the process would be slower.
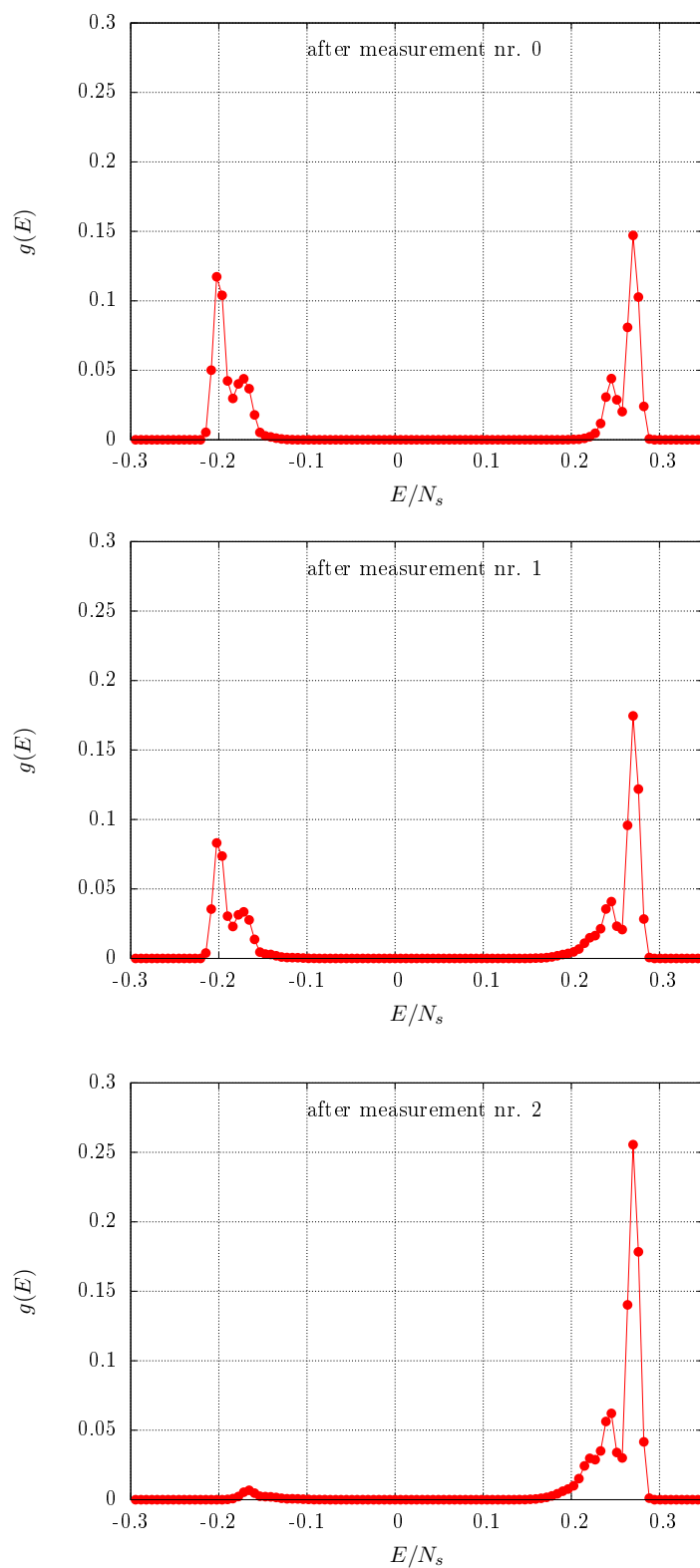
Figure 3.5: The distribution $g(E)$ is shown after each single-spin measurement for an initial two-peak $g(E)$ given in the first figure. The horizontal axis shows the energy per spin. The results are indicated by the dots which are connected by a line in order to guide the eye. Details of the calculation are given in the text.
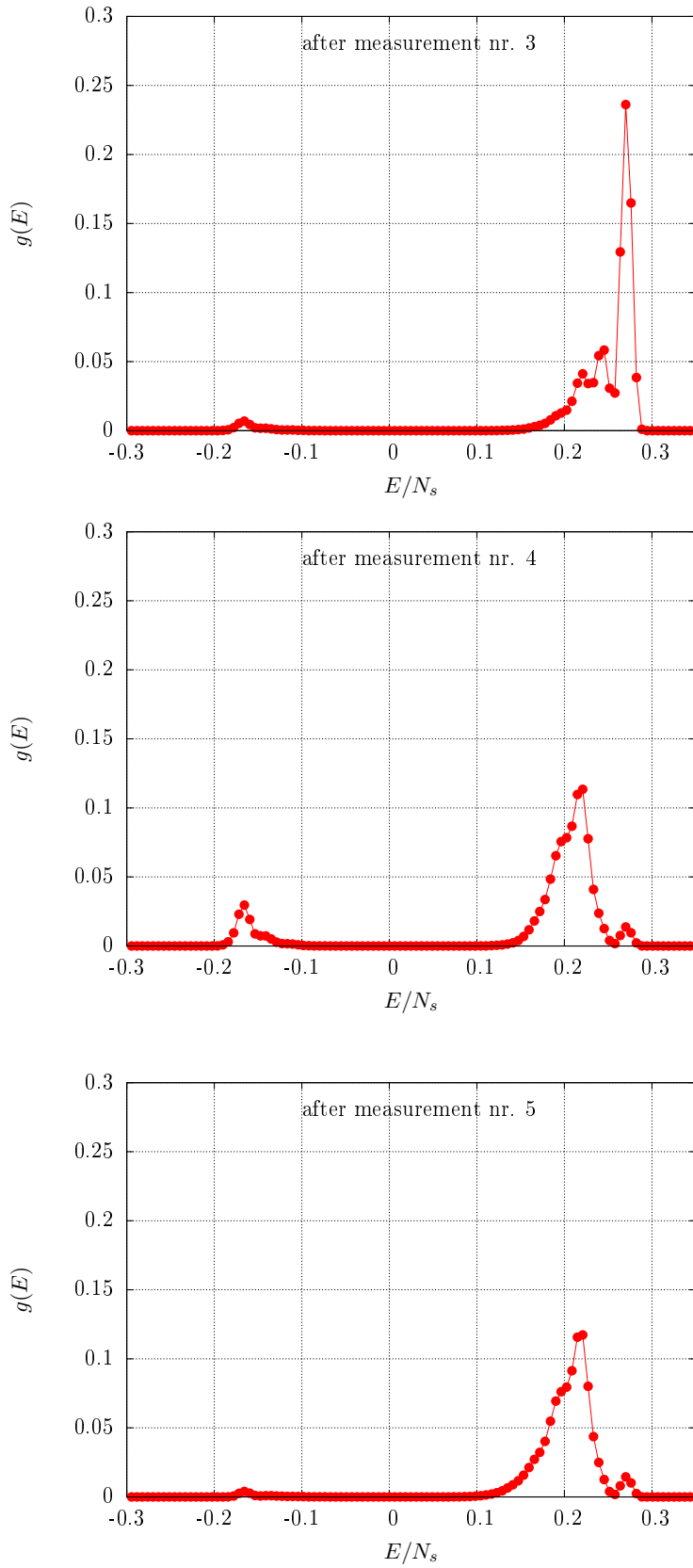
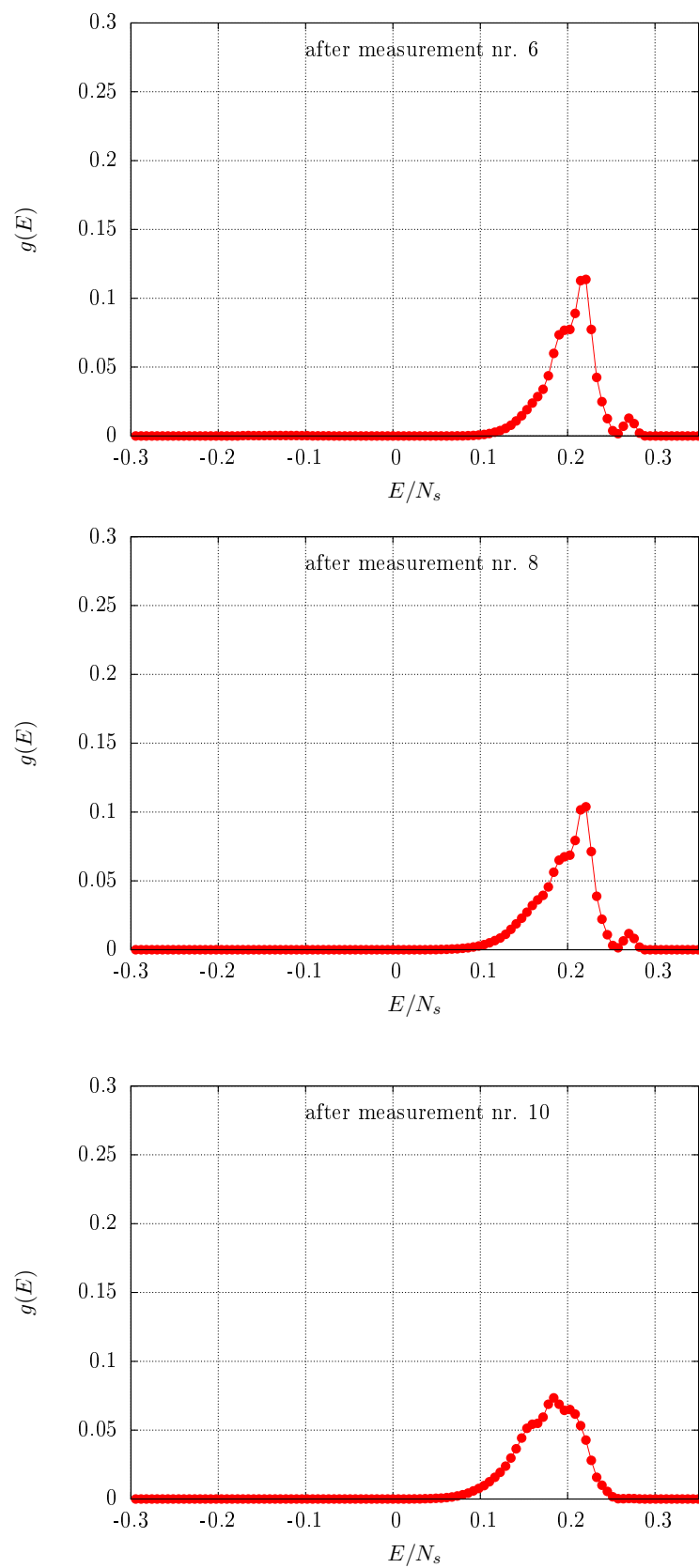Figure 3.6: Continuation of the figure on the previous page.

Figure 3.7: Continuation of the figure on the previous page.

Let us now have a closer look at the results in Fig. 3.5. The distribution $g(E)$ hardly changes after the first measurement but, after the second measurement, $g(E)$ changes significantly. This is consistent with the qualitative understanding that, for interacting systems, only the outcomes of spin-pair measurements are correlated with the total energy E. Consequently, the narrowing effect of spin-pair measurements is much stronger than that of single-spin measurements. In the figures, this is reflected by the fact that the modifications of $g(E)$ are stronger after measurements with an even number. Small modifications of $g(E)$ after measurements with odd numbers are due to the small external magnetic field ($H = 0.05$) and other possibly accidental weak correlations.

The outcome of the first spin-pair measurement favours energies which correspond to the peak at higher energies (right peak)[9]. Therefore, the right peak acquires a larger statistical weight than the left peak after $n = 2$. In contrast, the outcome of the second spin-pair measurement ($n = 4$) in Fig. 3.6, favours energies corresponding to the peak at lower energies (left peak). This process, where the effect of the subsequent measurement is opposite to the effect of the prior measurement, is possible in principle. However, such a reversed process is less probable because the probabilities for the outcomes of subsequent measurements are given by the post-measurement $g(E)$.

Finally, after the sixth individual measurement ($n = 6$), i.e, third spin-pair measurement in Fig. 3.7, the left peak becomes completely suppressed. For later measurements, it is rather improbable for the left peak to reappear again. In this sense, the effect of multiple measurements is effectively irreversible. Therefore, the main effects that take place after the third spin-pair measurement, are the heating and the broadening. These two processes correspond to the finite-size effect investigated in the previous section.

Let us now check the consistency between numerical and analytical results. The variance w_g^2 increases due to the broadening effect approximately according to the relation $w_{g,n}^2 \approx w_{g,0}^2 + n\epsilon_1^2$, cf. Sec. A.1. If we consider the energy distribution after the 10th measurement and neglect the initial variance, we obtain $w_{g,10} \approx \sqrt{10}\epsilon_1 \approx 3\epsilon_1$. Assuming that $\epsilon_1 \approx 1$, we obtain for the width $w_{g,10} \approx 3$ which leads to $\frac{w_{g,10}}{N_s} = \frac{3}{20} \approx 0.1$. This approximately corresponds to the width of the peak in the figure after the 10th measurement.

It is also noteworthy that the right peak exhibits a substructure which is a splitting of the peak into two narrow ones. This structure is due to an energy gap of the spectrum for the given Hamiltonian in Eq. (3.1) with the parameters in Eq. (3.14). The reason for this energy gap is the small magnetic field, which lifts the near degeneracy between the high-energy ferromagnetic states $|\uparrow\uparrow\uparrow \cdots\rangle$ and $|\downarrow\downarrow\downarrow \cdots\rangle$. As a result, the energy gap between these states is of the order HN_s and the energy gap in units "energy per spin" is of the order H. This estimate is consistent with the numerical results.

---

[9]The individual measurement outcomes were as follows: measurement 1: spin at site 3 is up, measurement 2: spin at site 4 is up, measurement 3: spin at site 1 is up, measurement 4: spin at site 2 is down, measurement 5: spin at site 18 is up, measurement 6: spin at site 19 is up, measurement 7: spin at site 14 is up, measurement 8: spin at site 15 is up, measurement 9: spin at site 17 is up, measurement 10: spin at site 18 is down.

3.3.2   Evolution of the stability measure $\Delta G(n)$

In this section, we investigate the stability of a two-peak $g(E)$ on the basis of the stability measure $\Delta G(n)$ introduced in Eq. (2.6). In order to do this, we directly simulate interacting spin systems of different sizes $16 \leq N_s \leq 24$[10]. The Hamiltonian is given in Eq. (3.1) with the parameters in Eq. (3.14).

The initial wave function is again a coherent superposition of two states corresponding to Gibbs energy distributions. The inverse temperatures are $\beta_1 = 10$ and $\beta_2 = -10$, cf. Sec. 3.1.2. After the preparation of the wave function, we first calculate the initial energy distribution $g_0(E)$ and then measure spin-pairs. For the measurement procedure, we randomly choose a spin pair and measure it with a random time delay chosen from the time interval $[0, 2]$. After each measurement, we calculate the energy distribution $g_n(E)$[11].

The measurement axes were chosen randomly for each individual measurement. This is different from the setting in the previous section, where the measurement axis was fixed along the z-axis. The reason for this choice is that a random measurement axis better resembles the process of random measurements mediated by environmental particles. The correlation between the outcome of a spin-pair measurement and the total energy E is particularly strong, if the spin-pair is measured along the same axis. When choosing the measurement axis randomly, such a measurement configuration may occur once per three spin-pair measurements. Therefore, the two-peak $g(E)$ is not always reduced to a single-peak $g(E)$. When averaging over many iterations, one should, therefore, keep in mind that, for a fraction of iterations, the measurements lead to the suppression of one peak while, for another fraction of iterations, both peaks survive until the last measurement[12].

The evolution of $\overline{\Delta G}(n)$ is shown in Figure 3.8. For the sake of convenience, we recall its definition[13]

$$\Delta G(n) \equiv \int_{-\infty}^{+\infty} |g_n(E) - g_0(E)| \, dE. \tag{3.16}$$

Since the main effect of the measurements is the suppression of one peak of $g_0(E)$, $\overline{\Delta G}(n)$ grows monotonically with n in Fig. 3.8. The complete suppression of one peak without any further modifications of $g(E)$ leads to $\Delta G(n) = 1$. Therefore, $\overline{\Delta G}(n)$ must satisfy

---

[10]In principle, we could extend our calculations to larger spin systems because, for $N_s = 24$, we did not reach the limitations due to the requirements for storage space. However, the time needed for gathering enough statistics is rather long. For example, the time needed to build the Hamiltonian for $N_s = 24$ approximately amounts to one hour, and the time for conducting 9 measurements including the calculation of intermediate energy distributions amounts to 2,5 hours for our algorithm.

[11]For the calculation of $g(E)$, we generate a time series of 2048 steps, where each step corresponds to a time interval of 0.025. Therefore, the total interval for the time propagation of the wave function is small enough such that the error of the Runge-Kutta method remains negligible, cf. Sec. 3.1.4.

[12]In order to gather good statistics, we averaged the results shown in this section over many iterations. The numbers of iterations are slightly different for different system sizes: $N_s = 16$: 100 iterations, $N_s = 17$: 100 iterations, $N_s = 18$: 100 iterations, $N_s = 19$: 98 iterations, $N_s = 20$: 57 iterations, $N_s = 21$: 122 iterations, $N_s = 22$: 116 iterations, $N_s = 23$: 63 iterations, $N_s = 24$: 42 iterations.

[13]In our numerical investigations, we obtain the energy distribution on a discrete energy axis, cf. Eq. (3.11) and Eq. (B.40), such that the integral in Eq. (3.16) turns into a sum over equally spaced energy values E_l

$$\Delta G(n) = \sum_l |g_n(E_l) - g_0(E_l)| . \tag{3.15}$$

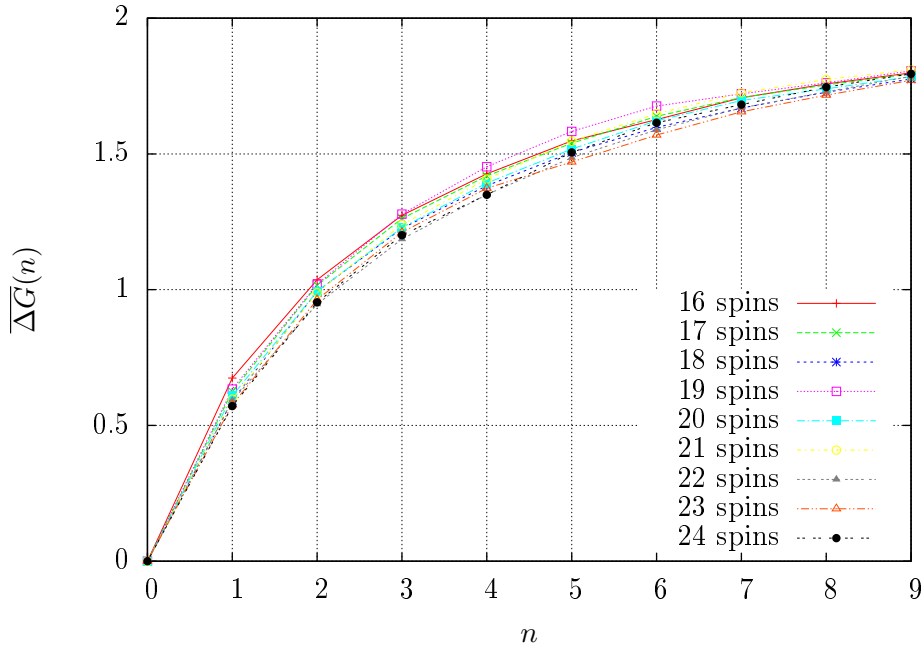This corresponds to a coarse-grained energy axis.

Figure 3.8: $\overline{\Delta G}(n)$ calculated for different system sizes as indicated in the legend. Individual dots are connected by a line in order to guide the eye. For further information, see text.

$\overline{\Delta G}(n) < 1$, cf. Fig. 2.2. However, the calculated stability measure $\overline{\Delta G}(n)$ in Fig. 3.8 seems to converge to $\overline{\Delta G}(n) = 2$. This deviation from the anticipated behaviour is due to the finite-size effects, in particular the heating effect which makes both peaks drift towards the energy values corresponding to higher entropy. The particular value of 2 comes from the fact that, if the initial $g_0(E)$ and the final $g_n(E)$ have zero overlap, the stability measure yields

$$\Delta G(n) = \sum_l |g_n(E_l) - g_0(E_l)| = \sum_l \Big(g_n(E_l) + g_0(E_l) \Big) = 2, \tag{3.17}$$

due to the normalisation $\sum_l g_n(E_l) = 1$. If the shift of the average energy of the individual peaks is of the order of the width of these peaks, the overlap can indeed become nearly zero. Since heating occurs for each individual realisation, the averaged value $\overline{\Delta G}(n)$ also converges to 2^{14}.

Comparing results for different system sizes in Fig. 3.8, $\overline{\Delta G}(n)$ grows slower for larger system sizes. This again confirms that the dynamics in Fig. 3.8 is mostly driven by the heating effect which is less pronounced for larger systems. If we were able to simulate even larger spin systems numerically, $\overline{\Delta G}(n)$ would grow even slower and, eventually, $\overline{\Delta G}(n)$ not become larger than 1.

Introduction of a two-bin energy axis

The results in Fig. 3.8 show that the finite-size effects contribute significantly to the evolution of $\overline{\Delta G}(n)$. In an effort to identify a stability measure less sensitive to these effects, we

---

[14]When $\overline{\Delta G}(n)$ approaches 2 in Fig. 3.8, the results for different system sizes seem to come closer to each other. In this regime, the overlap of tails of $g(E)$ presumably governs the behaviour of $\overline{\Delta G}(n)$, which seems to exhibit a behaviour independent on the system size.
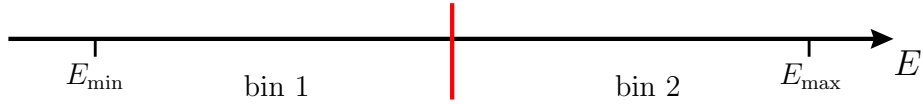
Figure 3.9: An illustration of the coarse-graining of the total energy axis into two large bins. As long as each peak is localised in one bin, the finite-size effects of the measurements can be neglected.

introduce a radical coarse-graining of the energy axis. Namely, we divide the total energy axis into two large energy bins as indicated in Fig. 3.9. These bins are defined such that the peaks contribute to different bins. Such a choice makes the heating effect negligible as long as each peak is localised in its own bin. This approach fails as soon as the peaks start overlapping. It is worth stressing that this approach is not universally applicable to any $g(E)$ but is mainly restricted to two-peak $g(E)$, where the distance between the peaks is much larger than the width of individual peaks.

The averaged stability measure $\overline{\Delta G}_2(n)$ obtained for the same setting as that for Fig. 3.8 but with two large energy bins is shown in Fig. 3.10. The increase of $\overline{\Delta G}_2(n)$ is much slower now. Moreover, we observe a ladder structure until the fourth measurement which implies that the modifications of $\overline{\Delta G}_2(n)$ are stronger after the spin-pair measurements. The reason for this ladder structure is that, for interacting spin systems, the outcome of the spin-pair measurements is correlated with the total energy E as shown in Chapter 2. The change of $\overline{\Delta G}_2(n)$ after the measurements with odd numbers are also non-zero because of other, possibly accidental, correlations between measurement outcomes and the total energy E. In contrast to Fig. 3.10, the ladder structure is completely washed out by the finite-size effect in Fig. 3.8.

Let us now try to understand the results shown in Fig. 3.10. In order to do this, we introduce the following notation

$$\Delta G(n) = \sum_l |g_n(E_l) - g_0(E_l)| = |p_{1,n} - p_{1,0}| + |p_{2,n} - p_{2,0}|, \qquad (3.18)$$

where $p_{1,n}$ is the statistical weight of the left peak after the n-th measurement and, likewise, $p_{2,n}$ for the right peak, cf. Fig. 3.9. Initially, $p_{1,0} = p_{2,0} = 0,5$ and $\overline{\Delta G}_2(0) = 0$. Let us now consider $\overline{\Delta G}_2(9)$ in Fig. 3.10 after the ninth measurement, where $\overline{\Delta G}_2(9) \approx 0.5$ approximately for all system sizes. For the statistical weights $p_{1,n}$ and $p_{2,n}$, this corresponds on average to the two cases

$$\text{either} \qquad p_{1,9} \approx 0.75 \quad \text{and} \quad p_{2,9} \approx 0.25 \qquad (3.19)$$

$$\text{or} \qquad p_{1,9} \approx 0.25 \quad \text{and} \quad p_{2,9} \approx 0.75, \qquad (3.20)$$

which means that the statistical weight of the larger peak is three times larger than the statistical weight of the smaller peak. However, this is to be understood only as the average case. In fact, for some cases, the measurements induce a complete suppression of one peak, i.e. either $p_{1,n} = 0$ or $p_{2,n} = 0$, whereas, for other cases, the initial balance remains conserved, i.e. $p_{1,n} = p_{2,n} = 0.5$.
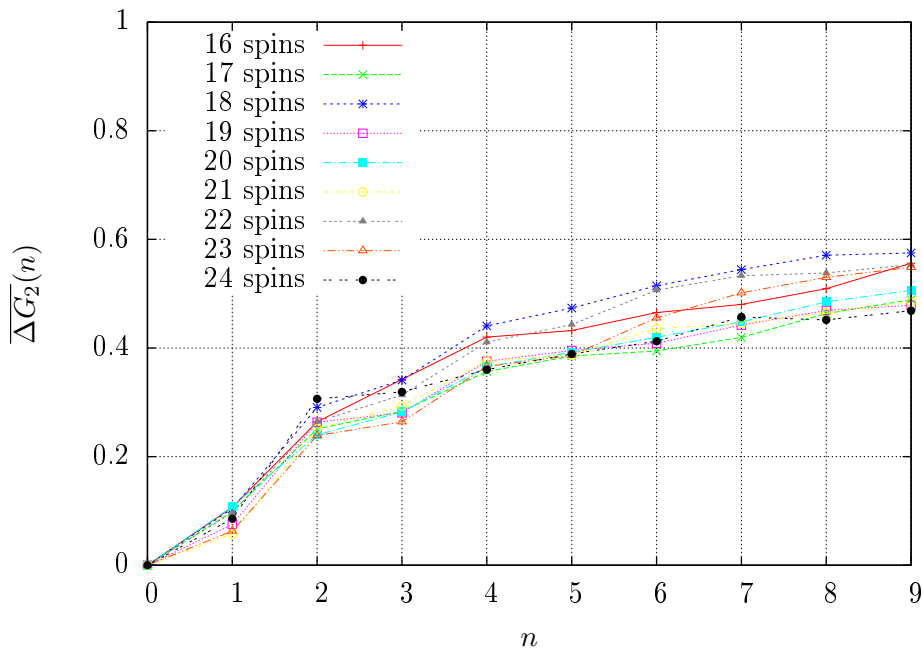
Figure 3.10: $\overline{\Delta G_2}(n)$ calculated for different system sizes as indicated in the legend and a coarse grained energy axis divided into two bins. Individual dots are connected by a line in order to guide the eye. The vertical axis has a different scaling as compared to the previous figure. For details of the calculations, see text.

Let us now cross check the assumption that, using the two-bin energy axis, the heating effect can be neglected. In Fig. 3.11, we show $g_n(E)$ for the system size $N_s = 16$. In this example, the initial two-peak $g(E)$ is not reduced to a one-peak $g(E)$. The heating effect is pronounced for this small system size to such extend that the two peaks start to overlap approximately after the 6th measurement. At the same time, Fig. 3.12 shows a similar example for the system size $N_s = 24$. In this case, the measurements strongly suppress the right peak. The heating effect is much less pronounced than that for $N_s = 16$ such that the two peaks to not start overlapping. To summarise, dividing the energy axis into two bins makes the finite-size effect negligible for larger system sizes whereas, for smaller ones, the peaks start to overlap during the measurements.

3.3.3 Other stability measures

Entropy of the energy distribution

The entropy $\mathrm{entr}(n)$ of the energy distribution $g_n(E)$ is defined as

$$\mathrm{entr}(n) \equiv -\sum_l g_n(E_l) \ln[g_n(E_l)], \tag{3.21}$$

where the sum extends over all energy eigenvalues[15]. The entropy is zero for the narrow peak $g_n(E_l) = \delta_{lk}$. For the two-peak distribution $g_n(E_l) = \frac{1}{2}(\delta_{lk} + \delta_{lp})$, the entropy is $\ln(2)$.

---

[15]In our numerical simulations, we obtain $g_n(E)$ on a coarse-grained energy axis. Therefore, in practice, the sum in Eq. (3.21) extends over the energy bins.
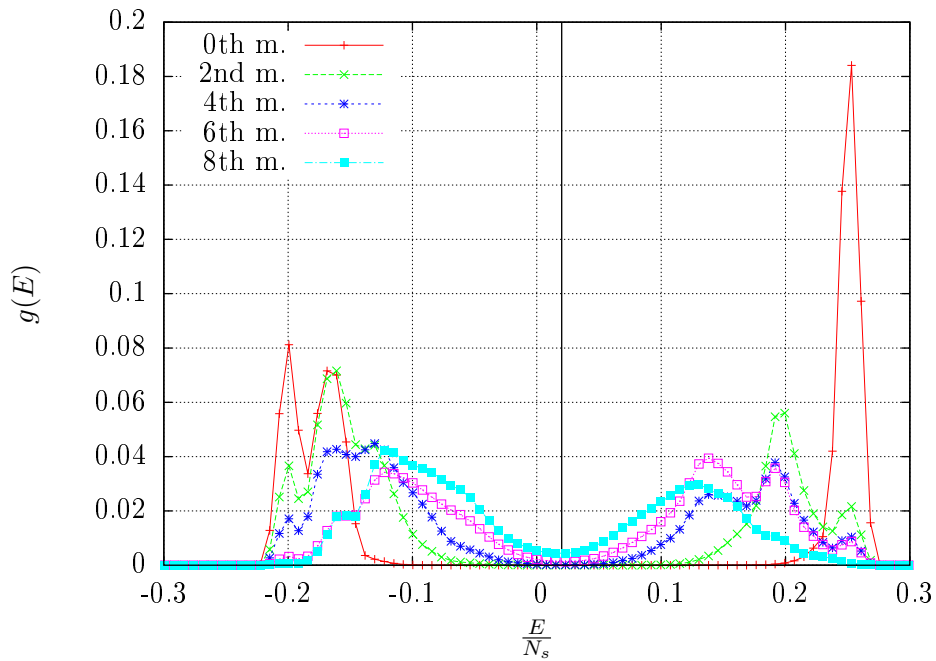
Figure 3.11: Plot of the energy distribution $g_n(E)$ for the system size $N_s = 16$ after n measurements as indicated in the legend. The vertical solid line indicates the possible partition into the two bins. At the border between the bins, $g(E)$ becomes non-zero. Therefore, the finite-size effects are not negligible completely.
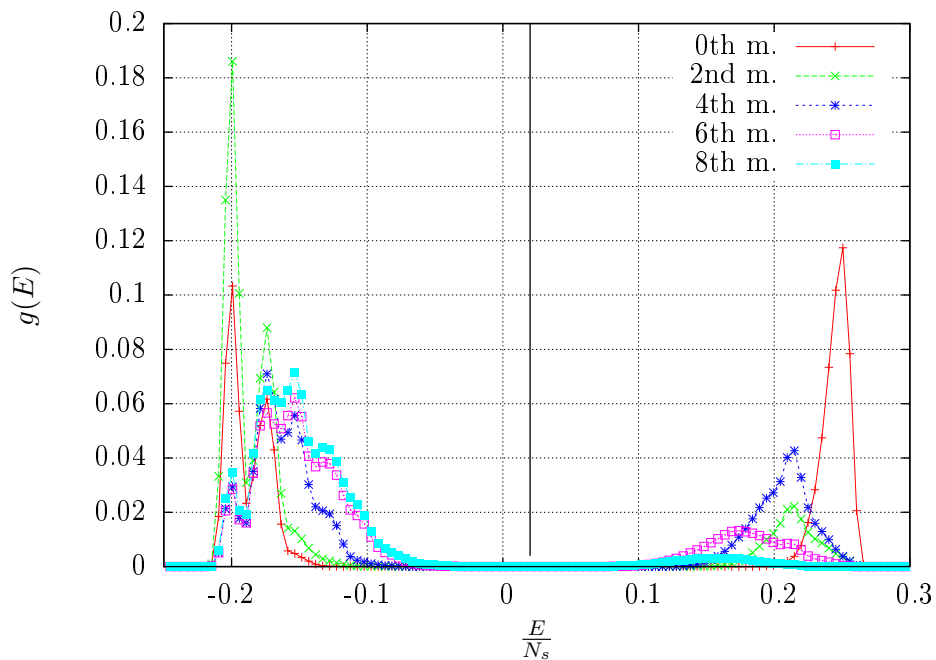

Figure 3.12: Plot of the energy distribution $g_n(E)$ for the system size $N_s = 24$ after n measurements as indicated in the legend. The vertical solid line indicates the possible partition into the two bins. In contrast to the case above, $g(E)$ remains zero at the border between the bins.

Therefore, if the measurements induce the suppression of one peak, this corresponds to a decrease of the entropy by $\ln(2) \approx 0.69$. The maximal entropy, one obtains for a completely flat distribution $g(E) = const.$.

In Fig. 3.13, we show the averaged entropy $\text{entr}(n)$ for different system sizes. In contrast to the expectation that the narrowing effect of measurements decreases the entropy, the entropy increases monotonically. This is again an impact of the finite-size effects of the measurement. Since the value contributed by finite-size effects to the entropy is larger than the contribution by the narrowing effect, the entropy increases.

Now, we introduce the same coarse-graining as for the stability measure $\Delta G(n)$. We split the energy axis into two large bins and calculate the entropy anew. The result is shown in Fig. 3.14. Now, the entropy decreases as anticipated. Moreover, its behaviour exhibits the ladder structure due to the correlations between the outcome of the spin-pair measurements and the total energy of the system. It is noteworthy that, for the new coarse-grained energy axis, the initial value $\text{entr}(0) = \ln(2)$ is the same for all system sizes.

The results obtained indicate that the entropy as defined in Eq. (3.21) can be used as a measure of stability. However, there are some disadvantages. One disadvantage is that entropy is very sensitive to the shape of $g(E)$. Small variations of the shape of $g(E)$ can induce large variations of the entropy. Further, entropy is prone to the finite-size effects. These effects completely reverse the behaviour of $\text{entr}(n)$ from decreasing to increasing as we have seen above. Moreover, the reduction of a two-peak $g(E)$ to a single-peak $g(E)$ corresponds to a change of the entropy by $\ln(2)$. Especially for macroscopic quantum systems, where the entropy of $g(E)$ can be significantly larger than $\ln(2)$, this term can readily become negligible.

Kurtosis of the energy distribution

The next stability measure that we are going to consider is the kurtosis which is defined as

$$\text{kurt}(n) \equiv \frac{\mu_{g,n}}{w_{g,n}^4}, \tag{3.22}$$

where $\mu_{g,n}$ is the fourth central moment of $g_n(E)$

$$\mu_{g,n} \equiv \sum_l (E_l - E_{\text{av},n})^4 \, g_n(E_l). \tag{3.23}$$

The kurtosis is a measure of the shape of $g(E)$. For a $g(E)$ with a Gaussian shape, we obtain $\text{kurt}(n) = 3$. For $g(E)$, which decay slower than a Gaussian function, $\text{kurt}(n) < 3$. An example hereby is a two-peaked $g(E)$, where $\text{kurt}(n) \approx 1$, cf. Appendix B.7. For $g(E)$, which decay faster than a Gaussian function $\text{kurt}(n) > 3$.

In Fig. 3.15, we show the results for the kurtosis. For all system sizes, initially $\text{kurt}(0) \approx 1$ which corresponds to a broad $g_0(E)$. With an increasing number of measurements, the kurtosis grows which indicates the narrowing effect of measurements. The plotted figures exhibit the ladder structure. This implies that the kurtosis is less prone to the finite-size effects as compared to the previous measures of stability, where the ladder structure became

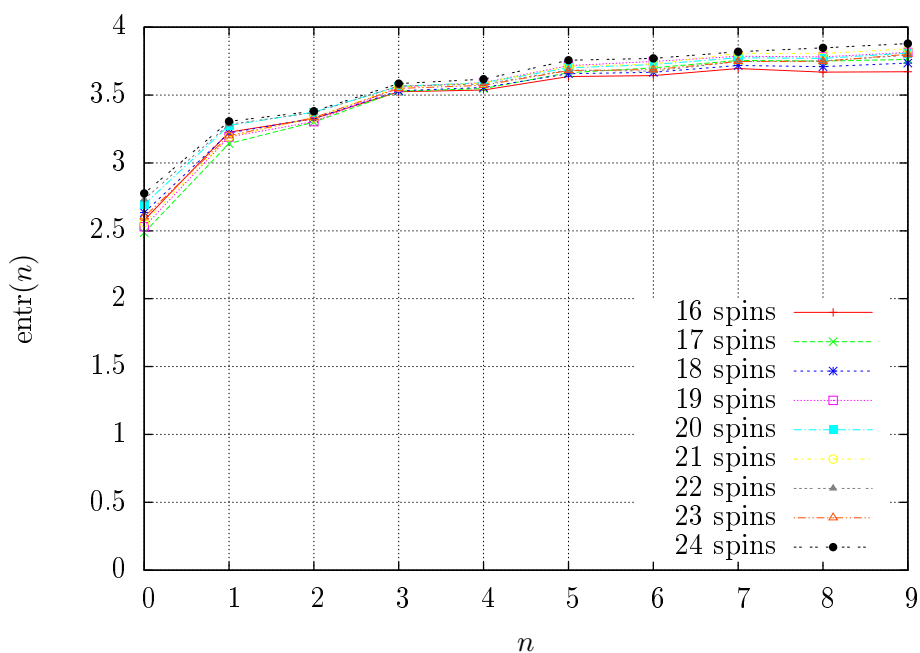Figure 3.13: Entropy of $g(E)$ as a function of the number of measurements n for different system sizes as indicated in the legend. For further explanations, see text.
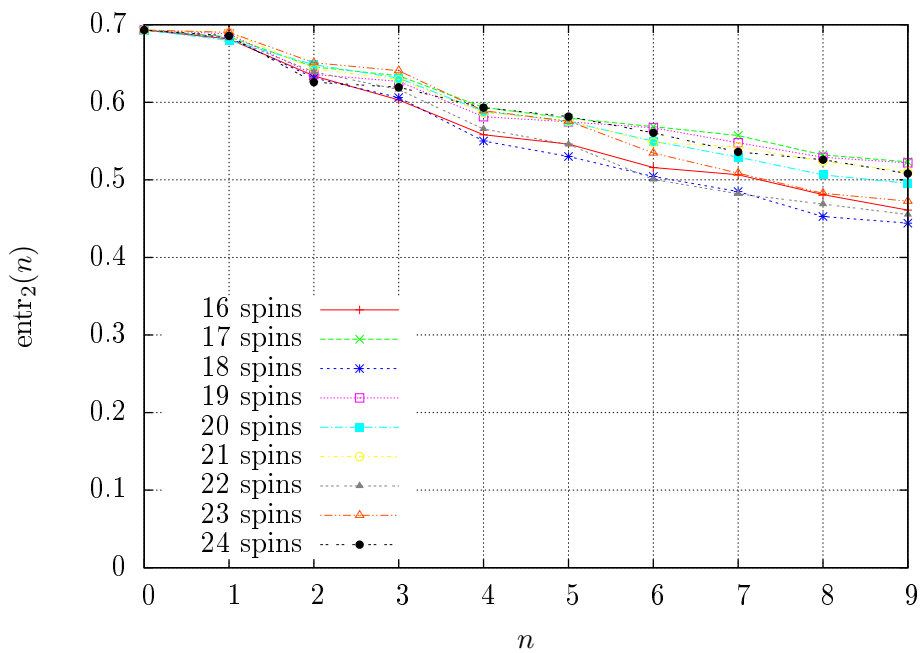

Figure 3.14: Entropy of $g(E)$ as a function of the number of measurements n for different system sizes as indicated in the legend. The entropy is calculated on the basis of two large bins. For further explanations, see text.
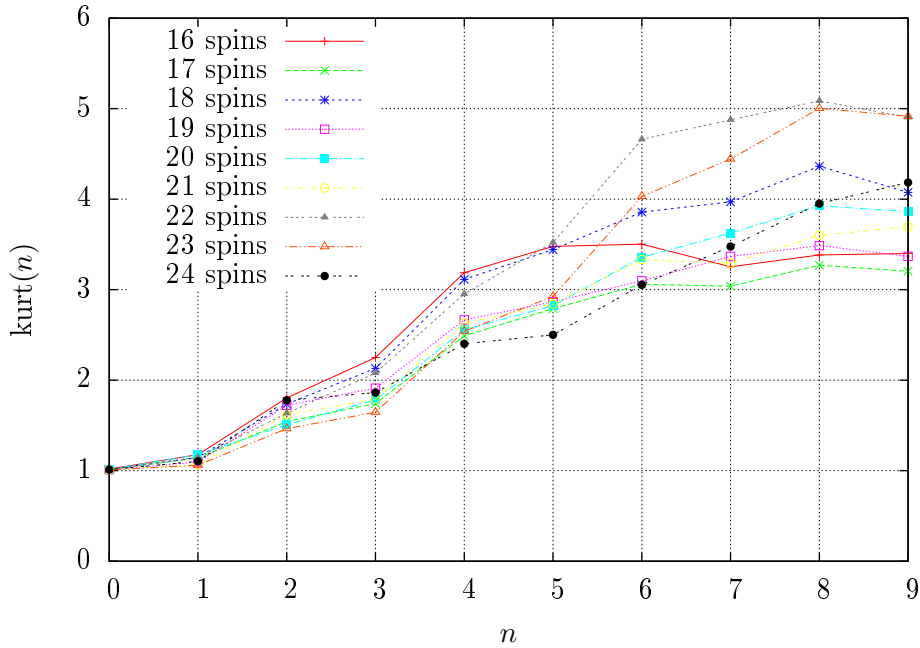
Figure 3.15: The averaged kurtosis $\mathrm{kurt}(n)$ as a function of the number of measurements n for different system sizes as indicated in the legend. For further explanations, see text.

visible only on the basis of the two-bin energy axis. In contrast, the results in Fig. 3.15 are obtained without the introduction of the two larger energy bins.

An essential disadvantage of the kurtosis as a measure of stability is that it is very sensitive to small variations on the tails of $g(E)$. Apparently insignificant variations of $g(E)$ can induce large variations of the kurtosis. Further, $\mathrm{kurt}(n)$ grows without a limit for narrow $g(E)$. Therefore, it is difficult to use kurtosis to compare the stability of different distributions $g(E)$.

Deviation of the average energy from its initial value

Let us now investigate the deviation of the average energy $E_{\mathrm{av},n}$ as a measure of the modifications of $g(E)$ due to the measurements. In order to quantify the deviation of $E_{\mathrm{av},n}$, we define[16]

$$\Delta E_{\mathrm{av}}(n) \equiv \frac{|E_{\mathrm{av},n} - E_{\mathrm{av},0}|}{w_{g,0}}, \tag{3.24}$$

where $w_{g,0}$ is the initial width of $g(E)$ and, approximately, the separation of the two peaks. Initially, $E_{\mathrm{av},0}$ is centred between the two peaks. If one of the peaks becomes suppressed due to the measurements, the average energy $E_{\mathrm{av},n}$ jumps towards the remaining peak. Therefore, a sudden jump of $\Delta E_{\mathrm{av}}(n)$ to $\Delta E_{\mathrm{av}}(n) \approx \frac{1}{2}$ corresponds to the complete suppression of one of the two peaks.

In Fig. 3.16, we show the results for $\Delta E_{\mathrm{av}}(n)$. We observe that the ladder structure is rather pronounced. For larger values of n, $\Delta E_{\mathrm{av}}(n)$ seems to saturate at the value

---

[16]Here, we need to consider the absolute value of the energy difference $|E_{\mathrm{av},n} - E_{\mathrm{av},0}|$ because $E_{\mathrm{av},n}$ can shift in both directions. This is in contrast to the investigation of the finite-size effects, where heating induced a shift of $E_{\mathrm{av},n}$ into one direction only.
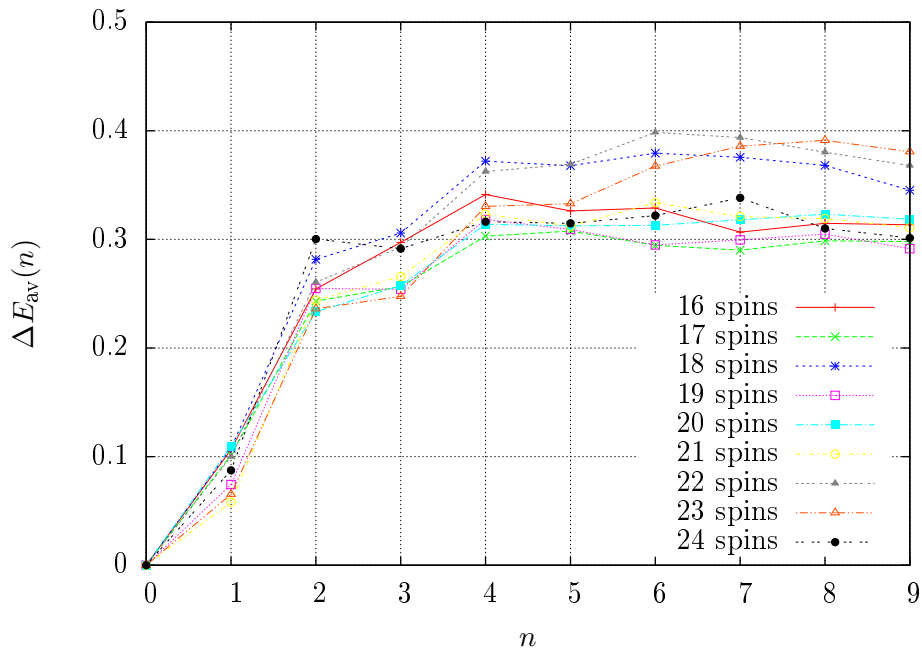
Figure 3.16: $\Delta E_{\text{av}}(n)$ is shown for different system sizes as indicated in the legend. For further explanations, see text.
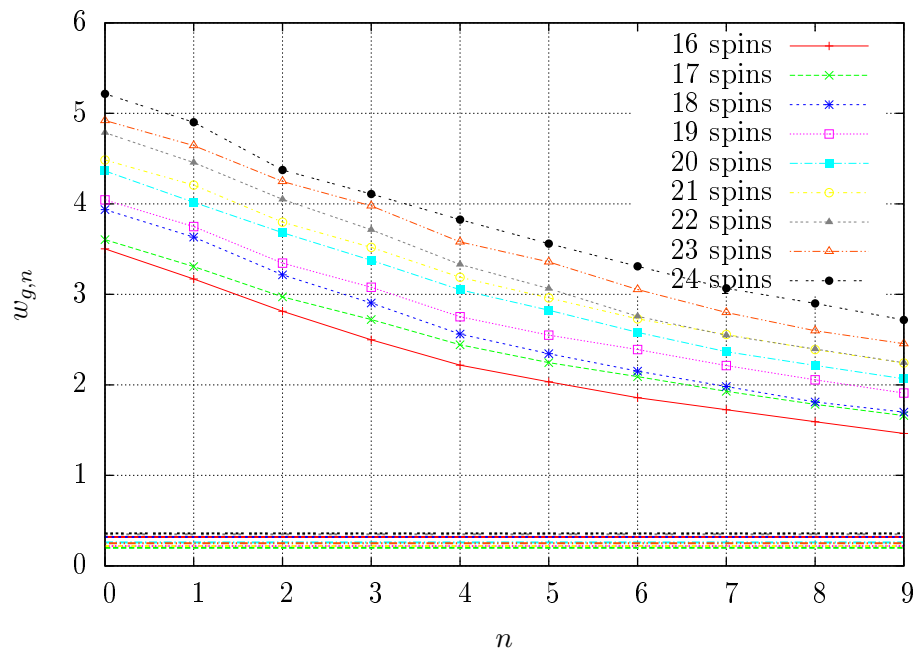

Figure 3.17: The width $w_{g,n}$ of $g_n(E)$ is shown as a function of n for different system sizes as indicated in the legend. The horizontal lines illustrate the widths of the initial individual thermal peaks. The colour of the horizontal lines indicates the system size. For further explanations, see text.

$\Delta E_{\mathrm{av}}(n) \approx 0.35$. The reason is that two effects compensate each other for this value. On the one hand, there are the finite-size effects decreasing $\Delta E_{\mathrm{av}}(n)$, and, on the other hand, narrowing effect which forces $\Delta E_{\mathrm{av}}(n)$ to increase.

In total, $\Delta E_{\mathrm{av}}(n)$ turns out to be suitable as a measure of stability. However, for $g(E)$ other than the two-peak $g(E)$, it is less suitable.

The width of the energy distribution

As the last proposal for the measure of stability, we consider the width $w_{g,n}$ as a function of n. The idea behind is that there are two characteristic widths of $g(E)$. There is the total width w_g of $g(E)$ corresponding to the separation of the peaks and there are the smaller widths of the individual peaks. By monitoring $w_{g,n}$, we can trace its value from the large initial value corresponding to the separation of the peaks to the small values corresponding to the width of a individual peaks.

The results are illustrated in Fig. 3.17, where the horizontal lines indicate the widths of the individual peaks. The plot shows a decent decrease of $w_{g,n}$. However, $w_{g,n}$ does not reach the width of the individual energy peaks. The reason is, on the one hand, that $g(E)$ is not reduced to one peak in all cases and, on the other hand, the broadening effect of the measurements. The finite-size effects again completely wash out the ladder structure.

The advantage of the width $w_{g,n}$ as a measure of stability is that, in principle, it is applicable to any $g(E)$. However, $w_{g,n}$ is prone to the finite-size effects as explained above.

3.4   Summary

In this chapter, we numerically investigate the stability of a two-peak $g(E)$ for an interacting spin system. First, we introduced the methods for the numerical investigation. Then, we considered the finite-size effects with respect to the local measurements. We gave an example for the narrowing effect of measurements by explicitly showing all intermediate $g_n(E)$ for a given initial wave function. Finally, we studied the evolution of the stability measure $\overline{\Delta G}(n)$ and other stability measures that we proposed.

In general, the results of the numerical investigations exhibit qualitatively all effects anticipated from the analytical treatment in Chapter 2, namely the narrowing effect, the broadening effect and the heating effect. The results of the numerical investigations are consistent with the analytical results. Further, the numerical investigations confirmed that the finite size effects are rather pronounced for microscopic systems. In fact, these effects dominate over the narrowing effect in some cases.

The study of the evolution of the different stability measures shows that it is, in general, difficult to define suitable stability measures for microscopic systems. In view of the finite-size effects with respect to local measurements, it is sometimes difficult to capture the narrowing effect even for a two-peak $g(E)$. If we were to study the narrowing effect for a general broad $g(E)$, it would be unclear how to separate the finite-size effects from the qualitative trends present in the macroscopic limit.

Chapter 4

Macroscopicity Measure for Quantum Superpositions

Until today, the applicability limits of quantum mechanics remain unknown. Despite the large number of conducted experiments, whose results are accurately described by quantum mechanics, several parameter regimes have not been covered yet experimentally [54]. One of these parameter regimes is the transition to the macroscopic limit. The objective hereby is to prepare quantum superpositions of macroscopically distinct states. A famous thought experiment was put forward by Erwin Schrödinger [78], where he proposed a setting aiming at creating a quantum superposition of a living and a dead cat. Such a quantum superposition can be called macroscopic meaning a superposition of macroscopically distinguishable quantum states.

In principle, quantum mechanics does not distinguish between the microscopic and the macroscopic systems. In practice, quantum superpositions have been observed in uncountable experiments on the microscopic scale, [56, 98, 63, 44, 83, 31, 14], while the observation of quantum superpositions of macroscopically distinct states remains elusive until today. In general, the quantum-to-classical transition and, in particular, the absence of the quantum interference on the scales of our everyday life are not well understood yet. Although the absence of the quantum interference on the macroscopic scales can be explained by the quantum decoherence theory, the observation of the quantum superposition of macroscopically distinct states is as such of fundamental interest. Aside from that, the difficulties to reconcile the quantum theory and the theory of general relativity make the tests of quantum mechanics at macroscopic scales even more compelling.

Although the notion of macroscopicity of quantum superpositions appears intuitive, its precise definition is difficult to formulate. Coming back to the above example of the Schrödinger's cat, it is unclear whether the number of molecules matters that the cat is made of or does the difference of the body temperature of the cat matter? If we were to consider the overlap of the wave functions describing the living and the dead cat, this would not constitute a proper measure of macroscopicity. The reason is that the overlap of two states already vanishes if the two states differ locally. For example, if we would displace a single hair of the cat, this would already lead to a state which is orthogonal to the previous

one.

The research field in the context of the macroscopicity measure has recently gained increased interest due to the experimental advances in cooling and isolating quantum systems of increasing size and complexity; see for example Refs. [65, 51, 92]. Many different macroscopicity measures have been proposed during the last years. However, all of them are system-specific, cf. Sec. 1.2.2. Given a measure of macroscopicity, which is applicable to a broad variety of many-body systems, one could in principle compare the macroscopicity reached in different experiments. Moreover, based on such a measure, decisions could be made about future experiments for searching for the limits of quantum mechanics.

In this chapter, we introduce a measure of macroscopicity for quantum superpositions. We call a quantum wave function[1] a macroscopic quantum superposition, when a single local measurement leads to a change of the density matrices of a macroscopic number of subsystems within the same system. Hereby, local means localised in the physical three-dimensional space, cf. Sec. 2.4.1. Local measurements can be, for example, measurements of individual particles, measurements of a pair of particles and so forth. This measure of macroscopicity can be understood as a measure of instability with respect to one local measurement applied to a given quantum superposition. While, in the context of the stability of quantum statistical ensembles, we considered the variation of the probability distribution of the total energy $g(E)$ due to multiple measurements, for the measure of macroscopicity of quantum superpositions, we consider the variation of the reduced density matrices of the subsystems due to a single measurement[2].

In order to understand why the above idea indeed gives rise to a notion of macroscopicity of quantum superpositions, let us for a moment consider a local measurement of a macroscopic classical system. We expect that a measurement on a small part of a macroscopic classical system does not affect remote subsystems of the same system. In nature, only the properties of nearby parts of the measured subsystem can be affected such that the macroscopicity of macroscopic classical systems is negligible. In contrast, for quantum states, even distant subsystems may be affected by a local measurement. An example hereby is the superposition of the ferromagnetic ground states

$$|\psi\rangle = \frac{1}{\sqrt{2}}\Big(|\uparrow\uparrow\uparrow\cdots\rangle + |\downarrow\downarrow\downarrow\cdots\rangle\Big), \tag{4.1}$$

where $|\uparrow\rangle$ is the eigenstate of the spin operator corresponding to the z-component of the spin with eigenvalue $+\frac{1}{2}$. If we measure the polarisation of an arbitrary spin along the z-axis, the state of all other spins changes according to the measurement outcome. Therefore, the macroscopicity of this state is extremely high[3].

---

[1]While we primarily focus on the stability of pure quantum states described by a quantum wave function, our approach is also applicable to mixed quantum states which describe incoherent mixtures of pure quantum states.

[2]During the completion of this thesis, we became aware of the article [82] by Shimizu and Miyadera, where the authors define the stability of quantum states with respect to local measurements. The definition in [82] is, in principle, equivalent to our definition of macroscopicity. However, Shimizu and Miyadera do not provide a stability measure. In contrast, we define a measure of macroscopicity which may become important, for example, for a comparison of different experiments.

[3]The example above also highlights the difference between the measure of macroscopicity of quantum

This chapter is organised as follows. First, we introduce the necessary objects for the formulation of the measure of macroscopicity and, subsequently, formulate the macroscopicity measure which is suitable for broad variety of many-body systems. Later, we apply this macroscopicity measure to lattices of spins-$\frac{1}{2}$ and also provide two explicit examples.

4.1 Preliminary considerations

We want to consider the overall effect of one local measurement on the subsystems of the total system. In order to characterise this effect, first, we introduce the decomposition of the total system into subsystems. Second, we quantify the effect on a given subsystem by introducing a distance measure for the density matrices. The overall effect of the local measurement is the sum of the changes of density matrices of the subsystems for a given decomposition. In this section, we introduce the above quantities.

Decomposition of the total system

There are many different possibilities to decompose the system into subsystems, cf. Fig. 4.1. In this thesis, we define the subsystems by dividing the physical three-dimensional space into non-overlapping regions. On the one hand, we assume that the volume of these subsystems is negligible with respect to the volume of the total system and, on the other hand, the subsystems' volume must be large enough such that not much less than one particle is contained in each subsystem on the average.

Distance between density matrices

We introduce the distance between the density matrices ρ_0 and ρ_1

$$d(\rho_0, \rho_1) \equiv \sqrt{\mathrm{Tr}\big[(\rho_0 - \rho_1)(\rho_0 - \rho_1)^\dagger\big]}, \tag{4.2}$$

---

states and the measure of stability of quantum statistical ensembles because both states $|\uparrow\uparrow\uparrow\cdots\rangle$ and $|\downarrow\downarrow\downarrow\cdots\rangle$ correspond to the same energy for a ferromagnetic Hamiltonian. Yet, the superposition of these states is unstable.
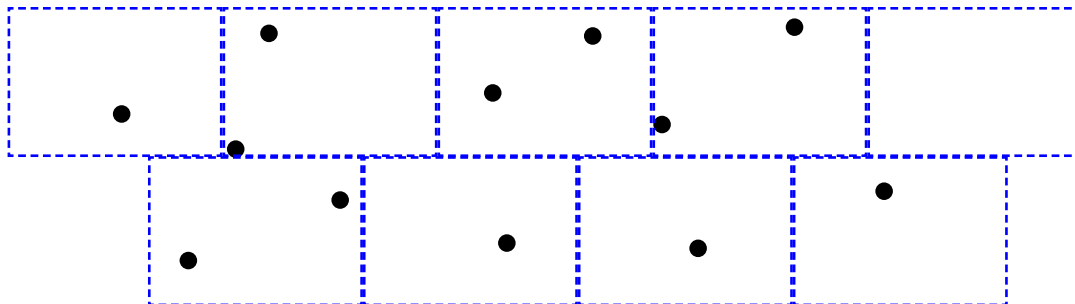

Figure 4.1: Schematic representation of an example for the decomposition of the system into subsystems. Dots indicate the particles of the system, and the blue dashed lines illustrate the decomposition into subsystems.

where the trace is to be taken over the degrees of freedom described by the density matrices. This distance is a metric in the space of the density matrices and it satisfies useful relations. For example, it is invariant under a basis transformation and also invariant under time evolution. Further, the distance can take on values in the range $0 \leq d(\rho_{1,m}, \rho_{0,m}) \leq \sqrt{2}$, cf. Appendix C[4].

4.2 Definition of the macroscopicity measure for quantum superpositions

Let ρ_0 be the density matrix describing the total system before the measurement and ρ_1 the density matrix immediately after the measurement[5]. Suppose now that we fix a decomposition of the total system into subsystems. We enumerate the subsystems and denote the reduced density matrices of the m-th subsystem before the measurement by $\rho_{0,m}$ and after the measurement by $\rho_{1,m}$.

In order to quantify the impact of the local measurement on the total system, we introduce

$$\Delta\Upsilon \equiv \sum_m d(\rho_{1,m}, \rho_{0,m}), \tag{4.3}$$

which is the sum of the changes of all subsystems' density matrices. Since the maximal value of the distance is $\sqrt{2}$, the maximal value of $\Delta\Upsilon$ is $\sqrt{2}N$, where N is the number of subsystems. If $\Delta\Upsilon \sim N$, this indicates a significant change of the density matrix for all subsystems.

The quantity $\Delta\Upsilon$ depends on the chosen decomposition of the system into subsystems. If we were to choose another decomposition, $\Delta\Upsilon$ could, in principle, vary significantly.

Definition: The measure of macroscopicity for quantum superpositions M is defined as

$$M \equiv \max\left[\Delta\Upsilon\right] = \max\left[\sum_m d(\rho_{1,m}, \rho_{0,m})\right], \tag{4.4}$$

where max denotes

- the maximum over all possible decompositions of the total system into subsystems,

- the maximum over the measurement basis because M is implied to be averaged over the possible measurement outcomes in a given basis.

Let us now make a two remarks.

1. We call a quantum state a *macroscopic superposition* (or mixture) if $M \sim N$.

2. The number of decompositions can become quite large especially for macroscopic systems. Therefore, finding a maximal value of $\Delta\Upsilon$ can become quite involved. However, the precise value of M is less important than its estimate. Finding an estimate for the

---

[4]It is noteworthy that the upper and lower bounds of $d(\rho_0, \rho_1)$ are independent of the size of the system described by the density matrices.

[5]This means that we disregard any time evolution after the measurement.

maximum over all possible decompositions can be simplified in the following way. If the properties of single particles change due to the measurement, the decomposition into subsystems, where each subsystem contains one particle on the average, is likely to give a good estimate for M. Furthermore, if the properties of single particles do not change, M is likely to be found for subsystems containing two directly interacting particles.

4.3 Formulation for lattices of spins-$\frac{1}{2}$

In this section, we apply the above measure of macroscopicity for quantum superpositions M to lattices of spins-$\frac{1}{2}$. In order to do this, we introduce a suitable parametrisation of the spin density matrices and provide an expression for M based on observable quantities.

4.3.1 Representation of the spin density matrix

Let us consider a single spin-$\frac{1}{2}$. The density matrix ρ_j of the spin at lattice site j can be written in the following form

$$\rho_j = \frac{1}{2} \sum_{\mu=0}^{3} P_{j\mu}\sigma_{j\mu}, \tag{4.5}$$

where $\sigma_{j\mu}$ is the μ-th Pauli matrix[6] acting on the Hilbert space corresponding to lattice site j[7] and $P_{j\mu}$ is the polarisation of the given spin in the direction μ. The polarisation $P_{j\mu}$ is given by

$$P_{j\mu} = \text{Tr}\left[\sigma_{j\mu}\rho_j\right] = 2\langle S_{j\mu}\rangle, \tag{4.6}$$

where $S_{i\mu} = \frac{1}{2}\sigma_{i\mu}$ is the corresponding spin operator. The parameters $P_{j\mu}$ can take on values from the interval $[-1, 1]$. Given that the density matrix of the total spin lattice is ρ, the above expression for $P_{j\mu}$ can also be written as $P_{j\mu} = \text{Tr}\left[\sigma_{j\mu}\rho\right]$, where the trace now extends over the larger Hilbert space.

The analogous expressions for the density matrix of 2 spins at lattice sites j and k are

$$\rho_{jk} = \frac{1}{4} \sum_{\mu,\nu=0}^{3} P_{jk\mu\nu}\ \sigma_{j\mu}\sigma_{k\nu}, \tag{4.7}$$

where

$$P_{jk\mu\nu} = \text{Tr}\left[\left(\sigma_{j\mu}\sigma_{k\nu}\right)\rho_{jk}\right] = 4\langle S_{j\mu}S_{k\nu}\rangle. \tag{4.8}$$

The parameters $P_{jk\mu\nu}$ contain not only the polarisations of the individual spins but also the spin-spin correlations. Density matrices of larger spin systems can be written in a form analogous to the ones given in Eq. (4.5) and Eq. (4.7).

---

[6]The zeroth Pauli matrix is defined as the unit matrix.

[7]In the following, we use the convention, that the indices for the lattice sites are indicated by Latin letters, while the indices for the spatial directions of the spin polarisations are indicated by Greek letters. The latter run over the values 0,1,2,3.

4.3.2   Macroscopicity measure for lattices of spins-$\frac{1}{2}$

Now, we calculate the measure of macroscopicity introduced in Eq. (4.4). We choose a decomposition of the system such that there is one spin in each subsystem. Substituting Eq. (4.5) into Eq. (4.2), we obtain

$$d(\rho_{1,j}, \rho_{0,j}) = \frac{1}{\sqrt{2}} \sqrt{\sum_{\mu=0}^{3} \left(P_{1,j\mu} - P_{0,j\mu} \right)^2}, \qquad (4.9)$$

where we used the following relation: $\sigma_\mu \sigma_\nu = \delta_{\mu\nu} \sigma_0 + i\varepsilon_{\mu\nu\kappa} \sigma_\kappa$. Hence, the distance between two density matrices is given by the differences of their individual parameters $P_{j\mu}$. The derivation of Eq. (4.9) is given in the Appendix C.

Further, substituting the expression for the parameters $P_{j\mu}$ in Eq. (4.6), we obtain

$$d(\rho_{1,j}, \rho_{0,j}) = \sqrt{2} \sqrt{\sum_{\mu=0}^{3} \left(\langle S_{j\mu} \rangle_1 - \langle S_{j\mu} \rangle_0 \right)^2}, \qquad (4.10)$$

where $\langle S_{j\mu} \rangle_1 \equiv \text{Tr}\big[S_{j\mu} \, \rho_1 \big]$ is the expectation value of $S_{j\mu}$ with respect to ρ_1 and likewise for $\langle S_{j\mu} \rangle_0$. Finally, substituting the expression in Eq. (4.10) into the expression for M, we obtain

$$M = \sqrt{2} \max \left[\sum_j \sqrt{\sum_{\mu=0}^{3} \left(\langle S_{j\mu} \rangle_1 - \langle S_{j\mu} \rangle_0 \right)^2} \right]. \qquad (4.11)$$

The result is that the measure of macroscopicity M is governed by the changes of the spin expectation values of all spins and in all directions.

For a decomposition of the system into subsystems each of which consists of two spins, we obtain along the lines to the above treatment

$$d(\rho_{1,jk}, \rho_{0,jk}) = 2 \sqrt{\sum_{\mu,\nu=0}^{3} \left(\langle S_{j\mu} S_{k\nu} \rangle_1 - \langle S_{j\mu} S_{k\nu} \rangle_0 \right)^2}, \qquad (4.12)$$

where $\langle S_{j\mu} S_{k\nu} \rangle_1 \equiv \text{Tr}\big[S_{j\mu} S_{k\nu} \, \rho_1 \big]$ and $\langle S_{j\mu} S_{k\nu} \rangle_0 \equiv \text{Tr}\big[S_{j\mu} S_{k\nu} \, \rho_0 \big]$. For the measure of macroscopicity M, we obtain

$$M = 2 \max \left[\sum_{jk} \sqrt{\sum_{\mu,\nu=0}^{3} \left(\langle S_{j\mu} S_{k\nu} \rangle_1 - \langle S_{j\mu} S_{k\nu} \rangle_0 \right)^2} \right], \qquad (4.13)$$

where $\sum_{jk}$ indicates the sum over the spin-pairs corresponding to the given decomposition of the system. This result is similar to the one given for the one-spin density matrices in Eq. (4.11).

4.4   Two examples for the macroscopicity measure

In this section, we apply the measure of macroscopicity M to quantum states describing a system of N_s spins-$\frac{1}{2}$.

- *Greenberger-Horne-Zeilinger (GHZ) state*

  Let us consider the measure of macroscopicity of the GHZ-state which is defined as

  $$|\psi_{\text{GHZ}}\rangle = \frac{1}{\sqrt{2}}\Big[|\uparrow\uparrow\uparrow\cdots\rangle + |\downarrow\downarrow\downarrow\cdots\rangle\Big]. \tag{4.14}$$

  This wave function describes a superposition of states, where all spins point either in the positive z-direction $|\uparrow\uparrow\uparrow\cdots\rangle$ or in the negative z-direction $|\downarrow\downarrow\downarrow\cdots\rangle$. The single-spin density matrix of each spin is

  $$\rho_{0,j} = \begin{pmatrix} \frac{1}{2} & 0 \\ 0 & \frac{1}{2} \end{pmatrix}, \tag{4.15}$$

  which leads to $\langle S_{jx}\rangle_0 = 0$, $\langle S_{jy}\rangle_0 = 0$ and $\langle S_{jz}\rangle_0 = 0$.

  Let us now assume that the state of an arbitrary spin after the measurement is

  $$|\psi(\vartheta,\varphi)\rangle = \cos\left(\frac{\vartheta}{2}\right)|\uparrow\rangle + \sin\left(\frac{\vartheta}{2}\right)e^{i\varphi}|\downarrow\rangle, \tag{4.16}$$

  where ϑ is the polar angle and φ the azimuthal angle of the spin polarisation. After the measurement, the density matrix of each spin except for the measured spin j is[8]

  $$\rho_{1,j} = \begin{pmatrix} \cos^2\left(\frac{\vartheta}{2}\right) & 0 \\ 0 & \sin^2\left(\frac{\vartheta}{2}\right) \end{pmatrix}, \tag{4.17}$$

  which leads to $\langle S_{jx}\rangle_1 = 0$, $\langle S_{jy}\rangle_1 = 0$ and $\langle S_{jz}\rangle_1 = \cos^2\left(\frac{\vartheta}{2}\right) - \frac{1}{2}$. In follows that the maximal change of the density matrix is given for the measurement along the z-axis. Therefore, M is maximal for measurement basis $|\uparrow\rangle_z$ and $|\downarrow\rangle_z$.

  Employing the expression in Eq. (4.11), we obtain

  $$M = \frac{1}{\sqrt{2}}N_s, \tag{4.18}$$

  which is the maximal value for the measure of macroscopicity[9]. Therefore, the GHZ-state describes a quantum superposition of macroscopically distinct states.

Induced symmetry breaking

The above example shows that a local measurement can induce a symmetry breaking. The measurement along the z-axis leads to a macroscopic magnetisation of the total

---

[8]The density matrix of the measured spin, in general, has in addition non-vanishing off-diagonal elements.

[9]The factor $\frac{1}{\sqrt{2}}$ comes from the particular definition of the distance measure d.

system $M_z \approx \langle S_{lz} \rangle_1 N_s = \pm \frac{1}{2} N_s$, whereas the magnetisation was zero before the measurement. Similar results can also be obtained for the anti-ferromagnetic state [43, 82].

- *A product state*

  A quantum state of the following form

  $$\psi_{\mathrm{p}} = |\uparrow\rangle |\downarrow\rangle |\uparrow\rangle \cdots |\uparrow\rangle, \tag{4.19}$$

  we call a product state. For the measure of macroscopicity of any such a state, we obtain

  $$M \lesssim 1. \tag{4.20}$$

  The reason is that the individual spins are not correlated with each other for the product states. This implies that the vast majority of subsystem's density matrices remains unchanged. The only density matrix that changes is the one of the measured spin. Therefore, a product state does not describe a quantum superposition of macro-scopically distinct states. In fact, the value in Eq. (4.20) is the minimal value for M.

Chapter 5

Summary and Conclusions

In this thesis, we resolve an outstanding issue of the foundation of quantum statistical physics. Namely, we show that the use of quantum statistical ensembles with narrow energy distributions for describing the equilibria of macroscopic quantum systems can be justified.

In Chapter 2, we formulate a stability criterion for statistical ensembles describing macroscopic systems which is suitable for a broad range of many-body systems. An ensemble is called "stable" when a small number of local measurements cannot significantly modify the probability distribution of the total energy of the system. We apply this stability criterion to lattices of spins-$\frac{1}{2}$ and analytically derive an expression which describes the effect of local measurements on the probability distribution of the total energy $g(E)$.

Based on the results obtained for lattices of spins-$\frac{1}{2}$, we show that even relatively rare random local measurements impose strict constraints on quantum statistical ensembles. Quantum statistical ensembles characterised by $g(E)$ which are significantly broader than that of the canonical ensemble are unstable. The lifetime of such $g(E)$ is extremely short such that narrow $g(E)$ can be assumed in all practical calculations. In contrast, ensembles characterised by $g(E)$ with a width which is of the same order as that of the canonical ensemble are nearly stable in the absolute sense. This means that the broadening effect and the narrowing effect compensate each other for this width.

The above results justify the use of statistical ensembles with narrow $g(E)$ for the equilibrium description of macroscopic systems, such as the canonical or microcanonical ensembles.

The analytical treatment of lattices of spins-$\frac{1}{2}$ is based on derivations which are system specific. Therefore, the results may be not directly applicable beyond spin lattices. However, the basic concept of the stability of statistical ensembles is applicable to all many-body systems in general. Moreover, we expect that similar results as that described above can also be obtained for other systems.

In Chapter 3, we numerically test the analytical results obtained in Chapter 2. We investigate the stability $g(E)$ by directly simulating interacting spin systems of different sizes with up to 24 spins.

First, we consider the finite-size effects with respect to the local measurements. Since, the finite-size effects are rather pronounced for microscopic systems, we limit our investigation to the two-peak $g(E)$ and study the evolution of the stability measure $\overline{\Delta G}(n)$ as well

as the evolution of other stability measures that we propose. The results of the numerical investigations are consistent with the analytical results in Chapter 2.

In Chapter 4, we introduce a macroscopicity measure M for quantum superpositions of macroscopically distinct states. We call a quantum superposition macroscopic if one local measurement induces significant modifications of the density matrices of a macroscopic number of subsystems. This measure is based the notion of the instability of individual quantum states with respect to one local measurement.

The definition of the macroscopicity measure M is suitable for a broad variety of many-body systems. We apply this measure to lattices of spins-$\frac{1}{2}$ and show that M is governed by the variations of the individual spin polarisations and the spin-spin correlations due to the local measurement. In the end, we give two examples by explicitly calculating the macroscopicity measure M.

Based on all the above results, we obtain the following constraints for experiments aiming at protecting unconventional statistical ensembles for finite spin systems. Such experiments should avoid: (i) external magnetic fields, (ii) long-range order, (iii) local constants of motion. Effectively, each of the above points increases the measurement frequency and thereby decreases the lifetime of a statistical ensemble.

In this thesis, we formulate a general concept of stability of quantum statistical ensembles. This concept is applicable to any physical system in principle. Further investigations could include the application of the stability criterion for quantum statistical ensembles to other physical systems, for example to systems with translational degrees of freedom.

Appendix A

Derivations for Chapter 2

A.1 Derivations for spins in magnetic field

In this Appendix, we present a rigorous derivation of Eq. (2.28). We defined the energy distribution $g_n(E)$ with respect to a coarse-grained energy axis. Here, we consider the occupation of individual energy levels and introduce the probability distribution of total energy $f_n(E)$ without any coarse-graining.

We consider N_s non-interacting spin in a uniform magnetic field H_z with the Hamiltonian in Eq. (2.27). The smallest energy eigenvalue for this system is $E_{\min} = -\frac{H_z N_s}{2}$ and the biggest energy eigenvalue is $E_{\max} = \frac{H_z N_s}{2}$. The eigenenergies are of the form

$$E = E_{\min} + H_z m, \tag{A.1}$$

where m is an integer $m \in [0, N_s]$. m is the number of spins pointing into the negative z-direction.

Now, let us consider the effect of the n-th measurement on the density matrix of the total system

$$\rho_{n-1} = \sum_i p(E_i) |E_i\rangle \langle E_i|. \tag{A.2}$$

The energy distribution $f_n(E)$ after the n-th measurement reads

$$f_n(E) = \frac{1}{B_n} \sum_k^{u(E)} \langle E_k | \mathcal{P}_n \rho_{n-1} \mathcal{P}_n | E_k \rangle = \frac{1}{B_n} \sum_k^{u(E)} \sum_i p(E_i) |\langle E_k | \mathcal{P}_n | E_i \rangle|^2, \tag{A.3}$$

where $u(E)$ is the subspace of the Hilbert space corresponding to the possibly degenerate eigenvalue E. The sum over the index k is, therefore, restricted to $|E_k\rangle \in u(E)$.

For the given Hamiltonian, a measurement of a single spin described by the projection operator $\mathcal{P}_n$ can induce transitions from an energy level E to two neighbouring energy levels $E - H_z$ and $E + H_z$. The sum over i in Eq. (A.3) is, hence, limited to $E_i = E$, $E_i = E - H_z$

and $E_i = E + H_z$

$$f_n(E) = \frac{1}{B_n} \sum_k^{u(E)} \left[p(E) \sum_i^{u(E)} |\langle E_k | \mathcal{P}_n | E_i \rangle|^2 + p(E + H_z) \sum_i^{u(E+H_z)} |\langle E_k | \mathcal{P}_n | E_i \rangle|^2 \right. \quad (A.4)$$
$$\left. + p(E - H_z) \sum_i^{u(E-H_z)} |\langle E_k | \mathcal{P}_n | E_i \rangle|^2 \right].$$

With $f(E) = p(E)\nu(E)$ and $\nu(E) = \dim[u(E)]$, we obtain

$$f_n(E) = \frac{1}{B_n} \left[f_{n-1}(E) \frac{\sum_k^{u(E)} \sum_i^{u(E)} |\langle E_k | \mathcal{P}_n | E_i \rangle|^2}{\dim[u(E)]} \right. \quad (A.5)$$
$$+ f_{n-1}(E + H_z) \frac{\sum_k^{u(E)} \sum_i^{u(E+H_z)} |\langle E_k | \mathcal{P}_n | E_i \rangle|^2}{\dim[u(E + H_z)]}$$
$$\left. + f_{n-1}(E - H_z) \frac{\sum_k^{u(E)} \sum_i^{u(E-H_z)} |\langle E_k | \mathcal{P}_n | E_i \rangle|^2}{\dim[u(E - H_z)]} \right].$$

Substituting the expression for the projection operator given in Eq. (2.12) and using that, for the given system,

$$\dim[u(E)] = \frac{N_s!}{m!(N_s - m)!}, \quad (A.6)$$

where m is defined by Eq. (A.1), the result reads[1]

$$f_n(E) = \frac{1}{B_n} \left[\left(\cos^4\left(\frac{\vartheta_n}{2}\right) - \frac{E - E_{\min}}{H_z N_s} \cos(\vartheta_n) \right) f_{n-1}(E) \right. \quad (A.7)$$
$$+ \frac{1}{4} \sin^2(\vartheta_n) \frac{E + H_z - E_{\min}}{H_z N_s} f_{n-1}(E + H_z)$$
$$\left. + \frac{1}{4} \sin^2(\vartheta_n) \left(1 - \frac{E - H_z - E_{\min}}{H_z N_s} \right) f_{n-1}(E - H_z) \right],$$

where

$$B_n = \frac{1}{2} + \left(\frac{1}{2} - \frac{E_{\text{av},n-1} - E_{\min}}{H_z N_s} \right) \cos(\vartheta_n). \quad (A.8)$$

When changing to the coarse-grained energy axis with a bin width $\Delta_E \gg H_z$ and correspondingly shifting from $f_n(E)$ to $g_n(E)$, we substitute $E \pm H_z \to E$ in the above equation and obtain for $g(E)$

$$g_n(E) = \frac{1}{B_n} \left(\frac{1}{2} - \frac{E - \frac{1}{2}(E_{\max} + E_{\min})}{E_{\max} - E_{\min}} \cos(\vartheta_n) \right) g_{n-1}(E), \quad (A.9)$$

where $E_{\max} - E_{\min} = H_z N_s$. Since $E_{\max} + E_{\min} = 0$ for the Hamiltonian given, we arrive at Eq. (2.28).

---

[1] The result depends only on the polar angle ϑ_n because of the axial symmetry of the problem.

A.1.1 Evolution of the average energy

The average energy $E_{\text{av},n}$ after the n-th measurement reads

$$
\begin{aligned}
E_{\text{av},n} &= \sum_E E\, f_n(E) \tag{A.10}\\
&= E_{\text{av},n-1} + \frac{1}{B_n}\left[\frac{1}{4}H_z \sin^2(\vartheta_n)\left(1 - \frac{E_{\text{av},n-1} - E_{\min}}{E_{\text{av},T=\infty} - E_{\min}}\right) - \frac{\cos(\vartheta_n)}{H_z N_s}w_{g,n-1}^2\right] \tag{A.11}
\end{aligned}
$$

where $w_{g,n-1}^2$ is the variance of $f_{n-1}(E)$ before the n-th measurement and

$$
E_{\text{av},T=\infty} \equiv \frac{1}{2}(E_{\max} - E_{\min}) + E_{\min} = \frac{1}{2}H_z N_s + E_{\min} \tag{A.12}
$$

is the average energy of the canonical ensemble at infinite temperature.

Now, we consider specific measurement outcomes.

$$
\vartheta = 0: \quad E_{\text{av},n} = E_{\text{av},n-1} - \frac{w_{g,n-1}^2}{E_{\max} - E_{\text{av},n-1}}, \tag{A.13}
$$

$$
\vartheta = \pi: \quad E_{\text{av},n} = E_{\text{av},n-1} + \frac{w_{g,n-1}^2}{E_{\text{av},n-1} - E_{\min}}, \tag{A.14}
$$

$$
\vartheta = \frac{\pi}{2}: \quad E_{\text{av},n} = E_{\text{av},n-1} + \frac{H_z}{2}\left(1 - \frac{E_{\text{av},n-1} - E_{\min}}{E_{\text{av},T=\infty} - E_{\min}}\right). \tag{A.15}
$$

If the measured spin is aligned parallel to the z-axis ($\vartheta = 0$, $\vartheta = \pi$), E_{av} increases for a spin pointing into the negative z-direction and decreases in the opposite case. This is an implication of the correlation between the measurement outcomes and the total energy. If the measured spin is polarised in the $x - y$ plane ($\vartheta = \frac{\pi}{2}$), the shift of the average energy does not depend on the particular spin polarisation in the plane. Such a measurement outcome induces a drift of E_{av} towards the value in the infinite-temperature limit $E_{\text{av},T=\infty}$ (higher entropy) and corresponds to heating.

Averaging $E_{\text{av},n}$ over all possible measurement outcomes, we obtain

$$
\begin{aligned}
\overline{E_{\text{av},n}} &= \int d\vartheta_n \sin(\vartheta_n)\, E_{\text{av},n}\, B_n \\
&= E_{\text{av},n-1} + \frac{H_z}{3}\left(1 - \frac{E_{\text{av},n-1} - E_{\min}}{E_{\text{av},T=\infty} - E_{\min}}\right). \tag{A.16}
\end{aligned}
$$

This means that the average behaviour of $E_{\text{av},n}$ is governed by the heating effect.

A.1.2 Evolution of the variance of the energy distribution

Now, we calculate the variance $w_{g,n}^2$ of $g_n(E)$ after the n-th measurement

$$
w_{g,n}^2 \equiv \sum_E \left(E - E_{\text{av},n}\right)^2 f_n(E). \tag{A.17}
$$

First, we split the above expression into two terms and consider each term separately

$$w_{g,n}^2 = \sum_E \left(E - E_{\mathrm{av},n-1} \right)^2 f_n(E) - \left(E_{\mathrm{av},n} - E_{\mathrm{av},n-1} \right)^2. \tag{A.18}$$

The first term yields

$$\sum_E \left(E - E_{\mathrm{av},n-1} \right)^2 f_n(E) \tag{A.19}$$

$$= w_{g,n-1}^2 + \frac{1}{B_n} \left[\frac{1}{4} H_z^2 \sin^2(\vartheta_n) \left(1 - \frac{w_{g,n-1}^2}{w_{T=\infty}^2} \right) - \frac{\cos(\vartheta_n)}{H_z N_s} \langle E^3 \rangle_{n-1} \right],$$

where $\langle E^3 \rangle_{n-1}$ is the third central moment of the total-energy distribution $f_{n-1}(E)$. The second term in Eq. (A.18) follows directly from Eq. (A.11) such that, in total, we obtain

$$w_{g,n}^2 = w_{g,n-1}^2 + \frac{1}{B_n} \left[\frac{1}{4} H_z^2 \sin^2(\vartheta_n) \left(1 - \frac{w_{g,n-1}^2}{w_{T=\infty}^2} \right) - \frac{\cos(\vartheta_n)}{H_z N_s} \langle E^3 \rangle_{n-1} \right] \tag{A.20}$$

$$+ \frac{1}{B_n^2} \left[\frac{1}{4} H_z \sin^2(\vartheta_n) \left(1 - \frac{E_{\mathrm{av},n-1} - E_{\min}}{E_{\mathrm{av},T=\infty} - E_{\min}} \right) - \frac{\cos(\vartheta_n)}{H_z N_s} w_{g,n-1}^2 \right]^2.$$

Now, let us evaluate Eq. (A.20) for some specific measurement outcomes

$$\vartheta_n = 0: \quad w_{g,n}^2 = w_{g,n-1}^2 - \left(\frac{w_{g,n-1}^2}{E_{\mathrm{av},n-1} - E_{\min}} \right)^2 + \frac{\langle E^3 \rangle_{n-1}}{E_{\mathrm{av},n-1} - E_{\min}}, \tag{A.21}$$

$$\vartheta_n = \pi: \quad w_{g,n}^2 = w_{g,n-1}^2 - \left(\frac{w_{g,n-1}^2}{E_{\max} - E_{\mathrm{av},n-1}} \right)^2 - \frac{\langle E^3 \rangle_{n-1}}{E_{\mathrm{av},n-1} - E_{\min}}, \tag{A.22}$$

$$\vartheta_n = \frac{\pi}{2}: \quad w_{g,n}^2 = w_{g,n-1}^2 + \frac{1}{2} H_z^2 \left(1 - \frac{w_{g,n-1}^2}{w_{T=\infty}^2} \right) - \frac{1}{4} H_z^2 \left(1 - \frac{E_{\mathrm{av},n-1} - E_{\min}}{E_{\mathrm{av},T=\infty} - E_{\min}} \right)^2 \tag{A.23}$$

If we assume for simplicity that $\langle E^3 \rangle_{n-1} = 0$, a measurement outcome which correlates with the total energy ($\vartheta_n = 0$ and $\vartheta_n = \pi$) narrows the energy distribution $w_{g,n}^2 - w_{g,n-1}^2 < 0$. On the contrary, the measurement outcome corresponding to heating ($\vartheta_n = \pi/2$) drives the variance to $w_{T=\infty}^2$.

Now, we average $w_{g,n}^2$ over all possible measurement outcomes[2]

$$\overline{w_{g,n}^2} = \int d\vartheta_n \sin(\vartheta_n) \, w_{g,n}^2 \, B_n \tag{A.24}$$

$$= w_{g,n-1}^2 + \frac{1}{3} H_z^2 \left(1 - \frac{w_{g,n-1}^2}{w_{T=\infty}^2} \right) \tag{A.25}$$

$$- \frac{1}{4} H_z^2 \left[\left(\frac{w_{g,n-1}^2}{w_{T=\infty}^2} \right)^2 k_1(x) + \frac{w_{g,n-1}^2}{w_{T=\infty}^2} k_2(x) + k_3(x) \right],$$

---

[2]It is worth noticing that, unlike for $\overline{E_{\mathrm{av},n}}$, the behaviour of $\overline{w_{g,n}^2}$ in Eq. (A.25) shows both effects, that of heating (second term in Eq. (A.25)), and that of narrowing (third term in Eq. (A.25)).

where

$$k_1(x) = \left| \frac{x - \operatorname{artanh}(x)}{x^3} \right| \tag{A.26}$$

$$k_2(x) = \left| \frac{x\left(\frac{4}{3}x^2 - 2\right) - 2(x^2 - 1)\operatorname{artanh}(x)}{x^3} \right| \tag{A.27}$$

$$k_3(x) = \left| \frac{x\left(\frac{5}{3}x^2 - 1\right) + (x^2 - 1)^2\operatorname{artanh}(x)}{x^3} \right|, \tag{A.28}$$

and $x = \frac{E_{\mathrm{av},n-1} - E_{\min}}{E_{\mathrm{av},T=\infty} - E_{\min}} - 1$ with $x \in [-1, +1]$. $x = -1$ corresponds to $E_{\mathrm{av},n-1} = E_{\min}$ and $x = 1$ to $E_{\mathrm{av},n-1} = E_{\max}$. The functions $k_2(x)$ and $k_3(x)$ are finite for all values of x, but $k_1(x)$ diverges for $x \to \pm 1$. Taking into account that the variance $w^2_{g,n-1}$ vanishes in these limits renders this divergence negligible.

The important term which determines the change of the variance $\overline{w^2_{g,n}} - w^2_{g,n-1}$ is thus $w^2_{g,n-1}/w^2_{T=\infty}$. If $w^2_{g,n-1}/w^2_{T=\infty} \ll 1$ corresponding to a narrow $f(E)$, then, according to Eq. (A.25), $\overline{w^2_{g,n}} - w^2_{g,n-1} \sim 1$. However, for a broad $f(E)$, the ratio $w^2_{g,n-1}/w^2_{T=\infty}$ can easily be of order N_s leading to a significant narrowing.

A.1.3   Stable variance and its relation to the canonical ensemble

Requiring $\overline{w^2_{g,n}} - w^2_{g,n-1} = 0$ in Eq. (A.25), we obtain

$$0 = -\frac{4}{3}\left(1 - \frac{w^2_{g,n-1}}{w^2_{T=\infty}}\right) + \left(\frac{w^2_{g,n-1}}{w^2_{T=\infty}}\right)^2 k_1(x) + \frac{w^2_{g,n-1}}{w^2_{T=\infty}} k_2(x) + k_3(x). \tag{A.29}$$

The solution is

$$\left[w^2_g\right]_{\mathrm{stab}}(x) = \frac{w^2_{T=\infty}}{k_1(x)}\left(k_2(x) + \frac{4}{3}\right)\left(-\frac{1}{2} + \sqrt{\frac{1}{4} + k_1(x)\frac{\frac{4}{3} - k_3(x)}{\left(k_2(x) + \frac{4}{3}\right)^2}}\right). \tag{A.30}$$

Figure A.1 shows $\frac{\left[w^2_g\right]_{\mathrm{stab}}(x)}{w^2_{T=\infty}}$ as a function of x. It is worth mentioning, hereby, that the stable variance $\left[w^2_g\right]_{\mathrm{stab}}(x)$ does not vanish at $x = \pm 1$ but remains finite.

For the canonical ensemble, the relation between x and the variance can be obtained by approximating the density of states using Stirlings formula and expanding the exponential until the second order

$$w^2_{\mathrm{can}}(x) \cong w^2_{T=\infty}(1 - x^2). \tag{A.31}$$

The relation between the canonical variance $w^2_{\mathrm{can}}(x)$ and the stable variance $\left[w^2_g\right]_{\mathrm{stab}}(x)$ is shown in Fig. A.2. For the particular case $x = 0$, we obtain

$$\left[w^2_g\right]_{\mathrm{stab}}(0) = (\sqrt{8} - 2)w^2_{T=\infty} \approx 0,8\ w^2_{T=\infty} = 0,8\ w^2_{\mathrm{can}}(0). \tag{A.32}$$
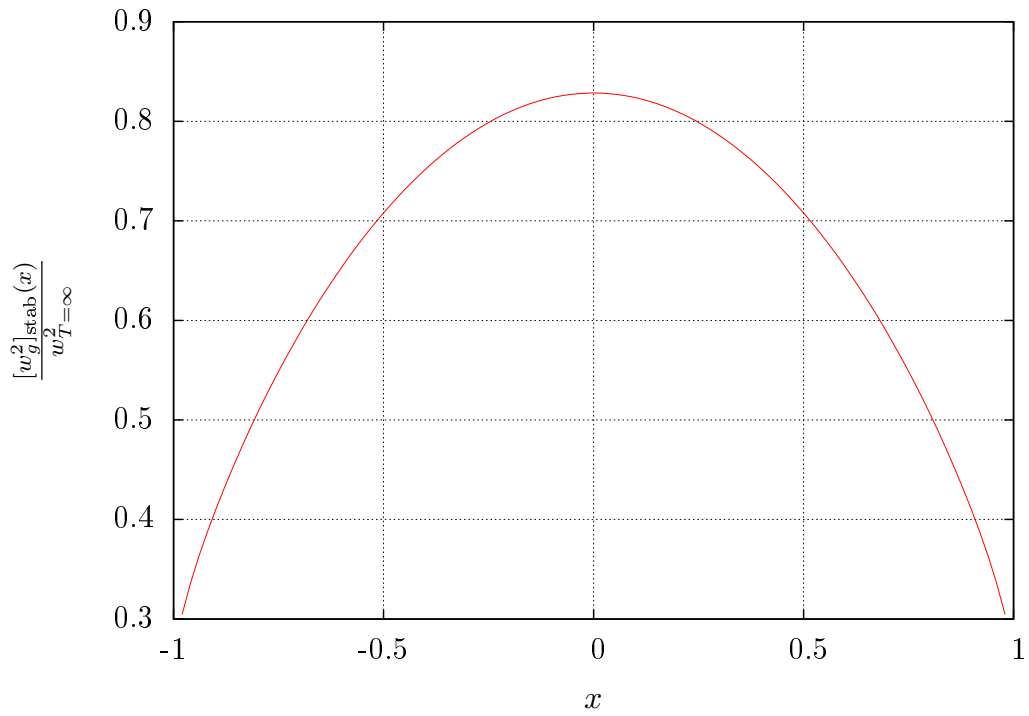
Figure A.1: The stable variance $\frac{\left[w_g^2\right]_{\text{stab}}(x)}{w_{T=\infty}^2}$ is shown as a function of x.
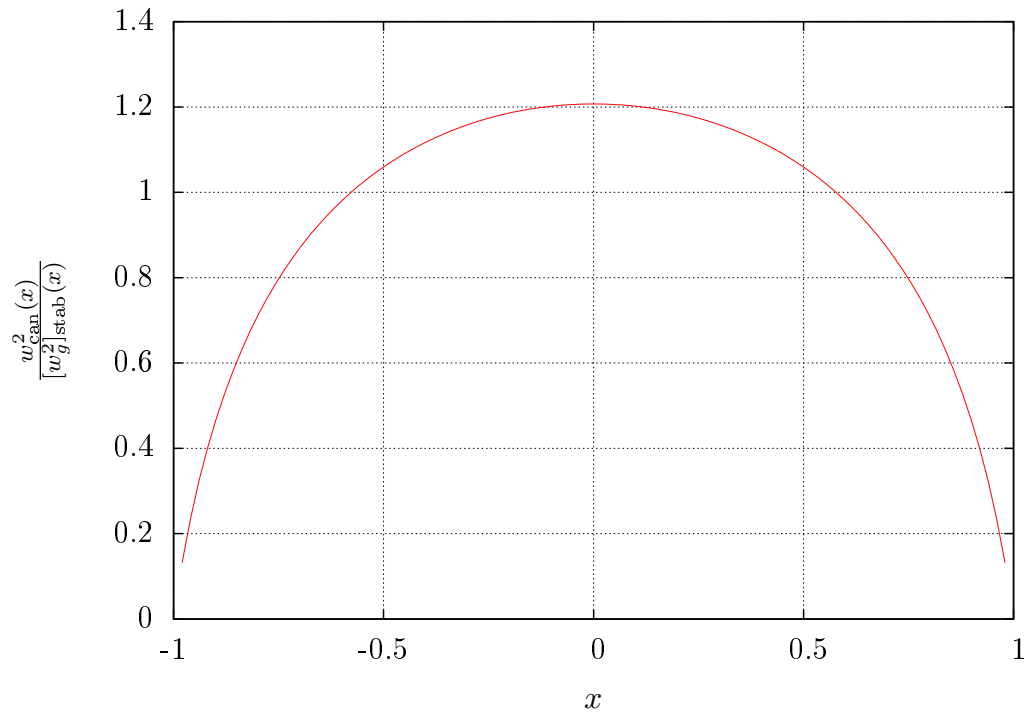

Figure A.2: The relation between the stable variance and the canonical variance $\frac{w_{\text{can}}^2(x)}{\left[w_g^2\right]_{\text{stab}}(x)}$ is shown as a function of x.

A.2 Coarse-graining of the energy axis

For a canonical ensemble, heating means that E_{av} drifts towards the values corresponding to higher entropy $S(E_{\text{av}})$, i.e., E_{av} increases for positive temperatures and decreases for negative ones. For positive temperatures T, the increase of E_{av} due to one measurement is of the order of one-particle energy ϵ_1.

Our definition of $g(E)$ implies averaging over energy bins whose width Δ_{e} satisfies the following inequalities

$$\epsilon_1 \ll \Delta_{\text{e}} \ll T(E_{\text{av}})\sqrt{C_V(E_{\text{av}})}. \tag{A.33}$$

In the case of negative temperatures, $|T(E_{\text{av}})|$ should be used instead.

The left inequality makes Δ_{e} larger than the energy range ϵ_1 connected by typical off-diagonal single-particle elements. This allows us to neglect the energy drift (heating) and also approximate the relation between $g_{n-1}(E)$ and $g_n(E)$ as being local in energy. The right inequality in Eq. (A.33) assures that the energy eigenstates within each bin correspond to approximately the same local density matrices.

Typically, Δ_{e} can be found such that both inequalities in (A.33) are satisfied for the whole energy range except for extremely low temperatures. We, however, assume that this energy interval makes a negligible contribution to $g(E)$, i.e., the integral of $g(E)$ over this energy interval is much smaller than 1.

Until now, we have considered the effect of a single measurement. Let us here for a moment consider the limit $n \ll \sqrt{N_s}$. After n measurements, the drift of E_{av} can be of the order $\epsilon_1 n$, cf. Appendix A.1. For $n \ll \sqrt{N_s}$, the maximal drift is much smaller than $\epsilon_1\sqrt{N_s}$. This condition is the same as the right inequality of Eq. (A.33) since $T(E_{\text{av}}) \sim \epsilon_1$. We require however that, even in the limit of $n \ll \sqrt{N_s}$, the drift of E_{av} remains smaller than Δ_{e}.

The broadening effect mentioned above can also be neglected on the same coarse-grained energy axis because the increase of the variance is $w_g^2 \cong n$. Therefore, for $n \ll \sqrt{N_s}$, the increase of the width w_g is smaller than $\sqrt[4]{N_s}\epsilon_1$.

Another possibility to deal with the heating effect is to introduce a detailed balance condition for the interaction between the system and the environment. According to this condition, the individual probabilities of measurement outcomes were to be modified such that, on average, E_{av} remains close to its initial value.

In principle, a detailed balance condition implies that the environment, which triggers the local measurements, is set to the same average energy. From this viewpoint, completely random measurements correspond to an environment in the infinite temperature limit.

A.3 Derivation of the general form of the cutting function

The transformation from ρ_{n-1} to ρ_n given in Eq. (2.19) can be iterated to obtain the transformation from ρ_0 to ρ_n

$$(\rho_n)_{kl} = \frac{1}{B}\langle E_k|\mathcal{O}\rho_0\mathcal{O}^\dagger|E_l\rangle, \tag{A.34}$$

where $|E_i\rangle$ is the energy eigenstate of the total system, $(\rho_n)_{kl} = \langle E_k|\rho_n|E_l\rangle$, B is the normalisation factor, and

$$\mathcal{O} = \mathcal{P}_n e^{-i\mathcal{H}(t_n - t_{n-1})}\mathcal{P}_{n-1}\cdots\mathcal{P}_2 e^{-i\mathcal{H}(t_2 - t_1)}\mathcal{P}_1 e^{-i\mathcal{H}t_1}. \tag{A.35}$$

In principle, the initial density matrix ρ_0 describes the ensemble of systems each of which is described by a quantum wave function with a given energy distribution $g_0(E)$. Such a density matrix is diagonal $\rho_0 = \sum_i (\rho_0)_{ii}|E_i\rangle\langle E_i|$. In practice, however, each density matrix ρ_0 corresponding to an individual pure quantum state with a given $g_0(E)$ for a generic quantum system typically leads to the same results as the above ρ_0 due to quantum typicality. In such a case, the off-diagonal elements of ρ_0 can be neglected given the dephasing between different energy eigenstates over each time interval $t_n - t_{n-1}$.

We are interested in the total-energy distribution and, therefore, focus on $(\rho_n)_{kk}$ (the diagonal elements of the density matrix)

$$\begin{aligned}
(\rho_n)_{kk} &= \frac{1}{B}\langle E_k|\mathcal{O}\left(\sum_i (\rho_0)_{ii}|E_i\rangle\langle E_i|\right)\mathcal{O}^\dagger|E_k\rangle \tag{A.36} \\
&= \frac{1}{B}(\rho_0)_{kk}\langle E_k|\mathcal{O}|E_k\rangle\langle E_k|\mathcal{O}^\dagger|E_k\rangle + \frac{1}{B}\langle E_k|\mathcal{O}\left(\sum_{i,i\neq k}(\rho_0)_{ii}|E_i\rangle\langle E_i|\right)\mathcal{O}^\dagger|E_k\rangle, \tag{A.37}
\end{aligned}$$

where, in the last step, we divided the sum into two parts. Using $|E_k\rangle\langle E_k| = \mathbf{1} - \sum_{i,i\neq k}|E_i\rangle\langle E_i|$, we further rewrite Eq. (A.37) as

$$\begin{aligned}
(\rho_n)_{kk} &= \frac{1}{B}(\rho_0)_{kk}\langle E_k|\mathcal{O}^\dagger\mathcal{O}|E_k\rangle \tag{A.38} \\
&\quad -\frac{1}{B}\sum_{i,i\neq k}(\rho_0)_{kk}\langle E_k|\mathcal{O}^\dagger|E_i\rangle\langle E_i|\mathcal{O}|E_k\rangle + \frac{1}{B}\sum_{i,i\neq k}(\rho_0)_{ii}\langle E_i|\mathcal{O}^\dagger|E_k\rangle\langle E_k|\mathcal{O}|E_i\rangle.
\end{aligned}$$

Now, we introduce the coarse-graining of the energy axis which means that we divide the energy axis into bins of width Δ_e introduced in Sec. A.2. The probability distribution $g_n(E)$ is defined in terms of these bins as follows

$$g_n(E) = \frac{1}{\Delta_e}\sum_k^{\text{bin}(E)}(\rho_n)_{kk}, \tag{A.39}$$

where the sum is taken over all energy eigenstates within the given bin. Substituting

Eq. (A.38) into Eq. (A.39), we obtain

$$
\begin{aligned}
g_n(E) \;=\; & \frac{1}{\Delta_{\mathrm{e}} B} \sum_{k}^{\mathrm{bin}(E)} (\rho_0)_{kk} \langle E_k | \mathcal{O}^\dagger \mathcal{O} | E_k \rangle \\
& -\frac{1}{\Delta_{\mathrm{e}} B} \sum_{k}^{\mathrm{bin}(E)} \sum_{i,i\neq k} (\rho_0)_{kk} \langle E_k | \mathcal{O}^\dagger | E_i \rangle \langle E_i | \mathcal{O} | E_k \rangle \\
& +\frac{1}{\Delta_{\mathrm{e}} B} \sum_{k}^{\mathrm{bin}(E)} \sum_{i,i\neq k} (\rho_0)_{ii} \langle E_i | \mathcal{O}^\dagger | E_k \rangle \langle E_k | \mathcal{O} | E_i \rangle ,
\end{aligned}
\tag{A.40}
$$

where $\sum$ [without $\mathrm{bin}(E)$] denotes a sum which is not restricted to the bin.

Now, we show that the first term in Eq. (A.40) makes the main contribution to $g_n(E)$, while the last two terms in Eq. (A.40) mainly compensate each other. To show this, we split each unrestricted sum into two sums, where one sum extends over the energy eigenstates within the bin, while the other one extends over the energy eigenstates outside the bin. The latter sum is to be denoted as $\sum^{\overline{\mathrm{bin}(E)}}$. We also use the relation $\langle E_k | \mathcal{O}^\dagger | E_i \rangle \langle E_i | \mathcal{O} | E_k \rangle = |\langle E_i | \mathcal{O} | E_k \rangle|^2$. Hence, we obtain for the last two terms in Eq. (A.40)

$$
-\frac{1}{\Delta_{\mathrm{e}} B} \left[\sum_{k}^{\mathrm{bin}(E)} \sum_{i,i\neq k}^{\mathrm{bin}(E)} (\rho_0)_{kk} |\langle E_i | \mathcal{O} | E_k \rangle|^2 + \sum_{k}^{\mathrm{bin}(E)} \sum_{i}^{\overline{\mathrm{bin}(E)}} (\rho_0)_{kk} |\langle E_i | \mathcal{O} | E_k \rangle|^2 \right.
$$
$$
\left. - \sum_{k}^{\mathrm{bin}(E)} \sum_{i,i\neq k}^{\mathrm{bin}(E)} (\rho_0)_{ii} |\langle E_k | \mathcal{O} | E_i \rangle|^2 - \sum_{k}^{\mathrm{bin}(E)} \sum_{i}^{\overline{\mathrm{bin}(E)}} (\rho_0)_{ii} |\langle E_k | \mathcal{O} | E_i \rangle|^2 \right]. \tag{A.41}
$$

Now, the two terms in Eq. (A.41) where both sums are restricted to $\mathrm{bin}(E)$ cancel each other. This can be readily seen after exchanging the summation indices i and k in one of these two terms. The remaining terms in Eq. (A.40) can be further rewritten as

$$
\begin{aligned}
g_n(E) \;=\; & \frac{1}{\Delta_{\mathrm{e}} B} \sum_{k}^{\mathrm{bin}(E)} (\rho_0)_{kk} \langle E_k | \mathcal{O}^\dagger \mathcal{O} | E_k \rangle \\
& -\frac{1}{\Delta_{\mathrm{e}} B} \sum_{k}^{\mathrm{bin}(E)} (\rho_0)_{kk} \left(\sum_{i}^{\overline{\mathrm{bin}(E)}} |\langle E_i | \mathcal{O} | E_k \rangle|^2 \right) \\
& +\frac{1}{\Delta_{\mathrm{e}} B} \sum_{i}^{\overline{\mathrm{bin}(E)}} (\rho_0)_{ii} \left(\sum_{k}^{\mathrm{bin}(E)} |\langle E_k | \mathcal{O} | E_i \rangle|^2 \right) .
\end{aligned}
\tag{A.42}
$$

The last two terms of Eq. (A.42) contain off-diagonal elements $|\langle E_i | \mathcal{O} | E_k \rangle|^2$ corresponding to transitions between energy bins, because E_k and E_i lie in different bins. Let us denote the characteristic energy range $|E_k - E_i|$ of the off-diagonal elements $\langle E_k | \mathcal{O} | E_i \rangle$ as $\Delta_{\mathcal{O}}$. This range is limited by the condition
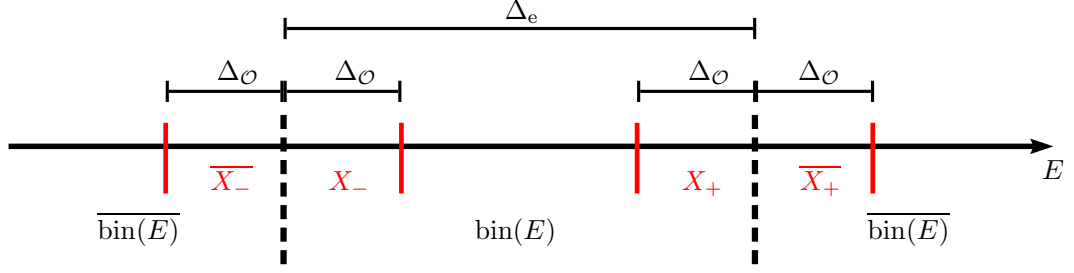
$$
\Delta_{\mathcal{O}} \sim \epsilon_1 n \ll \Delta_{\mathrm{e}} . \tag{A.43}
$$

Figure A.3: (Colour online) Schematic representation of the energy intervals $\mathrm{bin}(E)$, $\overline{\mathrm{bin}(E)}$, X_-, $\overline{X}_-$, X_+ and $\overline{X}_+$, introduced in the text. The characteristic size of the intervals Δ_e and $\Delta_\mathcal{O}$ are indicated above.

Therefore, only small energy intervals of length $\Delta_\mathcal{O}$ near the boundaries between the bins contribute to the sums. As shown in Fig. A.3, we label these energy intervals as X_-, $\overline{X}_-$, X_+ and $\overline{X}_+$. With such notations, Eq. (A.42) can be rewritten as

$$
\begin{aligned}
g_n(E) \;=\; & \frac{1}{\Delta_\mathrm{e}B} \sum_{k}^{\mathrm{bin}(E)} (\rho_0)_{kk} \langle E_k | \mathcal{O}^\dagger \mathcal{O} | E_k \rangle \\
& -\frac{1}{\Delta_\mathrm{e}B} \left[\sum_{k}^{X_-} (\rho_0)_{kk} \left(\sum_{i}^{\overline{X}_-} |\langle E_i|\mathcal{O}|E_k\rangle|^2 \right) + \sum_{k}^{X_+} (\rho_0)_{kk} \left(\sum_{i}^{\overline{X}_+} |\langle E_i|\mathcal{O}|E_k\rangle|^2 \right) \right] \\
& +\frac{1}{\Delta_\mathrm{e}B} \left[\sum_{i}^{\overline{X}_-} (\rho_0)_{ii} \left(\sum_{k}^{X_-} |\langle E_k|\mathcal{O}|E_i\rangle|^2 \right) + \sum_{i}^{\overline{X}_+} (\rho_0)_{ii} \left(\sum_{k}^{X_+} |\langle E_k|\mathcal{O}|E_i\rangle|^2 \right) \right].
\end{aligned}
\tag{A.44}
$$

Now, we show that the last four terms in Eq. (A.44) can be neglected in comparison with the first one, provided $g_0(E)$ does not change too fast. Specifically, we impose the condition

$$
\left| \frac{dg_0(E)}{dE} \right| \lesssim \frac{g_0(E)}{w_\mathrm{can}} \ll \frac{g_0(E)}{\Delta_\mathrm{e}},
\tag{A.45}
$$

where $w_\mathrm{can} = T(E_\mathrm{av})\sqrt{C_V(E_\mathrm{av})}$ is the width of the energy distribution corresponding to the canonical ensemble with the same initial average energy as that of $g_0(E)$. The condition in Eq. (A.45) must be satisfied within the energy interval, where $g_0(E)$ is large enough to make a non-negligible contribution to the normalisation integral $\int_{-\infty}^{\infty} g_0(E)dE = 1$.

In the first term of Eq. (A.44), we expect that, even if $(\rho_0)_{kk}$ and $\langle E_k|\mathcal{O}^\dagger\mathcal{O}|E_k\rangle$ fluctuate with respect to their bin-averaged values, they do it in an uncorrelated way. According to Eq. (A.39), the bin-averaged value of $(\rho_0)_{kk}$ is $\Delta_\mathrm{e}g_0(E)/N_\mathrm{bin}(E)$, where $N_\mathrm{bin}(E)$ is the number of states within the bin. We define the bin-average of $\langle E_k|\mathcal{O}^\dagger\mathcal{O}|E_k\rangle$ as

$$
\left[\mathcal{O}^\dagger \mathcal{O} \right]_\mathrm{diag}(E) \equiv \frac{1}{N_\mathrm{bin}(E)} \sum_{k}^{\mathrm{bin}(E)} \langle E_k|\mathcal{O}^\dagger\mathcal{O}|E_k\rangle.
\tag{A.46}
$$

Given the right inequalities in Eqs. (A.39) and (A.45), both bin-averages change very weakly

over the bin size Δ_e. Therefore, we can approximate the entire first term in Eq. (A.44) as

$$\frac{1}{\Delta_e B} \sum_k^{\text{bin}(E)} (\rho_0)_{kk} \langle E_k | \mathcal{O}^\dagger \mathcal{O} | E_k \rangle \approx \frac{1}{B} \left[\mathcal{O}^\dagger \mathcal{O} \right]_{\text{diag}} (E) \, g_0(E). \qquad (A.47)$$

Each of the remaining four terms in Eq. (A.44) has comparable values. Let us estimate the first of them. We use the following inequality

$$\sum_i^{\overline{X_-}} |\langle E_i | \mathcal{O} | E_k \rangle|^2 \leq \sum_i |\langle E_i | \mathcal{O} | E_k \rangle|^2 = \langle E_k | \mathcal{O}^\dagger \mathcal{O} | E_k \rangle, \qquad (A.48)$$

where, as before, the second sum extends over all energy eigenstates of the system. Employing this inequality together with the assumptions used for deriving Eq. (A.47), we obtain

$$\frac{1}{\Delta_e B} \sum_k^{X_-} (\rho_0)_{kk} \left(\sum_i^{\overline{X_-}} |\langle E_i | \mathcal{O} | E_k \rangle|^2 \right) \leq \frac{1}{\Delta_e B} \sum_k^{X_-} (\rho_0)_{kk} \langle E_k | \mathcal{O}^\dagger \mathcal{O} | E_k \rangle$$

$$\approx \frac{1}{\Delta_e B} \sum_k^{X_-} (\rho_0)_{kk} \left[\mathcal{O}^\dagger \mathcal{O} \right]_{\text{diag}} (E) \approx \frac{1}{B} \left[\mathcal{O}^\dagger \mathcal{O} \right]_{\text{diag}} (E) \frac{\Delta_{\mathcal{O}}}{\Delta_e} g_0(E). \qquad (A.49)$$

Since $\frac{\Delta_{\mathcal{O}}}{\Delta_e} \ll 1$, Eqs. (A.44), (A.47) and (A.49) imply that

$$g_n(E) \approx \frac{1}{B} \left[\mathcal{O}^\dagger \mathcal{O} \right]_{\text{diag}} (E) \, g_0(E), \qquad (A.50)$$

which is the same as Eq. (2.20).

A.4 Analytical approximation for $\overline{\Delta G}(n)$

In this Section, we derive the analytical approximation for $\overline{\Delta G}(n)$ used in Fig. 2.2. From relation (2.21), we obtain

$$g_n(E) = \prod_{i=1}^n \frac{1}{B_i} \left[\mathcal{P}_i \right]_{\text{diag}} (E) \, g_0(E). \qquad (A.51)$$

The substitution of this expression into Eq. (2.6) leads to

$$\Delta G(n) = \int_{-\infty}^{+\infty} \Big| \prod_{i=1}^n \frac{1}{B_i} \left[\mathcal{P}_i \right]_{\text{diag}} (E) - 1 \Big| g_0(E) dE, \qquad (A.52)$$

which, after averaging, gives Eq. (2.25).

For the initial distribution $g_0(E) = \frac{1}{2}[\delta(E - E_1) + \delta(E - E_2)]$, Eq. (A.51) leads to $g_n(E) = p_1 \delta(E - E_1) + p_2 \delta(E - E_2)$ with some probabilities p_1 and p_2 ($p_1 + p_2 = 1$). We further note that for $n \to \infty$, either $p_1 \to 0$ or $p_2 \to 0$, such that $\Delta G(n) = |p_1 - p_2| \to 1$.

In order to find an approximate expression for $\overline{\Delta G}(n)$, let us first observe that

$$\overline{\Delta G^2}(n) \approx \overline{[\Delta G(n) - \Delta G(n-1)]^2} + \overline{\Delta G^2}(n-1), \qquad (A.53)$$

because $\overline{\Delta G(n) - \Delta G(n-1)} \approx 0$. Therefore, we make the ansatz $\overline{\Delta G^2}(n) = \sum_{i=1}^{n} \overline{\gamma_i^2}$, where $\gamma_i = \Delta G(i) - \Delta G(i-1)$. The individual summands $\overline{\gamma_i^2}$ must become smaller as $\overline{\Delta G^2}(n)$ approaches 1. Therefore, we make the rough approximation $\overline{\gamma_i^2} \cong 1 - \overline{\Delta G^2}(n)$, which, in the continuum limit for n, leads to the differential equation

$$\frac{d\overline{\Delta G^2}(n)}{dn} = \lambda[1 - \overline{\Delta G^2}(n)], \qquad (A.54)$$

where λ is some constant. Assuming that $\overline{\Delta G^2}(n) \approx \overline{\Delta G}^2(n)$, we obtain

$$\overline{\Delta G}(n) \approx \sqrt{1 - e^{-\lambda n}}. \qquad (A.55)$$

We further adopt an approximation

$$\lambda = \kappa\, u^2\, (E_1 - E_2)^2\,, \qquad (A.56)$$

where $u = \overline{|\,[\mathcal{P}_n]'_{\text{diag}}(E_{\text{av}})|}$. κ is a fitting parameter. The expression in Eq. (A.56) can be justified by the following considerations. The parameter λ must be equal to 0, when $E_1 = E_2$. Also, λ must remain invariant under a sign-change of $E_1 - E_2$. Therefore, the lowest-order term allowed in an analytical expansion of λ around 0 is proportional to $(E_1 - E_2)^2$. Assuming that the value of λ is only controlled by u and $E_1 - E_2$, we conclude that u must also enter quadratically in order for λ to be dimensionless.

The above approximation can be further supported by a more detailed calculation of $\overline{\Delta G}(n)$ in which case the expression for $\Delta G(n)$ in Eq. (A.52) is to be averaged over all possible measurement outcomes. For this average, $\Delta G(n)$ must be weighed by the probability for a given set of n measurement outcomes, which equals the normalisation coefficient $\prod_{i=1}^{n} N_i = \int \prod_{i=1}^{n} [\mathcal{P}_i]_{\text{diag}}(E)\, g_0(E)dE$. Let us now make a simplifying assumption that the spin measurements are only done along the z-direction. Consequently, there are two possible measurement outcomes: positive ($\vartheta_n = 0$) and negative ($\vartheta_n = \pi$). According to Eq. (2.30), the projection operator is thus $[\mathcal{P}_i]_{\text{diag}}(E) = \frac{1}{2} \pm \frac{E}{E_{\max} - E_{\min}}$. After averaging over these two possibilities for each measurement, we obtain

$$\overline{\Delta G}(n) = \frac{1}{2} \sum_{k=0}^{n} |D_{np_1}(k) - D_{np_2}(k)|\,, \qquad (A.57)$$

where $D_{np}(k) = \binom{n}{k}p^k(1-p)^{n-k}$ is the binomial distribution and $p_i = \frac{1}{2} - \frac{E_i}{E_{\max} - E_{\min}}$. The value of $\overline{\Delta G}(n)$ is governed by the overlap as function of k between the two binomial distributions $D_{np_1}(k)$ and $D_{np_2}(k)$. With an increasing n, this overlap decreases approximately exponentially which is consistent with the asymptotic behaviour of $\overline{\Delta G}(n)$ that follows from Eq. (A.55) for large n.

Let us now consider a large n and approximate the binomial distribution $D_{np}(k)$ in

Eq. (A.57) by the Gaussian distribution $G_{np}(k)$. The expression in Eq. (A.57) in the integral form reads

$$\overline{\Delta G}(n) \approx \frac{1}{2} \int_{-\infty}^{\infty} |G_{np_1}(k) - G_{np_2}(k)| \, dk. \tag{A.58}$$

For a large n, the overlap of the two distributions $G_{np_1}(k)$ and $G_{np_2}(k)$ is typically governed by the small tails. Therefore, we make the following approximation

$$\overline{\Delta G}(n) \approx \frac{1}{2} \left[\int_{-\infty}^{k_0} G_{np_1}(k)dk + \int_{k_0}^{\infty} G_{np_2}(k)dk \right] \tag{A.59}$$

$$= 1 - \frac{1}{2} \left[\int_{k_0}^{\infty} G_{np_1}(k)dk + \int_{-\infty}^{k_0} G_{np_2}(k)(k)dk \right], \tag{A.60}$$

where k_0 is defined by $G_{np_1}(k_0) = G_{np_2}(k_0)$. The two remaining integrals above extend over the tails of the Gaussian distribution. For these integrals, we linearise the exponent round k_0 and obtain in the leading order for n

$$\overline{\Delta G}(n) \approx 1 - c \cdot e^{-n\lambda}, \tag{A.61}$$

where $\lambda \equiv \frac{1}{2\Sigma^2} \left(\frac{E_1 - E_2}{E_{\max} - E_{\min}} \right)^2$, $\Sigma \equiv \sqrt{p_1(1 - p_1)} + \sqrt{p_2(1 - p_2)}$ and c is some constant. The asymptotic formula for $\overline{\Delta G}(n)$ at large n in Eq. (A.61), therefore, exhibits the same functional form as that in Eq. (A.55).

A.5 Narrowing of a Gaussian probability distribution

For a Gaussian distribution

$$g_{n-1}(E) \sim \exp\left[-\frac{(E - E_{\text{av}})^2}{2w_{g,n-1}^2} \right] \tag{A.62}$$

with the variance $w_{g,n-1}^2 \ll (E_{\max} - E_{\min})^2$, the "cutting" by the linear function $[\mathcal{P}_n]_{\text{diag}}(E)$ can be expressed as

$$g_n(E) \sim [\mathcal{P}_n]_{\text{diag}}(E) \, e^{-\frac{(E - E_{\text{av}})^2}{2w_{g,n-1}^2}} = e^{\ln([\mathcal{P}_n]_{\text{diag}}(E)) - \frac{(E - E_{\text{av}})^2}{2w_{g,n-1}^2}}. \tag{A.63}$$

It changes the width according to the relation

$$\frac{1}{w_{g,n}^2} - \frac{1}{w_{g,n-1}^2} = \left(\frac{[\mathcal{P}_n]'_{\text{diag}}(E_{\text{av}})}{[\mathcal{P}_n]_{\text{diag}}(E_{\text{av}})} \right)^2, \tag{A.64}$$

where $[\mathcal{P}_n]'_{\text{diag}}(E_{\text{av}})$ is the derivative $d[\mathcal{P}_n]_{\text{diag}}(E_{\text{av}})/dE_{\text{av}}$. From Eq. (A.64), we obtain

$$\overline{\left[\frac{1}{w_{g,n}^2} \right]} \approx \frac{1}{w_{g,0}^2} + u^2 \, n, \tag{A.65}$$

where $u = \overline{|[\mathcal{P}_n]'_{\text{diag}}(E_{\text{av}})|}$, and we use $[\mathcal{P}_n]_{\text{diag}}(E_{\text{av}}) \sim 1$.

A.6 Estimate for the characteristic time τ_2

We assume that only outcomes of measurements of nearest neighbours are correlated with the total energy of the system. Since $\tau_2 \ll \tau_{\mathrm{corr}}$, each n-th measurement can, in principle, become correlated with any previous measurement. The probability for the second measurement not to become correlated with the first one is $P_2 = 1 - \frac{N_{\mathrm{NN}}}{N_s}$, where N_{NN} is the number of nearest neighbours. Correspondingly, the probability for the n-th measurement not to become correlated with any previous one is $P_n = 1 - (n-1)\frac{N_{\mathrm{NN}}}{N_s}$ for $n \ll N_s$. The probability that, among n measurements, there is no correlated pair, is

$$P(n) = \prod_{k=1}^{n} P_n = \prod_{k=1}^{n} \left(1 - (k-1)\frac{N_{\mathrm{NN}}}{N_s} \right) \approx \exp\left(-\frac{N_{\mathrm{NN}}}{N_s} \sum_{k=1}^{n} k \right) \approx e^{-n^2 \frac{N_{\mathrm{NN}}}{N_s}} \qquad (\mathrm{A.66})$$

for $1 \ll n \ll N_s$. Using the relation $n = N_s t/\tau_m$, we finally obtain the probability that, after time t, no correlated pair of measurements occurs,

$$P(t) \approx e^{-N_{\mathrm{NN}} N_s \frac{t^2}{\tau_m^2}}. \qquad (\mathrm{A.67})$$

Accordingly, $1 - P(t)$ is the probability that at least one correlated pair of measurements occurred. The characteristic time, thus, is

$$\tau_2 \approx \frac{1}{\sqrt{N_{\mathrm{NN}}}} \frac{\tau_m}{\sqrt{N_s}}. \qquad (\mathrm{A.68})$$

Since $\sqrt{N_s}$ is still large, τ_2 is certainly much smaller than any reasonable correlation time τ_{corr}. This is a consistency check of our initial assumption $\tau_2 \ll \tau_{\mathrm{corr}}$.

Appendix B

Derivations for Chapter 3

B.1   Block structure of a translational invariant Hamiltonian

In this section, we show that a translational invariant Hamiltonian $\mathcal{H}$ can be written in a block diagonal form. We consider N_s spins-$\frac{1}{2}$ arranged on a ring. For lattices of higher dimension, the calculations go along the lines. The translational invariance means that $[\mathcal{H}, \mathcal{R}] = 0$, where $\mathcal{R}$ is the displacement operator which moves all spins by one site simultaneously, cf. Fig. B.1,

$$\mathcal{R}|n_1, n_2, n_3, ..., n_{N_s}\rangle = |n_2, n_3, ..., n_{N_s}, n_1\rangle, \tag{B.1}$$

where the notation $|a, b, c, ...\rangle$ implies that the spin at lattice site one is in the state $|a\rangle$, the spin at lattice site two is in the state $|b\rangle$ and so forth.

Since $\mathcal{H}$ and $\mathcal{R}$ commute, the elements of the Hamiltonian matrix written in the eigenbasis of $\mathcal{R}$ are zero for states corresponding to two different eigenvalues of $\mathcal{R}$. This means that the Hamiltonian matrix can be written in a block-diagonal form, where each block corresponds to a different eigenvalue of $\mathcal{R}$.

Let us now obtain the eigenstates and eigenvalues of the operator $\mathcal{R}$. A displacement by one lattice site done N_s times on a ring is equivalent to no displacement at all which implies

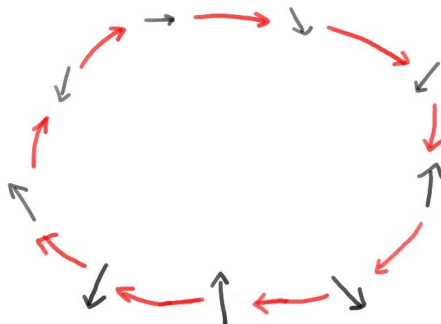$$\mathcal{R}^{N_s} = \mathbf{1}. \tag{B.2}$$

Figure B.1: Schematic representation of the action of the displacement operator $\mathcal{R}$. Black arrows represent spins, red arrows indicate the displacement.

Therefore, the eigenvalues of the displacement operator $\mathcal{R}$ must be of the following form

$$e^{i\lambda_k} \quad \text{for} \quad k \in \{0, 1, ..., N_s - 1\}, \tag{B.3}$$

where $\lambda_k \equiv \frac{2\pi}{N_s} k$. The eigenfunctions of $\mathcal{R}$ with the eigenvalue $e^{i\lambda_k}$ are[1]

$$|\psi_k\rangle \equiv \sum_{n=0}^{N_s-1} \left(e^{-i\lambda_k}\mathcal{R}\right)^n |\psi\rangle, \tag{B.4}$$

where $|\psi\rangle$ is an arbitrary wave function. We are going to prove this now. For the sake of concreteness, we assume that $|\psi\rangle$ is an Ising state. Applying the operator $\mathcal{R}$ to $|\psi_k\rangle$, we obtain

$$\mathcal{R}|\psi_k\rangle = \mathcal{R}\left[\sum_{n=0}^{N_s-1} \left(e^{-i\lambda_k}\mathcal{R}\right)^n |\psi\rangle\right] = \sum_{n=0}^{N_s-1} \left(e^{-i\lambda_k}\right)^n \left(\mathcal{R}\right)^{n+1}|\psi\rangle \tag{B.5}$$

$$= e^{i\lambda_k}\left[\sum_{n=0}^{N_s-1} \left(e^{-i\lambda_k}\mathcal{R}\right)^{n+1}|\psi\rangle\right] \tag{B.6}$$

$$= e^{i\lambda_k}\left[\sum_{n=1}^{N_s} \left(e^{-i\lambda_k}\mathcal{R}\right)^n |\psi\rangle\right] \tag{B.7}$$

$$= e^{i\lambda_k}\left[\sum_{n=0}^{N_s-1} \left(e^{-i\lambda_k}\mathcal{R}\right)^n |\psi\rangle\right] = e^{i\lambda_k}|\psi_k\rangle, \tag{B.8}$$

where, in the step to Eq. (B.8), we substituted Eq. (B.2) and used $e^{\lambda_k N_s} = 1$.

What we left aside so far is the possible internal translational symmetry of the state $|\psi\rangle$ in Eq. (B.4), i.e., $\mathcal{R}^l|\psi\rangle = |\psi\rangle$ with $l < N_s$. Such an internal symmetry can lead in certain cases to $|\psi_k\rangle = 0$, as for example in the case $|\psi\rangle = |\uparrow\downarrow\uparrow\downarrow\uparrow\downarrow\rangle$ with $N_s = 6$ ($l = 2$) and $k = 1$. This implies that a state $|\psi\rangle$ with internal symmetry must not be used for the definition of $|\psi_k\rangle$ for all values of k. In order to derive the conditions for the allowed values of k, let us assume that l is the smallest integer with the property $\mathcal{R}^l|\psi\rangle = |\psi\rangle$. We define $N' \equiv \frac{N_s}{l}$ and obtain

$$|\psi_k\rangle = \sum_{n=0}^{N_s-1} \left(e^{-i\lambda_k}\mathcal{R}\right)^n |\psi\rangle = \sum_{m=0}^{l-1}\sum_{n=0}^{N'-1} \left(e^{-i\lambda_k}\mathcal{R}\right)^{ln+m} |\psi\rangle \tag{B.9}$$

$$= \sum_{m=0}^{l-1}\sum_{n=0}^{N'-1} \left(e^{-i\lambda_k}\right)^{ln+m} \mathcal{R}^m|\psi\rangle \tag{B.10}$$

$$= \left[\sum_{n=0}^{N'-1} \left(e^{-i\lambda_k}\right)^{ln}\right] \sum_{m=0}^{l-1} \left(e^{-i\lambda_k}\mathcal{R}\right)^m |\psi\rangle. \tag{B.11}$$

---

[1]The wave functions in Eq. (B.4) are not normalised.

We obtain $|\psi_k\rangle = 0$ if the first term in Eq. (B.11) vanishes

$$\sum_{n=0}^{N'-1} \left(e^{-i\lambda_k}\right)^{ln} = \sum_{n=0}^{N'-1} \exp\left(-i\frac{2\pi}{N_s}kl\right)^n = \begin{cases} \frac{N_s}{l} & \text{if } \frac{kl}{N_s} \in \mathbb{N}_0 \\ 0 & \text{else.} \end{cases} \tag{B.12}$$

Therefore, the allowed values of k for a state with an internal tranlational symmetry l are those satisfying

$$\frac{kl}{N_s} \in \mathbb{N}_0. \tag{B.13}$$

For the sake of completeness, let us show that the states $|\psi_k\rangle$ are orthogonal

$$\langle\psi_k|\psi_{k'}\rangle = \langle\psi| \left[\frac{N_s}{l} \sum_{n'=0}^{l-1} \left(e^{\lambda_k}\mathcal{R}^\dagger\right)^{n'} \frac{N_s}{l} \sum_{n=0}^{l-1} \left(e^{-\lambda_{k'}}\mathcal{R}\right)^n \right] |\psi\rangle \tag{B.14}$$

$$= \frac{N_s^2}{l^2} \sum_{n=0}^{l-1} e^{i\frac{2\pi}{N_s^2}n(k-k')} = \frac{N_s^2}{l^2} l \, \delta_{k,k'} = \frac{N_s^2}{l}\delta_{k,k'}. \tag{B.15}$$

Therefore, the propely normalised eigenstates of $\mathcal{R}$ are

$$|\psi_k\rangle \equiv \frac{1}{\sqrt{l}} \sum_{n=0}^{l-1} \left(e^{-\lambda_k}\mathcal{R}\right)^n |\psi\rangle, \tag{B.16}$$

where l is the smallest integer satisfying $\mathcal{R}^l|\psi\rangle = |\psi\rangle$. In the following, we refer to the states (B.16) as the *translational invariant basis* and indicate it with the subscript k.

To summarise, in order to obtain the translational invariant basis $|\psi_k\rangle$, one should go through all Ising states $|\psi\rangle$ and apply the transformation described by Eq. (B.4) for the allowed values of k as shown in Eq. (B.13). If two states $|\psi\rangle$ and $|\phi\rangle$ are related to each other by $|\psi\rangle = \mathcal{R}^n|\phi\rangle$ with some integer n, then $|\psi_k\rangle = |\phi_k\rangle$.

B.2 An additional symmetry of the Hamiltonian

In this section, we show that the Hamiltonian

$$\mathcal{H} = -\sum_{i<j} \left[J_{ij}^x S_{ix}S_{jx} + J_{ij}^y S_{iy}S_{jy} + J_{ij}^z S_{iz}S_{jz} \right] - \sum_j H_j S_{jz}, \tag{B.17}$$

conserves the quantity

$$[N_\downarrow \mod 2], \tag{B.18}$$

where $N_\downarrow$ is the number of spins down in z-direction. In order to do this, we consider an arbitrary Ising state $|\psi\rangle$ which has either an odd or an even number of spins down.

Suppose now that we act with the Hamiltonian on this state $\mathcal{H}|\psi\rangle$. What is the effect of each individual term of the Hamiltonian $\mathcal{H}$ in Eq. (B.17)? For last two terms of $\mathcal{H}$, which contain only the operator S_z for the z-components of the spin, each Ising state $|\psi\rangle$ is an eigenstate. For the effect of the first two terms of the Hamiltonian in Eq. (B.17), let us

recall that the operators S_x and S_y flip the z-projection of the spin, i.e.,

$$S_x|\!\uparrow\rangle = +\frac{1}{2}|\!\downarrow\rangle, \quad S_x|\!\downarrow\rangle = +\frac{1}{2}|\!\uparrow\rangle, \tag{B.19}$$

$$S_y|\!\uparrow\rangle = +\frac{1}{2}|\!\downarrow\rangle, \quad S_y|\!\downarrow\rangle = -\frac{1}{2}|\!\uparrow\rangle. \tag{B.20}$$

Since $\mathcal{H}$ is quadratic in S_x and S_y, $\mathcal{H}|\psi\rangle$ contains admixtures of states where the z-projections of two spins are flipped with respect to $|\psi\rangle$. Therefore, $[N_\downarrow \mod 2]$ in Eq. (B.18) remains unchanged for $\mathcal{H}|\psi\rangle$. This also implies that $[N_\downarrow \mod 2]$ remains unchanged with time.

It is also important to notice that each state of the translational invariant basis in Eq. (B.16) has a well-defined number of spins down. Therefore, the translational symmetry and the symmetry with respect to the conservation of $[N_\downarrow \mod 2]$ are mutually compatible.

B.3   Sparsity of the Hamiltonian

In this section, we first show that the matrix of the Hamiltonian in Eq. (B.17), which describes spins with nearest-neighbour interaction, is sparse in the Ising basis. Later, we show that the Hamiltonian is also sparse in the block-diagonal form.

Let us apply the Hamiltonian (B.17) to an Ising state $|\psi\rangle$ and count the Ising states $|\phi\rangle$ with non-zero overlap $\langle\phi|\mathcal{H}|\psi\rangle$. First, there is the diagonal element $|\phi\rangle = |\psi\rangle$ due to the last two terms of $\mathcal{H}$ in Eq. (B.17). Second, the number of off-diagonal elements $|\phi\rangle \neq |\psi\rangle$ is N_s because there are N_s different terms of $\mathcal{H}$ which are not diagonal in the Ising basis. In total, we obtain $N_s + 1$ states $|\phi\rangle$ with $\langle\phi|\mathcal{H}|\psi\rangle \neq 0$. The fraction of the non-zero elements is extremely small

$$\frac{(N_s + 1)2^{N_s}}{(2^{N_s})^2} = \frac{N_s + 1}{2^{N_s}} \ll 1. \tag{B.21}$$

For example, $\frac{N_s+1}{2^{N_s}} \approx 2 \cdot 10^{-5}$ for a system of $N_s = 20$ spins.

If the interaction is not restricted to the nearest neighbours, the number of non-zero elements of the Hamiltonian matrix is $(rN_s + 1)2^{N_s}$, where r is the range of the interaction in terms of the number of neighbours it extends over. For any value of r, the Hamiltonian matrix is sparse.

Let us now consider the one-dimensional nearest-neighbour Hamiltonian (B.17) in the translational invariant basis and focus on one block on the diagonal corresponding to the eigenvalue $e^{i\lambda_k}$. In analogy to the calculation above, we again determine the number of non-zero elements by counting the states $|\phi_k\rangle$ such that $\langle\phi_k|\mathcal{H}|\psi_k\rangle \neq 0$ for a given $|\psi_k\rangle$.

Since the translational invariant states $|\phi_k\rangle$ are eigenstates of the z-z term of the Hamiltonian, the diagonal element is $\langle\psi_k|\mathcal{H}|\psi_k\rangle \neq 0$ in general. Now, let us consider the off-diagonal elements due to the first two terms of the Hamiltonian (B.17). For this sake, we

rewrite the first two terms of the Hamiltonian using the displacement operator $\mathcal{R}$

$$-\sum_{n=1}^{N_s} \left[J^x S_{nx} S_{(n+1)x} + J^y S_{ny} S_{(n+1)y} \right] = -\sum_{n=1}^{N_s} \left[J^x \mathcal{R}^n S_{1x} S_{2x} (\mathcal{R}^\dagger)^n + J^y \mathcal{R}^n S_{1y} S_{2y} (\mathcal{R}^\dagger)^n \right],$$

(B.22)

where the adjoint operator $\mathcal{R}^\dagger$ acts as a displacement operator in the opposite direction. For the sake of clarity, let us for a moment focus only on the interaction in x-direction. We obtain

$$
\begin{aligned}
-J^x \sum_{n=1}^{N_s} S_{nx} S_{(n+1)x} |\psi_k\rangle &= -J^x \sum_{n=1}^{N_s} \mathcal{R}^n S_{1x} S_{2x} (\mathcal{R}^\dagger)^n \frac{1}{\sqrt{l}} \sum_{m=0}^{l-1} \left(e^{-i\lambda_k} \mathcal{R} \right)^m |\psi\rangle && \text{(B.23)} \\
&= -J^x \sum_{n=1}^{N_s} \mathcal{R}^n S_{1x} S_{2x} \frac{1}{\sqrt{l}} \sum_{m=0}^{l-1} e^{-i\lambda_k m} \mathcal{R}^{m-n} |\psi\rangle && \text{(B.24)} \\
&= -J^x \sum_{n=1}^{N_s} \mathcal{R}^n S_{1x} S_{2x} \frac{1}{\sqrt{l}} \sum_{m'=0}^{l-1} e^{-i\lambda_k (m'+n)} \mathcal{R}^{m'} |\psi\rangle && \text{(B.25)} \\
&= -J^x \sum_{n=1}^{N_s} e^{-i\lambda_k n} \mathcal{R}^n S_{1x} S_{2x} \frac{1}{\sqrt{l}} \sum_{m'=0}^{l-1} \left(e^{-i\lambda_k} \mathcal{R} \right)^{m'} |\psi\rangle && \text{(B.26)} \\
&= -J^x \sum_{n=1}^{N_s} \left(e^{-i\lambda_k} \mathcal{R} \right)^n S_{1x} S_{2x} |\psi_k\rangle, && \text{(B.27)}
\end{aligned}
$$

where, in Eq. (B.25), $m' = m - n$. The state $|\psi_k\rangle$ is a translational invariant basis vector being a superposition of $l \leq N_s$ vectors of the Ising basis. The operator $S_{1x} S_{2x}$ acts on each of the l Ising states such that the resulting state $S_{1x} S_{2x} |\psi_k\rangle$ in not translational invariant. Instead, it is a superposition of some l Ising states $|\psi'_i\rangle$. Taking into account the y-y term of the Hamiltonian and repeating the steps of Eqs. (B.23)-(B.27), we obtain

$$-\sum_{n=1}^{N_s} \left[J^x S_{nx} S_{(n+1)x} + J^y S_{ny} S_{(n+1)y} \right] |\psi_k\rangle = \sum_{n=1}^{N_s} \left(e^{-i\lambda_k} \mathcal{R} \right)^n \sum_{i=0}^{l-1} c_i |\psi'_i\rangle = \sum_{i=0}^{l-1} c_i |\psi'_{i,k}\rangle,$$

(B.28)

where $|\psi'_{i,k}\rangle$ are translational invariant basis vectors and c_i are some coefficients . On the right-hand side of Eq. (B.28), there is a superposition of $l \leq N_s$ translational invariant basis vectors. Therefore, there are $l + 1$ states $|\phi_k\rangle$ such that $\langle \phi_k | \mathcal{H} | \psi_k \rangle \neq 0$ in total.

B.4 Sampling of a wave function corresponding to the infinite temperature limit

If we randomly draw the wave functions from the Hilbert space without any constraints, the corresponding energy distributions can, to a good accuracy, be approximated by $g_\infty(E)$ for the overwhelming majority of wave functions, where

$$g_\infty(E) = p \sum_i \delta(E - E_i),$$

(B.29)

is the energy distribution corresponding to the infinite temperature limit. The reason is the property quantum typicality. The random wave functions typically exhibit behaviour which is similar to the behaviour for the infinite-temperature limit.

In the numerical calculations, we need to randomly sample the individual p_i such that we obtain a typical wave function subject only to the constraint

$$\sum_i p_i = 1. \tag{B.30}$$

What is the probability distribution $P(p)$ for the individual occupation probabilities p corresponding to a typical wave function? Suppose, we fix an arbitrary state k with occupation probability p_k and rewrite the above constraint as

$$1 - p_k = \sum_{i \neq k} p_i. \tag{B.31}$$

This relation describes a $2^{N_s} - 1$ dimensional sphere with radius $\sqrt{1 - p_k}$ for the variables $\sqrt{p_i}$. The probability distribution $P(p_k)$ for the arbitrarily chosen state k, therefore, scales as the volume of that sphere

$$P(p_k) \cong \frac{(2\pi)^{(2^{N_s}-2)/2}\sqrt{1-|c_p|^2}^{2^{N_s}-2}}{(n/2-1)!} \cong (1-p_k)^{2^{N_s}-2} \approx e^{-\Lambda p_k}, \tag{B.32}$$

where $\Lambda \equiv 2^{N_s-2}$ is a large number. In total, if the occupation probabilities p_k are distributed according to $P(p_k)$ in Eq. (B.32), we obtain a typical wave function which exhibits behaviour similar to the infinite-temperature limit.

Suppose now that only one random-number generator is available for the numerical calculations. This random-number generator delivers random numbers y in the interval $[0, 1]$ with a flat probability distribution $P_y(y) = 1$. The question now is how to obtain $P(p)$ in Eq. (B.32) using the above random-number generator. The solution is to consider

$$P(p)dp = P_y(y)dy = dy, \tag{B.33}$$

which leads to

$$\frac{dy(p)}{dp} = P(p) = \frac{1}{\Lambda}e^{-\Lambda p}. \tag{B.34}$$

The solution is

$$y(p) = -e^{-\Lambda p} + y_0 \tag{B.35}$$

and, therefore,

$$p(y) \cong -\log(y_0 - y). \tag{B.36}$$

From the constraint $0 \leq p \leq 1$ follows that $y_0 = 1$.

In total, the algorithm for obtaining a typical wave function is given by the following scheme

1. Draw a number y_i from the interval $[0, 1]$ at random.

2. Set $p_i = -\log(y_i)$.

3. Normalise the coefficients p_i according to Eq. (B.30).

4. Set the quantum-mechanical amplitudes according to $c_i = \sqrt{p_i}e^{\phi_i}$ with a random phase ϕ_i.

B.5   Discrete Fourier transformation

In order to obtain the energy distribution $g(E)$ of a wave function $|\psi\rangle$, we calculate the power spectrum of a time series by applying the discrete Fourier transform. The procedure consists of the following steps:

1. We calculate the discrete time series $X(k)$ of length N with an appropriately chosen time step Δt

$$X(k) \equiv f(\Delta t\ k) = \langle \psi(\Delta t\ k)|\psi(0)\rangle. \tag{B.37}$$

2. We multiply $X(k)$ by the Kaiser-Bessel function

$$\mathcal{K}(k) \equiv \frac{I_0\left(\pi\alpha\sqrt{1 - \left(\frac{2k}{N-1} - 1\right)^2}\right)}{I_0(\pi\alpha)}, \tag{B.38}$$

where I_0 is the zeroth-order modified Bessel function of the first kind, and α is a non-negative real number which determines the shape of the window. In our calculations, we use $\alpha = 3$.

3. We obtain the Fourier coefficients $Y(\omega_l)$ with $\omega = \frac{2\pi}{N}l$, where l is an integer in the interval $[0, N-1]$,

$$Y(\omega_l) \equiv \sum_k \left[X(k)\mathcal{K}(k)\right]e^{i\omega_l k}. \tag{B.39}$$

In practice, we use the Fast-Fourier-Transform (FFT) algorithm for the efficient computation of the discrete Fourier transform.

4. Finally, we compute the energy distribution by

$$g(\omega_l) \cong |Y(\omega_l)|^2, \tag{B.40}$$

and normalise $g(\omega_l)$.

The typical shape of the time series $X(k)$ is the following: $X(k)$ has a peak at $t = 0$ because of $\langle\psi(0)|\psi(0)\rangle = 1$, and otherwise $X(k)$ fluctuates around the value 0 with a small amplitude. When applying the above scheme, we obtain good results when the point $t = 0$ is in the middle of the time series and not at the beginning. In practice, this means that $X(k)$ must be computed $\frac{N}{2}$ steps backwards in time and, likewise, $\frac{N}{2}$ steps forward in time. In this way, the peak at $t = 0$ is not cut away by the Kaiser-Bessel window in contrast to the case when $t = 0$ is the starting point of $X(k)$. This is illustrated in Fig. B.2.
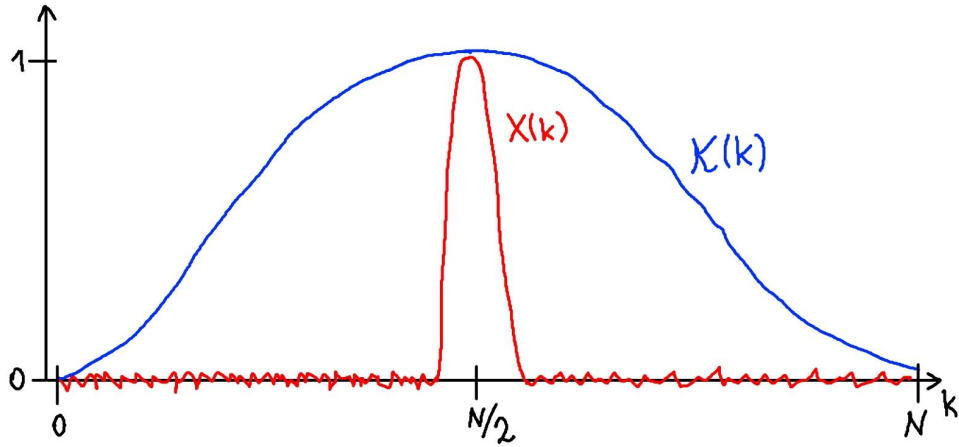
Figure B.2: Illustration of the time series $X(k)$ and the Kaiser-Bessel window $\mathcal{K}(k)$. The initial point $t = 0$ is at $\frac{N}{2}$. If it were at $N = 0$, it would be cut away by the window function $\mathcal{K}(k)$.

B.6 Examples for the finite-size effects

In this section, we give explicit examples for the finite-size effects of local measurements. We plot $g_n(E)$ for different n for the system sizes $N_s = 16$, $N_s = 20$ and $N_s = 24$ in Figs. B.3, B.4 and B.5, respectively. The Hamiltonian and the initial conditions are the same as those in Sec. 3.2.

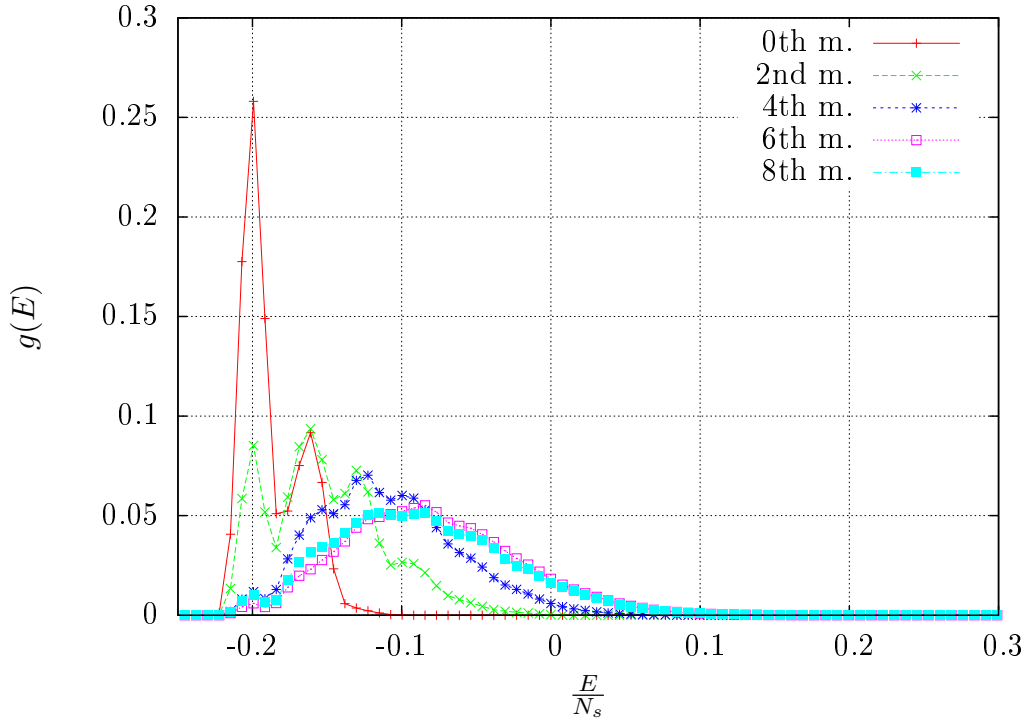Both the heating effect and the broadening effects are clearly visible in the figures.

Figure B.3: The energy distribution $g_n(E)$ is shown for different n. The system size is $N_s = 16$. The points have been connected by lines in order to guide the eye. For further information, see text.
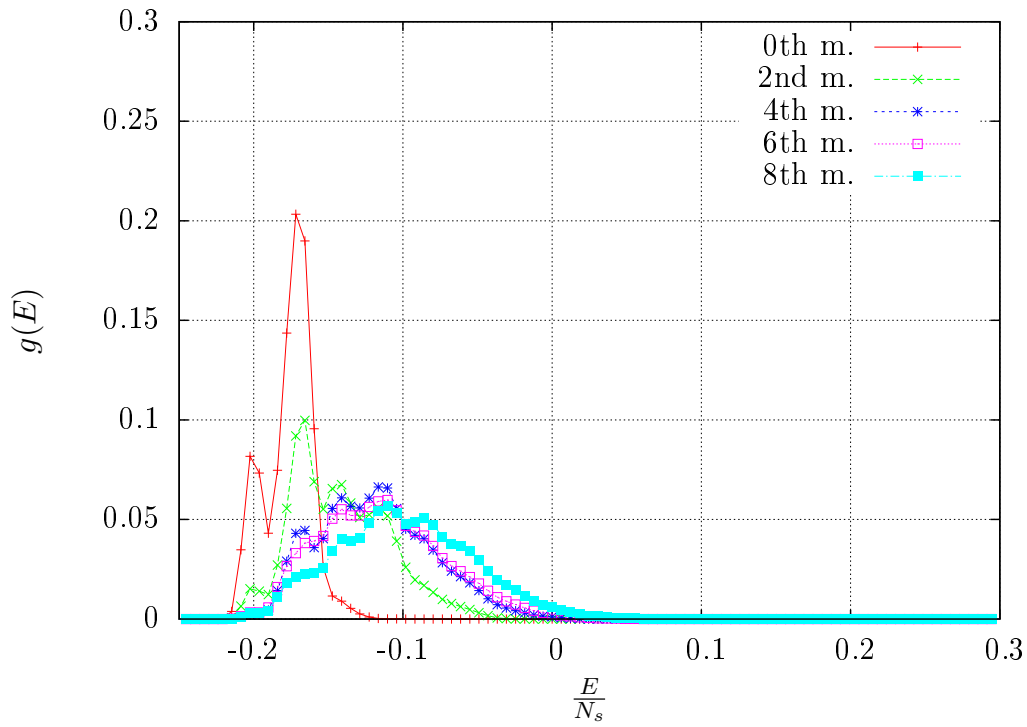
Figure B.4: The energy distribution $g_n(E)$ is shown for different n. The system size is $N_s = 20$. The points have been connected by lines in order to guide the eye. For further information, see text.
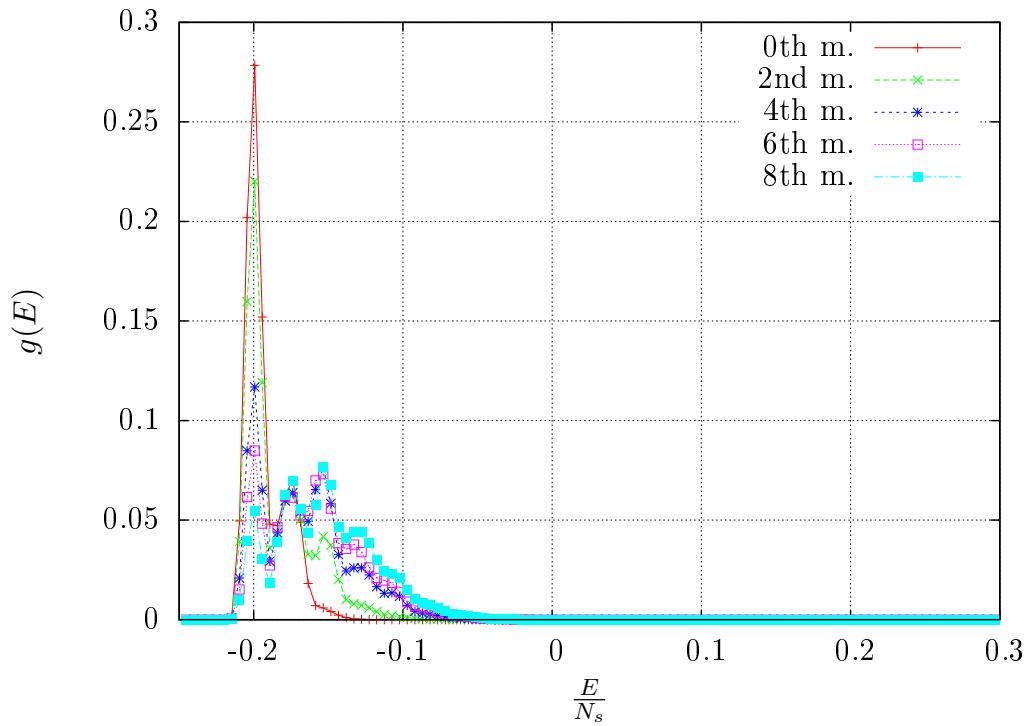

Figure B.5: The energy distribution $g_n(E)$ is shown for different n. The system size is $N_s = 24$. The points have been connected by lines in order to guide the eye. For further information, see text.

Moreover, the finite-size effects become less pronounced for increasing system sizes. For further information, we refer the reader to Sec. 3.2.

B.7   Kurtosis of a two-peak energy distribution

In this section, we derive the kurtosis defined in Eq. (3.22) for the two-peak distribution illustrated in Fig. B.6

$$f(x) = \frac{1}{2}\Big[G_a(x) + G_{-a}(x)\Big], \tag{B.41}$$

where $G_a(x)$ is a normalised Gaussian function centred around a

$$G_a(x) = \frac{1}{\sqrt{2\pi}\sigma}e^{-\frac{(x-a)^2}{2\sigma^2}}. \tag{B.42}$$

The first moment of this function is

$$\int_{-\infty}^{\infty} G_a(x)x\,dx = a, \tag{B.43}$$

the second central moment is

$$\int_{-\infty}^{\infty} G_a(x)(x-a)^2dx = \sigma^2, \tag{B.44}$$

and the fourth central moment is

$$\int_{-\infty}^{\infty} G_a(x)(x-a)^4dx = 3\sigma^4. \tag{B.45}$$

With these results, we obtain that the first moment of the function $f(x)$ vanishes

$$\int_{-\infty}^{\infty} f(x)x\,dx = 0. \tag{B.46}$$
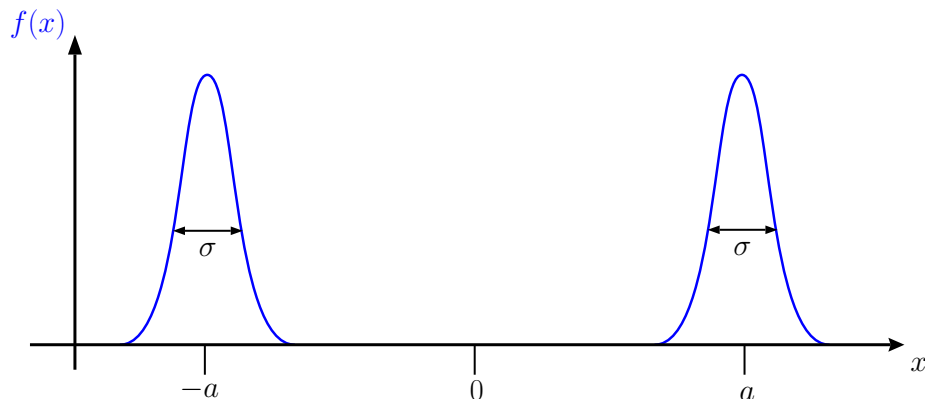

Figure B.6: Illustration of the function $f(x)$ given in Eq. (B.41)

The second central moment of $f(x)$ is

$$\int_{-\infty}^{\infty} f(x)x^2 dx = \sigma^2 + a^2, \tag{B.47}$$

and the fourth central moment is

$$\int_{-\infty}^{\infty} f(x)x^4 dx = 3\sigma^4 + 6\sigma^2 a^2 + a^4. \tag{B.48}$$

Combining these results, we obtain for the kurtosis of $f(x)$

$$\text{kurt}[f(x)] = 3 - \frac{2a^4}{(\sigma^2 + a^2)^2}. \tag{B.49}$$

If the distance between the two Gaussians in Fig. B.6 is much larger than their width, i.e., $a \gg \sigma$, we obtain $\text{kurt}[f(x)] = 1$. The kurtosis grows if the distance decreases such that, for $a \approx \sigma$, we obtain $\text{kurt}[f(x)] = 2.5$. If we set $a = 0$, which corresponds to a single Gaussian function, we obtain $\text{kurt}[f(x)] = 3$.

Appendix C

Derivations for Chapter 4

C.1   Distance between two-spin density matrices

In this section, we first prove the inequalities $0 \leq d(\rho_1, \rho_0) \leq \sqrt{2}$ and, later, derive an expression similar to Eq. (4.9). For the sake of convenience, we repeat here the definition of the distance

$$d(\rho_1, \rho_0) \equiv \sqrt{\mathrm{Tr}\big[(\rho_1 - \rho_0)^2\big]}, \tag{C.1}$$

cf. Eq. (4.2). The inequality $0 \leq d(\rho_1, \rho_0)$ can be readily shown by diagonalising the Hermitian operator $\rho_1 - \rho_0$ and then considering $(\rho_1 - \rho_0)^2$. The diagonal elements of this operator are non-negative. Therefore, we obtain $0 \leq d(\rho_1, \rho_0)$.

In order to show the inequality $d(\rho_1, \rho_0) \leq \sqrt{2}$, let us rewrite the expression for the distance

$$d(\rho_1, \rho_0) = \sqrt{\mathrm{Tr}\big[\rho_1^2\big] + \mathrm{Tr}\big[\rho_0^2\big] - 2\mathrm{Tr}\big[\rho_0\rho_1\big]}. \tag{C.2}$$

The diagonal elements of a density matrix are non-negative. This leads to $\mathrm{Tr}\big[\rho_0\rho_1\big] \geq 0$. Therefore, we obtain

$$d(\rho_1, \rho_0) = \sqrt{\mathrm{Tr}\big[\rho_1^2\big] + \mathrm{Tr}\big[\rho_0^2\big] - 2\mathrm{Tr}\big[\rho_0\rho_1\big]} \tag{C.3}$$

$$\leq \sqrt{\mathrm{Tr}\big[\rho_1^2\big] + \mathrm{Tr}\big[\rho_0^2\big]} \tag{C.4}$$

$$\leq \sqrt{2}, \tag{C.5}$$

where, in the last step, we used $\mathrm{Tr}\big[\rho_1^2\big] \leq \mathrm{Tr}\big[\rho_1\big] = 1$.

Now, we derive an expression for the distance between two density matrices. We consider two-spin density matrices. The derivation of Eq. (4.9) goes along the lines. Using Eq. (4.7), we can write

$$\rho_1 - \rho_0 = \frac{1}{4} \sum_{\mu,\nu \in \{0,1,2,3\}} \Big(P_{1,\mu\nu} - P_{0,\mu\nu}\Big)\sigma_\mu \otimes \sigma_\nu, \tag{C.6}$$

where we omitted the indices for the lattice sites for simplicity. For the expression inside the trace in Eq. (C.1), we obtain

$$(\rho_1 - \rho_0)^2 = \frac{1}{4^2} \sum_{\mu,\nu \in \{0,1,2,3\}} \sum_{\kappa,\lambda \in \{0,1,2,3\}} \Big(P_{1,\mu\nu} - P_{0,\mu\nu}\Big)\Big(P_{1,\kappa\lambda} - P_{0,\kappa\lambda}\Big)\sigma_\mu\sigma_\kappa \otimes \sigma_\nu\sigma_\lambda \tag{C.7}$$

The product of the Pauli-matrices in the above expression can be rewritten using $\sigma_\mu \sigma_\nu = \delta_{\mu\nu} \sigma_0 + i\varepsilon_{\mu\nu\kappa}\sigma_\kappa$. For the distance, we obtain

$$d(\rho_1, \rho_0) = \sqrt{\text{Tr}\left[\frac{1}{4^2} \sum_{\mu,\nu\in\{0,1,2,3\}} \left(P_{1,\mu\nu} - P_{0,\mu\nu}\right)^2 \sigma_0 \otimes \sigma_0\right]} \tag{C.8}$$

$$= \frac{1}{2}\sqrt{\sum_{\mu,\nu\in\{0,1,2,3\}} \left(P_{1,\mu\nu} - P_{0,\mu\nu}\right)^2}, \tag{C.9}$$

where we used $\text{Tr}\left[\sigma_0 \otimes \sigma_0\right] = 4$. This concludes the derivation.

Let us now briefly consider two limiting cases. If $\rho_1 = \rho_0$ which implies $P_{1,\mu\nu} = P_{0,\mu\nu}$, this clearly leads to

$$d(\rho_1, \rho_0) = 0 \tag{C.10}$$

which is the minimal value of the distance. The distance reaches its maximal value $d(\rho_1, \rho_0) = \sqrt{2}$ when ρ_1 and ρ_0 describe two mutually excluding situations. An example of such a situation is when ρ_0 describes two spins pointing into the positive x-direction which corresponds to

$$P_{0,xx} = 1 \tag{C.11}$$

$$P_{0,x0} = 1 \tag{C.12}$$

$$P_{0,0x} = 1 \tag{C.13}$$

and the other parameters are zero. Suppose that the density matrix ρ_1 describes two spins, where one spins still point into the positive x-direction whereas the other spin now points into the negative x-direction. This case corresponds to

$$P_{0,xx} = -1 \tag{C.14}$$

$$P_{0,x0} = 1 \tag{C.15}$$

$$P_{0,0x} = -1 \tag{C.16}$$

and the other parameters are zero. The distance is

$$d(\rho_1, \rho_0) = \frac{1}{2}\sqrt{\left(P_{1,xx} - P_{0,xx}\right)^2 + \left(P_{1,0x} - P_{0,0x}\right)^2} = \frac{1}{2}\sqrt{8} = \sqrt{2}. \tag{C.17}$$

Appendix D

Acknowledgements

First of all, I would like to express my sincere gratitude to my supervisor Boris Fine for his encouraging support, his patient explanations and the numerous stimulating discussions throughout these years. I am specially thankful to him for introducing me into the foundations of quantum statistical physics and pointing out the unsolved problem that has been addressed in the present thesis.

I would like to thank Prof. Manfred Salmhofer for being referee for this thesis.

Additionally, I want to thank all my colleagues at the Institute for theoretical Physics; especially Frank Hantschel, my room-mates Martin Bies and Michele Pastena (thanks also to both of them for proofreading parts of this manuscript), and Tarek Elsayed for his help in programming.

It is also a pleasure to mention my former colleagues and now friends Armen Hayrapetyan and Oleksiy Kovtun for discussions about physics and beyond. Further, this work would not be possible without the continuous support of my family and my friends! Thank you!

Finally, it is an overwhelming pleasure to say thank you to my wife Alina for making my life enjoyable.

Appendix E

Bibliography

[1] Gert Aarts, Gian Franco Bonini, and Christof Wetterich. On thermalization in classical scalar field theory. *Nuclear Physics B*, 587:403 − 418, 2000.

[2] M. R. Andrews, C. G. Townsend, H.-J. Miesner, D. S. Durfee, D. M. Kurn, and W. Ketterle. Observation of interference between two bose condensates. *Science*, 275(5300):637–641, 1997.

[3] Markus Arndt, Olaf Nairz, Julian Vos-Andreae, Claudia Keller, Gerbrand van der Zouw, and Anton Zeilinger. Wave-particle duality of c60 molecules. *Nature*, 401:680–682, 1999.

[4] M. C. Bañuls, J. I. Cirac, and M. B. Hastings. Strong and weak thermalization of infinite nonintegrable quantum systems. *Phys. Rev. Lett.*, 106:050405, Feb 2011.

[5] Miguel Ballesteros, Martin Fraas, Jürg Fröhlich, and Baptiste Schubnel. Indirect retrieval of information and the emergence of facts in quantum mechanics. *arXiv:1506.01213*.

[6] Michel Bauer and Denis Bernard. Convergence of repeated quantum nondemolition measurements and wave-function collapse. *Phys. Rev. A*, 84:044103, Oct 2011.

[7] C. Beck and E.G.D. Cohen. Superstatistics. *Physica A: Statistical Mechanics and its Applications*, 322:267 − 275, 2003.

[8] Gunnar Björk and Piero G Luca Mana. A size criterion for macroscopic superposition states. *Journal of Optics B: Quantum and Semiclassical Optics*, 6(11):429, 2004.

[9] Vladimir B. Braginsky and Farid Ya. Khalili. *Quantum Measurement*. 1992.

[10] S. Braun, J. P. Ronzheimer, M. Schreiber, S. S. Hodgman, T. Rom, I. Bloch, and U. Schneider. Negative absolute temperature for motional degrees of freedom. *Science*, 339(6115):52–55, 2013.

[11] Heinz-Peter Breuer and Francesco Petruccione. *The Theory of Open Quantum Systems*. 2002.

[12] Dorje C. Brody and Lane P. Hughston. The quantum canonical ensemble. *Journal of Mathematical Physics*, 39(12):6502–6508, 1998.

[13] M A Cazalilla and M Rigol. Focus on dynamics and thermalization in isolated quantum many-body systems. *New Journal of Physics*, 12(5):055006, 2010.

[14] Keng-Yeow Chung, Sheng-wey Chiow, Sven Herrmann, Steven Chu, and Holger Müller. Atom interferometry tests of local lorentz invariance in gravity and electrodynamics. *Phys. Rev. D*, 80:016002, Jul 2009.

[15] Govinda Clos, Diego Porras, Ulrich Warring, and Tobias Schaetz. Time-resolved observation of thermalization in an isolated quantum system. *arXiv*, 1509.07712, 2015.

[16] J. M. Deutsch. Quantum statistical mechanics in a closed system. *Phys. Rev. A*, 43:2046–2049, Feb 1991.

[17] Wolfgang Dür, Christoph Simon, and J. Ignacio Cirac. Effective size of certain macroscopic quantum superpositions. *Phys. Rev. Lett.*, 89:210402, Oct 2002.

[18] Tarek A. Elsayed and Boris V. Fine. Regression relation for pure quantum states and its implications for efficient computing. *Phys. Rev. Lett.*, 110:070404, Feb 2013.

[19] Boris V. Fine. Typical state of an isolated quantum system with fixed energy and unrestricted participation of eigenstates. *Phys. Rev. E*, 80:051130, Nov 2009.

[20] Boris V Fine and Frank Hantschel. An alternative to the conventional micro-canonical ensemble. *Physica Scripta*, 2012(T151):014078, 2012.

[21] Barbara Fresch and Giorgio J. Moro. Typicality in ensembles of quantum states: Monte carlo sampling versus analytical approximations. *The Journal of Physical Chemistry A*, 113(52):14502–14513, 2009.

[22] Barbara Fresch and Giorgio J. Moro. Emergence of equilibrium thermodynamic properties in quantum pure states. i. theory. *The Journal of Chemical Physics*, 133(3), 2010.

[23] Barbara Fresch and Giorgio J. Moro. Emergence of equilibrium thermodynamic properties in quantum pure states. ii. analysis of a spin model system. *The Journal of Chemical Physics*, 133(3), 2010.

[24] Jonathan R. Friedman, Vijay Patel, W. Chen, S. K. Tolpygo, and J. E. Lukens. Quantum superposition of distinct macroscopic states. *Nature*, 406:43–46, 2000.

[25] Florian Fröwis and Wolfgang Dür. Measures of macroscopicity for quantum spin systems. *New Journal of Physics*, 14(9):093039, 2012.

[26] J. Gemmer and G. Mahler. Distribution of local entropy in the hilbert space of bipartite quantum systems: origin of jaynes' principle. *The European Physical Journal B - Condensed Matter and Complex Systems*, 31(2):249–257.

[27] Jochen Gemmer, M. Michel, and Günter Mahler. *Quantum Thermodynamics*. Springer-Verlag Berlin Heidelberg, 2009.

[28] S. Genway, A. F. Ho, and D. K. K. Lee. Dynamics of thermalization in small hubbard-model systems. *Phys. Rev. Lett.*, 105:260402, Dec 2010.

[29] Sheldon Goldstein, Joel L. Lebowitz, Roderich Tumulka, and Nino Zanghì. Canonical typicality. *Phys. Rev. Lett.*, 96:050403, Feb 2006.

[30] Philippe Grangier, Juan Ariel Levenson, and Jean-Philippe Poizat. Quantum non-demolition measurements in optics. *Nature*, 396, 1998.

[31] R. E. Grisenti, W. Schöllkopf, J. P. Toennies, G. C. Hegerfeldt, and T. Köhler. Determination of atom-surface van der waals potentials from transmission-grating diffraction intensities. *Phys. Rev. Lett.*, 83:1755–1758, Aug 1999.

[32] Christine Guerlin, Julien Bernu, Samuel Deléglise, Clément Sayrin, Sébastien Gleyzes, Stefan Kuhr, Michel Brune, Jean-Michel Raimond, and Serge Haroche. Progressive field-state collapse and quantum non-demolition photon counting. *Nature (London)*, 448:889–893, 2007.

[33] Lucia Hackermuller, Klaus Hornberger, Bjorn Brezger, Anton Zeilinger, and Markus Arndt. Decoherence of matter waves by thermal emission of radiation. *Nature*, 427:711–714, 2004.

[34] Anthony Hams and Hans De Raedt. Fast algorithm for finding the eigenvalue distribution of very large matrices. *Phys. Rev. E*, 62:4365–4377, Sep 2000.

[35] T. Hime, P. A. Reichardt, B. L. T. Plourde, T. L. Robertson, C.-E. Wu, A. V. Ustinov, and John Clarke. Solid-state qubits with current-controlled coupling. *Science*, 314(5804):1427–1429, 2006.

[36] Michael Hohmann, Farina Kindermann, Tobias Lausch, Daniel Mayer, Felix Schmidt, and Artur Widera. Single-atom thermometer for ultracold gases. *Phys. Rev. A*, 93:043607, Apr 2016.

[37] Klaus Hornberger, Stefan Uttenthaler, Björn Brezger, Lucia Hackermüller, Markus Arndt, and Anton Zeilinger. Collisional decoherence observed in matter wave interferometry. *Phys. Rev. Lett.*, 90:160401, Apr 2003.

[38] E. T. Jaynes. Information theory and statistical mechanics. *Phys. Rev.*, 106:620–630, May 1957.

[39] E. T. Jaynes. Information theory and statistical mechanics. ii. *Phys. Rev.*, 108:171–190, Oct 1957.

[40] F. Jelezko, T. Gaebel, I. Popa, A. Gruber, and J. Wrachtrup. Observation of coherent oscillations in a single electron spin. *Phys. Rev. Lett.*, 92:076401, Feb 2004.

[41] E. Joos and H. D. Zeh. The emergence of classical properties through interaction with the environment. *Z. Phys. B*, 59:223–243, 1985.

[42] Erich Joos, H. Dieter Zeh, Claus Kiefer, Domenico J. W. Giulini, Joachim Kupsch, and I. O. Stamatescu. *Decoherence and the Appearance of a Classical World in Quantum Theory.* 2003.

[43] M. I. Katsnelson, V. V. Dobrovitski, and B. N. Harmon. Néel state of an antiferro-magnet as a result of a local measurement in the distributed quantum system. *Phys. Rev. B*, 63:212404, May 2001.

[44] D. W. Keith, M. L. Schattenburg, Henry I. Smith, and D. E. Pritchard. Diffraction of atoms by a transmission grating. *Phys. Rev. Lett.*, 61:1580–1583, Oct 1988.

[45] Toshiya Kinoshita, Trevor Wenger, and David S. Weiss. A quantum newton's cradle. *Nature*, 440:900–903, 2006.

[46] M. Kliesch, C. Gogolin, M. J. Kastoryano, A. Riera, and J. Eisert. Locality of temperature. *Phys. Rev. X*, 4:031019, Jul 2014.

[47] Corinna Kollath, Andreas M. Läuchli, and Ehud Altman. Quench dynamics and nonequilibrium phase diagram of the bose-hubbard model. *Phys. Rev. Lett.*, 98:180601, Apr 2007.

[48] J. I. Korsbakken, F. K. Wilhelm, and K. B. Whaley. The size of macroscopic superposition states in flux qubits. *EPL (Europhysics Letters)*, 89(3):30003, 2010.

[49] Jan Ivar Korsbakken, K. Birgitta Whaley, Jonathan Dubois, and J. Ignacio Cirac. Measurement-based measure of the size of macroscopic quantum superpositions. *Phys. Rev. A*, 75:042106, Apr 2007.

[50] L. D. Landau and E. M. Lifshitz. *Statistical Physics*, volume 5. 3 edition, 1980.

[51] F. Lecocq, J. B. Clark, R. W. Simmonds, J. Aumentado, and J. D. Teufel. Quantum nondemolition measurement of a nonclassical state of a massive object. *Phys. Rev. X*, 5:041037, Dec 2015.

[52] Chang-Woo Lee and Hyunseok Jeong. Quantification of macroscopic quantum superpositions within phase space. *Phys. Rev. Lett.*, 106:220401, May 2011.

[53] A. J. Leggett. Macroscopic quantum systems and the quantum theory of measurement. *Progress of Theoretical Physics Supplement*, 69:80–100, 1980.

[54] A J Leggett. Testing the limits of quantum mechanics: motivation, state of play, prospects. *Journal of Physics: Condensed Matter*, 14(15):R415, 2002.

[55] Hans Maassen and Burkhard Kümmerer. Purification of quantum trajectories. *IMS Lecture Notes-Monograph Series*, 48:252–261, 2006.

[56] H. Maier-Leibnitz and T. Springer. Ein interferometer für langsame neutronen. *Zeitschrift für Physik*, 167(4):386–402.

[57] Artur S. L. Malabarba, Luis Pedro García-Pintos, Noah Linden, Terence C. Farrelly, and Anthony J. Short. Quantum systems equilibrate rapidly for most observables. *Phys. Rev. E*, 90:012121, Jul 2014.

[58] Florian Marquardt, Benjamin Abel, and Jan von Delft. Measuring the size of a quantum superposition of many-body states. *Phys. Rev. A*, 78:012109, Jul 2008.

[59] William Marshall, Christoph Simon, Roger Penrose, and Dik Bouwmeester. Towards quantum superpositions of a mirror. *Phys. Rev. Lett.*, 91:130401, Sep 2003.

[60] Ugo Marzolino and Daniel Braun. Precision measurements of temperature and chemical potential of quantum gases. *Phys. Rev. A*, 88:063609, Dec 2013.

[61] Markus P. Müller, David Gross, and Jens Eisert. Concentration of measure for quantum states with a fixed expectation value. *Communications in Mathematical Physics*, 303(3):785–824, 2011.

[62] Stefan Nimmrichter and Klaus Hornberger. Macroscopicity of mechanical quantum superposition states. *Phys. Rev. Lett.*, 110:160403, Apr 2013.

[63] A Peters, K Y Chung, and S Chu. High-precision gravity measurements using atom interferometry. *Metrologia*, 38(1):25, 2001.

[64] Igor Pikovski, Magdalena Zych, Fabio Costa, and Caslav Brukner. Universal decoherence due to gravitational time dilation. *Nature Physics*, 2015.

[65] J.-M. Pirkkalainen, E. Damskägg, M. Brandt, F. Massel, and M. A. Sillanpää. Squeezing of quantum noise of motion in a micromechanical resonator. *Phys. Rev. Lett.*, 115:243601, Dec 2015.

[66] D. Poilblanc, T. Ziman, J. Bellissard, F. Mila, and G. Montambaux. Poisson vs. goe statistics in integrable and non-integrable quantum hamiltonians. *EPL (Europhysics Letters)*, 22(7):537, 1993.

[67] A. V. Ponomarev, S. Denisov, and P. Hänggi. Thermal equilibration between two quantum systems. *Phys. Rev. Lett.*, 106:010405, Jan 2011.

[68] Sandu Popescu, Anthony J. Short, and Andreas Winter. Entanglement and the foundations of statistical mechanics. *Nature Physics*, 2:754–758, 2006.

[69] E. M. Purcell and R. V. Pound. A nuclear spin system at negative temperature. *Phys. Rev.*, 81:279–280, Jan 1951.

[70] Peter Reimann. Foundation of statistical mechanics under experimentally realistic conditions. *Phys. Rev. Lett.*, 101:190403, Nov 2008.

[71] Marcos Rigol, Vanja Dunjko, and Maxim Olshanii. Thermalization and its mechanism for generic isolated quantum systems. *Nature*, 452:854–858, 2008.

[72] Marcos Rigol, Vanja Dunjko, Vladimir Yurovsky, and Maxim Olshanii. Relaxation in a completely integrable many-body quantum system: An *Ab Initio* study of the dynamics of the highly excited states of 1d lattice hard-core bosons. *Phys. Rev. Lett.*, 98:050405, Feb 2007.

[73] O. Romero-Isart, A. C. Pflanzer, M. L. Juan, R. Quidant, N. Kiesel, M. Aspelmeyer, and J. I. Cirac. Optically levitating dielectrics in the quantum regime: Theory and protocols. *Phys. Rev. A*, 83:013803, Jan 2011.

[74] J. J. Sakurai. *Modern Quantum Mechanics*. 1994.

[75] Philipp Schindler, Daniel Nigg, Thomas Monz, Julio T Barreiro, Esteban Martinez, Shannon X Wang, Stephan Quint, Matthias F Brandl, Volckmar Nebendahl, Christian F Roos, Michael Chwalla, Markus Hennrich, and Rainer Blatt. A quantum information processor with trapped ions. *New Journal of Physics*, 15(12):123012, 2013.

[76] Maximilian Schlosshauer. *Decoherence and the Quantum-to-Classical Transition*. 2007.

[77] Erwin Schrödinger. *Statistical Thermodynamics*. Cambridge University Press, 2nd edition, 1952.

[78] Erwin Schrödinger. *Collected papers*. Verlag der Österr. Akad. d. Wiss., 1984.

[79] Marlan O. Scully and M. Suhail Zubairy. *Quantum Optics*. Cambridge University Press, 1997.

[80] Pavel Sekatski, Nicolas Gisin, and Nicolas Sangouard. How difficult is it to prove the quantumness of macroscropic states? *Phys. Rev. Lett.*, 113:090403, Aug 2014.

[81] Pavel Sekatski, Nicolas Sangouard, and Nicolas Gisin. Size of quantum superpositions as measured with classical detectors. *Phys. Rev. A*, 89:012116, Jan 2014.

[82] Akira Shimizu and Takayuki Miyadera. Stability of quantum states of finite macroscopic systems against classical noises, perturbations from environments, and local measurements. *Phys. Rev. Lett.*, 89:270403, Dec 2002.

[83] Fujio Shimizu, Kazuko Shimizu, and Hiroshi Takuma. Double-slit interference with ultracold metastable neon atoms. *Phys. Rev. A*, 46:R17–R20, Jul 1992.

[84] A. I. Shnirelman. *Usp. Mat. Nauk*, 29:181, 1974.

[85] Mark Srednicki. Chaos and quantum thermalization. *Phys. Rev. E*, 50:888–901, Aug 1994.

[86] R. Steinigeweg, A. Khodja, H. Niemeyer, C. Gogolin, and J. Gemmer. Pushing the limits of the eigenstate thermalization hypothesis towards mesoscopic quantum systems. *Phys. Rev. Lett.*, 112:130403, Apr 2014.

[87] Robin Steinigeweg, Jochen Gemmer, and Wolfram Brenig. Spin-current autocorrelations from single pure-state propagation. *Phys. Rev. Lett.*, 112:120601, Mar 2014.

[88] Sho Sugiura and Akira Shimizu. Canonical thermal pure quantum state. *Phys. Rev. Lett.*, 111:010401, Jul 2013.

[89] S. Trotzky, Y-A. Chen, A. Flesch, I. P. McCulloch, U. Schollwock, J. Eisert, and I. Bloch. Probing the relaxation towards equilibrium in an isolated strongly correlated one-dimensional bose gas. *Natrue Physics*, 8:325–330, 2012.

[90] Constantino Tsallis. Possible generalization of boltzmann-gibbs statistics. *Journal of Statistical Physics*, 52(1):479–487.

[91] A. N. Wenz, G. Zürn, S. Murmann, I. Brouzos, T. Lompe, and S. Jochim. From few to many: Observing the formation of a fermi sea one atom at a time. *Science*, 342(6157):457–460, 2013.

[92] E. E. Wollman, C. U. Lei, A. J. Weinstein, J. Suh, A. Kronwald, F. Marquardt, A. A. Clerk, and K. C. Schwab. Quantum squeezing of motion in a mechanical resonator. *Science*, 349(6251):952–955, 2015.

[93] William K. Wootters. Random quantum states. *Foundations of Physics*, 20(11):1365–1378, 1990.

[94] B. Wouters, J. De Nardis, M. Brockmann, D. Fioretto, M. Rigol, and J.-S. Caux. Quenching the anisotropic heisenberg chain: Exact solution and generalized gibbs ensemble predictions. *Phys. Rev. Lett.*, 113:117202, Sep 2014.

[95] Benjamin Yadin and Vlatko Vedral. Quantum macroscopicity versus distillation of macroscopic superpositions. *Phys. Rev. A*, 92:022356, Aug 2015.

[96] Benjamin Yadin and Vlatko Vedral. General framework for quantum macroscopicity in terms of coherence. *Phys. Rev. A*, 93:022122, Feb 2016.

[97] Shengjun Yuan, Mikhail I. Katsnelson, and Hans De Raedt. Decoherence by a spin thermal bath: Role of spin-spin interactions and initial state of the bath. *Phys. Rev. B*, 77:184301, May 2008.

[98] A. Zeilinger, R. Gaehler, C. G. Shull, and W. Treimer. Experimental status and recent results of neutron interference optics. *AIP Conference Proceedings*, 89(1), 1982.

[99] Wojciech Hubert Zurek. Decoherence, einselection, and the quantum origins of the classical. *Rev. Mod. Phys.*, 75:715–775, May 2003.